

Copyright

by

Fergal Robert Mullally

2007

The Dissertation Committee for Fergal Robert Mullally
certifies that this is the approved version of the following dissertation:

Substellar Companions to White Dwarves

Committee:

D. E. Winget, Supervisor

Ted von Hippel

S. O. Kepler

W. Cochran

J. Craig Wheeler

Frank N. Bash

Substellar Companions to White Dwarves

by

Fergal Robert Mullally, B.Sc., M.A.

Dissertation

Presented to the Faculty of the Graduate School of

The University of Texas at Austin

in Partial Fulfillment

of the Requirements

for the Degree of

Doctor of Philosophy

The University of Texas at Austin

August 2007

For Anna Livia

Acknowledgments

As the years roll by, the number of people you need to thank continues to grow. This long work would never have been completed without the help of many of the people listed below, and many more besides. My gratitude to all who helped, whether you are mentioned below or not.

First in precedence are my advisors, Don Winget and Ted von Hippel, who were the inspiration, motivation, and guidance for the projects herein described. None of this would have been done without them. Next, my parents: who never understood why, but never belittled my choice of living for so long so far away.

I have had the privilege of meeting many wonderful people during my time at Texas. The white dwarf group at Texas consists of many more people than just my advisors. I have had the benefit of working with such fine minds as Mike Montgomery, Mukremin Kilic and Agnès Kim, from whom I have learned much. Among the former students, Diane Paulson and Nairn Baliber must be singled out for special mention. Nairn shared many a cloudy night at the observatory with me, and many a sunny afternoon at the Crown and Anchor. He deserves much credit for making this the friendly department that it is. In contrast, Diane never stayed later than 4 in the afternoon, but instilled in me her sensible attitude toward graduate school that as long as the work gets done it doesn't matter whether you are seen to be working long hours.

More recently, I have spend many long nights and long conversations with

Amy Forestell, Anna Frebel, and Casey Deen who will bear the responsibility for keeping the department a fun place to work for at least the next year. Speaking of fun, this town would be a shadow of itself without the irrepressible Tom Montemayor who appears out of nowhere, throws an incredible party, and disappears again for weeks on end.

A considerable portion of the observations that make up this dissertation were made at McDonald Observatory, and were made considerably easier by the friendly and hard working people who live and work there, available at all hours of the day and night when something went wrong (as it inevitably did). In particular, Dave Doss' nightly visits to the dome to check on the observer were appreciated more than he knows.

The three happiest years of my graduate career were spent at Laurel House Co-operative where I was assured good food and better companionship. There were always people around to talk to, argue against and celebrate with. I'm sad to see the old building go, but I hope the new Laurel House will be every bit as good.

And finally, to Susan, who has endured so much, smiled through most of it, and brightened the darker hours for me. Thank you.

FERGAL ROBERT MULLALLY

The University of Texas at Austin

August 2007

Substellar Companions to White Dwarves

Publication No. _____

Fergal Robert Mullally, Ph.D.

The University of Texas at Austin, 2007

Supervisor: D. E. Winget

We search for planets and brown dwarves around white dwarves (WDs). Finding extra-solar planets is the first step toward establishing the existence and abundance of life in the Universe. The low mass and luminosity of WDs make them ideal stars to search for low mass companion objects. Theoretical predictions generally agree that a star will consume and destroy close-in, low mass planets as it ascends the red giant and asymptotic giant branch evolutionary tracks, but larger mass objects and those further out will survive. The matter ejected from the star as it evolves into a white dwarf may also be accreted onto daughter planets, or may coalesce into a disk from which planets can then form.

We employ two techniques to search for planets and brown dwarves (BDs)

around WDs. A subset of pulsating white dwarf stars have a pulsational stability that rivals pulsars and atomic clocks. When a planet is in orbit around a such a star the orbital motion of the star around the centre of mass is detectable as a change in arrival times of the otherwise stable pulsations. We search for, and find, a sample of suitable pulsators, monitor them for between three and four years, and place limits on companions by constraining the variation in the pulse arrival times. For one star, we detect a variation consistent with a $2.4 M_J$ planet in a 4.6 year orbit.

We also observe a large sample of WDs to search for a mid-infrared excess caused by the presence of sub-stellar companions. We present evidence for a potential binary system consisting of a WD and a BD on the basis of an observed excess flux at near and mid-infrared wavelengths. We also place limits on the presence of planetary mass companions around these stars and compare our results to predictions of planetary survival theories. Our findings do not support suggestions of planet formation or accretion of extra mass during stellar death.

Contents

Acknowledgments	v
Abstract	vii
List of Tables	xi
List of Figures	xii
Chapter 1 Introduction	1
1.1 Planets	3
1.1.1 Theories of formation	3
1.1.2 Methods of planet detection	5
1.2 White Dwarf Stars	7
1.2.1 Metals in White Dwarf atmospheres	8
1.2.2 Will planets survive white dwarf formation?	8
1.3 Brown Dwarf Stars	11
1.3.1 Defining Brown Dwarves and Planets	11
1.3.2 The L and T spectral types	12
1.3.3 Do BDs form like stars or planets?	12
1.4 Current surveys	14
1.5 Finding planets around pulsating white dwarf stars	16
1.5.1 The pulsations of DAV stars	16
1.5.2 The effect of a planet on the observed pulsations	18
1.5.3 Doppler shift of pulsations	21
1.6 Infrared Planet Limits with <i>Spitzer</i>	21
1.7 Summary	22
Chapter 2 Eleven New DAVs from the Sloan Survey	24
2.1 Introduction	24
2.2 Object Selection and Observation	26
2.3 Characteristics of the Instability Strip	28

Chapter 3	A Candidate Planet around a White Dwarf	34
3.1	Introduction	34
3.2	Observations and Reductions	37
3.3	Analysis	38
3.3.1	The 302s mode	38
3.3.2	The 271.7s mode	42
3.4	Discussion	46
3.4.1	Confirmation by Direct Detection	47
3.5	Conclusion	50
Chapter 4	Limits on Planets around Other White Dwarves	54
4.1	Motivation	54
4.2	The Survey	58
4.3	Results	64
4.3.1	Notes on Individual Stars	65
4.4	Discussion and Conclusion	68
Chapter 5	A <i>Spitzer</i> White Dwarf Infrared Survey	73
5.1	Introduction	73
5.2	Target Selection, Observations and Reductions	75
5.3	Results	77
5.3.1	Notes on Individual Objects	77
5.4	Discussion	89
5.5	Conclusion	90
Chapter 6	Planet Limits with <i>Spitzer</i>	97
6.1	Introduction	97
6.2	Observations and Reductions	99
6.2.1	The Survey	99
6.2.2	Testing our models and photometry	99
6.2.3	Constraining the excess at $4.5\,\mu\text{m}$	102
6.2.4	Measuring the Contrast	103
6.2.5	Range of orbital separation probed	108
6.3	Results and Discussion	110
6.4	Conclusion	113
Chapter 7	Finis	116
	Bibliography	118
	Vita	124

List of Tables

2.1	Wavelengths used to calculate equivalent width of Balmer lines	27
2.2	Journal of Observations	30
2.3	Observed Periods and Amplitudes	31
2.4	Properties of new DAVs	32
2.5	Table of Objects not Observed to Vary	33
3.1	List of Observed Periods in GD66	40
3.2	Orbital Parameters for Planet around GD66	42
3.3	χ_r^2 for Fits of Different Models to the Data	44
3.4	Journal of Observations	51
3.4	Journal of Observations	52
3.4	Journal of Observations	53
4.1	Modes used to construct O-C diagrams	59
4.2	Initial and Final Masses	66
5.1	Classifications of Observed Stars	87
5.2	Infrared Fluxes for Stars in this Sample	92
5.2	Infrared Fluxes for Stars in this Sample	93
5.2	Infrared Fluxes for Stars in this Sample	94
5.2	Infrared Fluxes for Stars in this Sample	95
5.3	Survey Objects with Detected Photospheric Metals	96
6.1	Infrared Fluxes and Excesses	104
6.1	Infrared Fluxes and Excesses	105
6.2	Upper mass limits on Planets	114
6.2	Upper mass limits on Planets	115

List of Figures

1.1	Planet limits from other works	15
1.2	DAV pulse shapes	17
1.3	Theoretical Limits on Planet Detection	20
1.4	Combined SED of a white dwarf and planet	22
2.1	Lightcurves and Fourier Transforms	26
2.2	Lightcurves and Fourier Transforms (cont.)	28
2.3	The instability strip	29
3.1	FT of GD66	36
3.2	O-C diagram of the 302s mode	39
3.3	Amplitude of 302s and 271.7s modes	41
3.4	χ^2 of 302s mode	43
3.5	O-C diagram for the 271.7 second mode	44
3.6	O-C diagram for 198s triplet	45
3.7	Infrared Excess as function of Planet Mass	49
4.1	WD0018+0031	55
4.2	WD0111+0018	56
4.3	WD0214−0823	58
4.4	WD0913+4036	60
4.5	WD1015+0306	61
4.6	Aliases in Fourier Transforms	61
4.7	WD1354+0108	63
4.8	WD1355+5454	63
4.9	WD1724+5835	64
4.10	WD2214−0025	65
4.11	G117−B15A	67
4.12	G185−32	68
4.13	G238−53	69
4.14	GD244	70

4.15	R548	70
5.1	Spectral energy distributions for 124 WDs	85
5.2	SED of WD1234+481	88
5.3	SED fit to WD1234+481	88
5.4	Histogram of Excesses and Deficits	91
6.1	Histogram of Excess over Model	100
6.2	Histogram of Excess over Blackbody	101
6.3	Planet Limits as a Function of Age	107
6.4	Comparing Photometric and Spectroscopic Distance Determinations	109
6.5	Limits on Old Planets	110
6.6	Limits on Young Planets	111
6.7	Histogram of Limits on Planets	112
6.8	Companion Limits for Massive WDs	113

Chapter 1

Introduction

I can mar a curious tale in telling it

Kent, King Lear, Act 1 Scene 2

Planets are important to humans. After all, we live on one. This attachment to a small, unremarkable rock around a small, unremarkable star has given humans a rather biased perspective on the universe. When we look out into space hoping to meet and nod hello to our neighbours, we tend to expect extraterrestrial life to live a lot like us: bound to small unremarkable rocks, breathing deep from an oxygen rich atmosphere and washing down hearty meals of amino acids and complex sugars with big glasses of liquid water.

The question of whether extraterrestrial life exists and where best to look for it has long been purely an academic question, but may not remain so for much longer. Astronomical missions (e.g. Kepler) are being designed and built that will be able to detect planets as small as the Earth around the nearest stars, and some (e.g. Darwin, or the Terrestrial Planet Finder, TPF) may even be able to characterise the composition of the atmospheres of any planets found. And although detecting chemicals in the atmosphere of a planet is more akin to spying on our neighbours through the window blinds than it is greeting them at their door, even this small

step would be an incredible achievement for a species that until recently still thought they inhabited the centre of the universe.

It is easy to argue that this approach of looking for life only in places we would find hospitable is narrow minded and blinkered. After all, life on Earth is only a single data point in a universe that is not only stranger than we imagine, but stranger than we can imagine¹. It is only to be expected that Nature will do things differently in different locations. By restricting our searches by our prejudices we risk failing in our efforts.

However, the opposite argument is also valid. Although the Earth is the only place that we know life exists, we can list many places where we have failed to find life, e.g. the planets of our own solar system². At larger distances, we see no evidence for life on scales as large as interstellar gas clouds or galaxies. Moreover, if extraterrestrial life very much different from our own does exist, we may have difficulty recognising it as such. Far better to search for life we understand in places we know it can survive.

This thesis unashamedly flaunts its prejudice and asserts that planets are interesting astrophysical objects, if only because the author is rather fond of his own. Our technology is only beginning to become sensitive to planets as small as the Earth, and there is much to be learned about the frequency of planets and the details of their formation and destruction by studying the bestiary of Neptune and Jupiter mass extra-solar planets that are more easily detectable. Ernest Rutherford once divided all of science into physics and stamp collecting, but there is value in stamp collecting, or *surveys* in astronomical jargon. In order to study planets, we must first find them, and that is still a considerable observational challenge worthy even of a physicist. The focus of this thesis therefore is searching for and characterising extra-solar planets (and their somewhat larger relation, brown dwarves) around a particular remarkable type of star known as a white dwarf.

¹This quote is variously attributed to Arthur Eddington and John Haldane.

²At least we have found no evidence of macroscopic plant or animal life on Mars, although many people still hope to find microscopic life.

1.1 Planets

1.1.1 Theories of formation

Until recently all our information on planetary properties, formation and frequency came from studies of just one system, our own. The dramatic increase in knowledge over the past decade has added twists and turns to our understanding, but the basic paradigm has survived markedly unscathed. First proposed by Laplace in his “nebular hypothesis”, planets are still generally believed to form from disks around new stars. Left over material from stellar formation, gas and dust, collects into a circumstellar disk, which provides raw material from which planets form.

Support for this paradigm comes from the detection of disks around T Tauri (Mendoza 1966, 1968) and other young stars. Disks around these stars frequently show rings or gaps where the density of material drops suddenly (e.g. Forrest *et al.* 2004), which can be explained by accretion onto a unseen planet forming in the gap (Varnière *et al.* 2006). Other evidence comes from the discovery of both a planet (Hatzes *et al.* 2000) and a disk (Aumann 1988; Greaves *et al.* 2005) around the main sequence star ε Eridani and Benedict *et al.* (2006) measured that the disk is aligned with the plane of the planet’s orbit. Separately, Quillen & Thorndike (2002) used numerical simulations of the gravitational interaction of the disk particles with the planet to explain observed structure of lumps in the disk.

Under the most popular theory, known as core accretion (see Pollack *et al.* 1996, for a further description), dust particles first collide and coalesce to form snowflakes. The snowflakes combine to form rocks and boulders, which then further combine to form planetesimals and eventually planets. The larger a planet grows, the more efficient it becomes at accreting material, preferentially leading to a few large planetoids rather than many small ones, a process known as competitive accretion. If a planetoid mass exceeds a critical value (of the order of 10 Earth masses, Ida & Lin 2004), gas from the disk collapses onto the surface, rapidly increasing the growth rate and forming a gas-giant planet.

The problems with this theory are threefold. Firstly, evidence from asteroids in our solar systems shows them to be structurally weak objects, and collisions

tend to break large asteroids into many smaller ones, rather than building up into larger objects. The second problem is one of timescales. Observations of infrared (IR) excesses around young objects (e.g. Haisch *et al.* 2001; Carpenter *et al.* 2005; Silverstone *et al.* 2006) show that the gas and dust in disks survives for between 3 and 10 million years (depending on the star). Models of planet formation through core accretion (e.g. Pollack *et al.* 1996; Hubickyj *et al.* 2005) can create planets on this short a timescale, but some delicate fine tuning is required. Finally, many models of Jupiter’s interior find its core is smaller than $5 M_J$ and possibly non-existent (Saumon & Guillot 2004). If giant planets do not have a core, it is difficult to invoke core accretion to explain their formation.

An alternative theory, first proposed by Cameron (1978) and championed in a series of papers by Alan Boss (e.g. Boss 1995, 2005) is one of disk instability. In this theory, Earth-mass (terrestrial) planets form through oligarchic growth (as in core accretion), on timescales of many tens of millions of years. However, the rotating proto-planetary disk suffers from gravitational instability leading to the formation of vortexes and creating dense clumps of gas that form gas giant planets directly without recourse to a core accretion stage. Current hydrodynamical simulations show that these instabilities form easily, but do not have the resolution to determine whether these clumps stay bound and coalesce into a planet, or are torn apart by torques from the rest of the disk. Another problem with this model is that in order to form planets, simulations require an order of magnitude more material to be present in the disk than the minimum mass necessary for the disk that created our own solar system (Boss 1997)

Gonzalez (1997) first noted a correlation between detected planet frequency and host star metallicity. Because the sensitivity of radial velocity surveys are generally biased toward metal rich stars (which have more absorption lines permitting better measurement accuracy) it took a series of papers culminating in Fischer & Valenti (2005) to determine that the probability a star hosts a planet scales with the square of the metal abundance. The core accretion model is sensitive to the metallicity of the disk. More metals means more dust means more collisions between dust particles which should lead to faster growth rates for planets. The collision rate increases with the square of the number of particles, so the frequency of planets should scale with the square of the stellar metallicity. Alternatively, Laughlin &

Adams (1997) suggested that the star cannibalised one or more daughter planets that migrated too close, and therefore have a higher than primordial metallicity. This pollution would only be present in the convection zone near the surface of the star, and not at the core. However Fischer & Valenti (2005) found no correlation between metallicity and convection zone depth, confirming the link between stellar metallicity and abundances of planets.

The results appeared to sound the death knell for the disk instability model which predicted no (Boss 2002) or inverse (Cai *et al.* 2006) dependence of planetary frequency on stellar abundance. However, the question is not fully resolved. The core accretion model does not explain the result of Santos *et al.* (2004) that frequency of planet detection is observationally *independent* of metallicity for stars with sub-solar abundances. Rice *et al.* (2003) compromise, noting that disk instability favours producing high-mass planets, and that there is no evidence of host metallicity dependence for high-mass ($>5 M_J$) planets, and argue that massive planets are formed through disk instability, but core accretion applies for lower masses. Sozzetti (2004) claims to see a weak correlation between the orbital period of a planet and the host star metallicity, in reality this is just a different interpretation of the Rice result as larger mass planets generally are found with longer orbital periods. Perhaps high-mass planets are formed quickly by disk instability at large separations, while lower mass planets are formed over longer timescales by disk instability and suffer inward migration to produce the close-in “hot jupiters”.

1.1.2 Methods of planet detection

Theories stand and fall on their ability to predict and explain observations, and by far the most popular and successful method of discovering new planets is the radial velocity method (Struve 1952). As the star orbits the centre of mass of a planetary system, its small velocity toward and away from us ($\sim 10\text{m/s}$ for the sun due to the influence of Jupiter) can be detected by precise measurements of the Doppler shifts in the spectral lines. At this time of writing 229 planets have been discovered with this method – by far the majority. The technique is most suitable for bright stars (that can be studied with high resolution spectrographs), with lots of metal lines, slow rotation velocities and low activity from star spots (or chromospheres) that

could mimic the effect of a planet in the radial velocity signal. As a result, these surveys are limited to F, G and K stars, with surveys ongoing for early M stars (e.g. Endl *et al.* 2006). Because close-in planets have short orbital periods, and provoke correspondingly faster reflex orbital velocities in their parent stars, sensitivity to planets of a given mass falls off with increasing distance making it difficult to detect Jovian planets at larger (solar system-like) separations with current technology. As Figure 1.1 shows, radial velocity surveys are not able to detect Saturn around the sun, while Jupiter is currently at the limit of detectability. Despite the successes of this technique over the past decade, we still don't know if our solar system is a common configuration or a rare arrangement.

In terms of number of planets detected, the next most successful technique is that of transit photometry. In rare cases, the orbit of a planet aligns exactly with the line of sight from the Earth to the star and the planet can be observed as an obscuration of the stellar disk and a corresponding drop in the observed brightness of the star. Combined with orbital properties from radial velocity studies, transiting planets can reveal a surprising amount of information about the planet. The mass and radius (from the depth of the transit) give the density, the Rossiter-McLaughlin effect (Rossiter 1924; McLaughlin 1924) provides the inclination of the planet's orbit to the stellar rotation axis, a prediction of the nebular hypothesis, and precise measurements of small changes in the times of transits may reveal the presence of other low-mass planets or even moons (Sartoretti & Schneider 1999).

Ultimately, the future of planet detection lies in space. The *Spitzer* space telescope has already produced the first spectra of extra-solar planets, albeit of almost useless S/N (Richardson *et al.* 2007; Grillmair *et al.* 2007). Kepler, scheduled for launch in 2008, is expected to discover over 1000 new transiting planet detections³, while SIM, hopefully to launch in 2015, will astrometrically search for periodic oscillations in the positions of stars in an effort to detect otherwise invisible planets. JWST will provide a mid-IR capability to image and take spectra of planets, although its small field of view will make it unsuitable for large surveys. Considerable technical difficulties will need to be overcome before TPF or Darwin are able to achieve the holy grail of taking the spectrum of an Earth-mass planet to search for "biosignatures", chemical markers of extra-terrestrial life. In the meantime, there is

³See <http://kepler.nasa.gov/sci/basis/results.html>. Numerous assumptions apply, *caveat lector*.

plenty of opportunity for smaller, niche techniques to advance our understanding of planetary properties, formation and history, and it is in this category that searches around white dwarves firmly sits.

1.2 White Dwarf Stars

Despite their reputation, even stars are mortal. When a star exhausts its supply of usable hydrogen in its core it swells up to become a red giant star. The many details of the final stages of stellar evolution need not concern us here, but a star with initial mass $\lesssim 8 M_{\odot}$ will swell to a radius of between 1 and 5 AU (Pols *et al.* 1998) while helium in the core is transmuted into carbon, oxygen, and for the heavier stars, neon, silicon and possibly iron as well. The outer layers of the star are blown off in a strong stellar wind leaving the hot dense core behind. Despite the wide range of initial stellar masses that produce a white dwarf, the mass distribution of these remnants is narrowly peaked with a FWHM of $0.15 M_{\odot}$ around $0.59 M_{\odot}$ (Kepler *et al.* 2007) squeezed into a volume less than twice the radius of the Earth. Nuclear burning has effectively ceased in these objects, and subsequent evolution is one of slow, predictable cooling. WDs come in two main spectral flavours, hydrogen atmosphere DA stars, and helium atmosphere DBs. There are also a small number of unusual objects with other atmospheric compositions.

WDs are an interesting place to look for planets. Their chief advantage is their low luminosity which lowers the contrast between the star and the planet making direct-detection of the companion orders of magnitude easier than compared to main sequence systems. Studies of WDs will also reveal the eventual fate of planets after the death of their parent star, and whether they will survive or be destroyed. The existence of variable WDs with extreme stability in pulsational period and phase (see §1.5) also permits a planet search that preferentially detects lower mass planets at larger orbital separations, searching a region of parameter space complementary to that of the radial velocity and other methods.

1.2.1 Metals in White Dwarf atmospheres

The extremely high gravity on the surface of WDs (typically 10^5 that of the earth⁴) is effective at fractionating material by mass (Schatzman 1958). We can be confident that there is no hydrogen hiding beneath the helium layer in DBs. However, approximately 25% of isolated DAs show evidence of contamination by Calcium or other metals (Zuckerman *et al.* 2003), and are known as DAZs. Koester & Wilken (2006) showed that such material should diffuse out of the atmosphere on timescales of millions of years to weeks, and is therefore presumably being currently accreted from an external source. The source of these metals is still being debated, but the leading contenders are currently the interstellar medium (Dupuis *et al.* 1993; Koester & Wilken 2006) or a disrupted asteroid or comet (Alcock *et al.* 1986; Jura 2003). Recently, von Hippel *et al.* (2007) suggested that asteroids are the source of metals in all DAZs, with the implication that metal line contamination might be a marker for planetary systems. This (as yet untested) hypothesis could have far reaching consequences. If every DAZ is caused by accretion from the debris of a planetary system and 25% of DAs are DAZs then the fraction of stars with planetary systems is 25%, far greater than the minimum value of 5–10% determined by radial velocity methods.

1.2.2 Will planets survive white dwarf formation?

The end point of stellar evolution is undoubtedly a distressing time for any sub-stellar companions, and planets are not guaranteed to remain in the system. A planet will become gravitationally unbound if the star suddenly loses more than half its mass. A $1 M_{\odot}$ progenitor will lose approximately half its mass while nearly 90% of an $8 M_{\odot}$ star will be ejected. However, as discussed in Burleigh *et al.* (2002), the mass loss must take at least $\sim 10^4$ and probably $\sim 10^6$ years, which is long on the timescales of planetary orbits (typically less than a few hundred years) and so we do not expect planets to be ejected from the system by this mechanism.

However, as a star loses mass we expect its planets to drift outward in order

⁴Stellar surface gravities are typically written as the logarithm to base 10 of the acceleration due to gravity in cgs units. So $\log g = 8.0$ implies $g=10^8 \text{cm.s}^{-2}$ or 10^6m.s^{-2} .

to conserve angular momentum. The effect of mass loss on orbital migration was rigourously derived by Jeans (1924), but the special case of a circular orbit illustrates the argument quite well. If a planet of mass m_p is in a circular orbit around a star of mass M_* (where $M_* \gg m_p$) at a distance $r_1(t)$ and an orbital velocity $\dot{\theta}(t)$, the energy of the planet is given by

$$E = \frac{1}{2}m_p(\dot{r}_1^2 + (r_1\dot{\theta})^2) - \frac{GM_*m_p}{r_1} \quad (1.1)$$

The first term in this equation corresponds to the kinetic energy of the planet, and the second is the potential energy in the presence of a gravitational field. Because the orbit is circular, $\dot{r}_1 = 0$. The specific angular momentum of the planet, or angular momentum per unit mass, is given by

$$\ell = r_1\dot{\theta} \quad (1.2)$$

Therefore,

$$E = \frac{1}{2}m_p\ell^2 - \frac{GM_*m_p}{r_1} \quad (1.3)$$

where the first term is a constant of the motion. When the star evolves into a less massive white dwarf, the mass of the star reduces to M_{WD} . If we assume that the planet does not interact either with a third body or with the material being expelled from the star, then both the energy and angular momentum of the planet are conserved. Therefore

$$\frac{1}{2}m_p\ell^2 - \frac{GM_*m_p}{r_1} = E = \frac{1}{2}m_p\ell^2 - \frac{GM_{WD}m_p}{r_2} \quad (1.4)$$

or more succinctly,

$$\frac{r_1}{r_2} = \frac{M_*}{M_{WD}} \quad (1.5)$$

If the star is surrounded by a multi-planet system, the planets will pass through regions of orbital resonance which could cause dynamical instability. Dun-

can & Lissauer (1998) performed a numerical integration of the orbits of the giant planets in our solar system (Jupiter, Saturn, Uranus and Neptune) while reducing the mass of the sun smoothly from 1 to $0.5 M_{\odot}$. They found that while our solar system was likely to be stable during this process, in systems where the star lost $>90\%$ of its mass the planetary orbits would cross on timescales of the order of 10 million years. As discussed in Debes & Sigurdsson (2002), the result of this close interaction is either collision, ejection or orbital rearrangement. The most likely scenario is that one planet gets inserted into a short period orbit while the other is either ejected or lifted into a orbit $\sim 10^3$ times greater (in terms of semi-major axis) than before.

However, the planets may be destroyed before the parent star becomes a WD. Livio & Soker (1984) concluded that a planet engulfed in the stellar envelope would spiral in toward the stellar core due to gas drag and either be destroyed, or accrete enough mass to become a close-in sub-stellar companion. For planets outside the AGB envelope, Villaver & Livio (2007) predict that the hot wind from the pre-white dwarf will strip material from the atmosphere of any planets and cause them to be evaporated. However, they found that a $3 M_J$ planet at 2 AU from the $0.56 M_{\odot}$ (post mass loss) pre-white dwarf would lose less than half its mass in this manner.

An intriguing idea suggested by Jura & Turner (1998), is that planets could form from stellar material ejected during WD formation, but which never escaped the system. If such material is left behind, it may well form into a disk and form planets with the same efficiency as around young stars ⁵.

Livio *et al.* (2005) also noted that a large ($\sim 0.007 M_{\odot}$) disk of circumstellar material is left around a WD formed from the merger of two lower mass WDs. The energy released in such a merger would heat the disk enough to drive nuclear reactions, so such a disk would be high in carbonates and silicates (much like debris disks) and could coalesce to form planets. WD mergers do not produce low-mass WDs, so this formation mechanism would only be feasible for planets found around high-mass ($> 0.8 M_{\odot}$) WDs.

⁵Although this idea has been suggested, it has not been properly studied. For example, it is not known if such material could be left behind, whether it would be effectively removed from the system, or even if the strong ultraviolet flux from the young WD would interfere with the formation of dust grains.

As well as the importance for this work, the ability of a planet to survive is of broader interest. Our own planet orbits a star fated to become a WD, and answering the question of planetary survivability will resolve the ultimate destiny of our own home.

1.3 Brown Dwarf Stars

1.3.1 Defining Brown Dwarves and Planets

What constitutes a planet? This question received considerable public attention in 2006 when Pluto was unceremoniously stripped of its planetary status and demoted to a “dwarf planet”, or a mere oversized asteroid. A common, if incorrect, definition is that while stars shine by their own light, planets can be seen by reflected light only. A more formal definition could be that planets are gravitationally bound astrophysical objects in orbit around a star and of too low mass to support nuclear fusion of hydrogen. This definition makes sense: stars burn hydrogen to produce heat and light, while planets do not. It rests on the observationally obtainable quantity of mass (objects composed primarily of hydrogen can support fusion for masses above $0.08 M_{\odot}$) and does not depend on the unobservable details of whether the object formed from a nebula or the disk around a new star. It excludes exotic objects such as black holes, neutron stars and WDs and suggests a natural division between planets and asteroids – objects where inter-crystalline forces are strong enough to prevent them from assuming a nearly spherical shape are not bound by gravity and are therefore asteroids. Most appealingly, there is no requirement for the ad hoc, single object classification of “dwarf planet” ignominiously assigned to Pluto. However, this definition would promote Ceres and any other spherical bodies currently called asteroids to the class of planet.

There is one type of object that resists this definition. Objects with masses between about $13 M_J$ (0.012 and $0.08 M_{\odot}$) are too low mass to support anything but fleeting fusion of hydrogen, but do burn the small amounts of Deuterium (and sometimes Lithium) present during formation. This ability to produce energy from nuclear reactions is more akin to stellar than planetary behaviour and sug-

gests a new stellar class, the brown dwarf (BD). The existence of brown dwarves was first suggested by Kumar (1963) who approached the concept from the opposite direction, attempting to determine the nature of an object that formed like a star but was of too low mass to support fusion⁶. To accommodate BDs as a separate class of object we amend our definition of a planet to “gravitationally bound astrophysical objects in orbit around a star and of too low mass to support hydrogen or deuterium burning”. The dividing line between planets and deuterium-burning BDs is approximately $13 M_J$ (Burrows *et al.* 2001)

1.3.2 The L and T spectral types

The division between stars and brown dwarves fortuitously falls close to the temperature range where the strength of Titanium Oxide (TiO) absorption lines in stellar atmospheres weaken and absorption lines of metal hydrides (e.g. CrH, FeH) strengthen instead. As TiO was the distinguishing feature of the lowest-mass spectral class of stars, the M stars, it makes sense to assign a new spectral class to these cooler dwarves, the L type. At even cooler temperatures, the spectrum becomes dominated by absorption bands of water (H_2O) and these objects are known as T dwarves. The spectral classifications do not correspond exactly to the mass based definitions of stars, planets and BDs. The lowest mass stars are spectral type mid L, while young massive BDs start off as late M objects before they cool and become L, and later T dwarves. Finally, as the surface temperatures of the hot Jupiters often exceeds the temperature of the latest type of T dwarf, they too should be considered as T dwarves. For a complete description of these new spectral types, see the review of Kirkpatrick (2005).

1.3.3 Do BDs form like stars or planets?

As an intermediate object between planets and stars, the question naturally arises whether the BD formation mechanism is planet-like (i.e. from disks around forming stars), star-like (from contraction and fragmentation of giant molecular clouds) or a

⁶Kumar labeled these objects as black dwarf stars, instead of the more common brown dwarf used today.

mixture of the two. This question is complicated by the fact that neither planet nor star formation is well understood, but progress can still be made. The distribution of BDs around main sequence stars argues against a planetary formation mechanism. Radial velocity surveys show that high-mass planets are rarer than lower mass planets, at least down to the limits achieved by large surveys. Marcy & Butler (2000) state that less than 0.5% of main sequence stars have a BD companion within 3 AU. It appears that the disks that give birth to planets do not contain enough mass to create a BD.

If BDs form like stars on the other hand, their space density as a function of mass (Initial Mass Function, or IMF) should be similar to that of low-mass stars. Muench *et al.* (2002) studied the young cluster Trapezium and found that, in common with other stellar associations, the space density of stars, Φ , declines with increasing mass as $\Phi \propto M_*^\alpha$, with $\alpha \in [-1.7, -1.0]$. However, below $0.6 M_\odot$, the IMF flattens off, and around the brown dwarf limit the slope becomes positive, $\Phi \propto M_*^{+1.0}$. Large mass BDs are more common than lower mass ones, at least down as far as $0.02 M_\odot$ (or $20 M_J$). However, as the IMF is continuous and smooth it suggests that the difference between BDs and low-mass stars is one of degree, not of different mechanisms.

Cloud collapse models indicate that low-mass objects should continue to accrete material until they cross the mass threshold for hydrogen burning, so theoretical work on BD formation has concentrated on interrupting the accretion process somehow. For single BDs forming in clusters there are two popular theories, disk interaction and ejection. In the first, the close passage of an object near a proto-star disrupts the accretion disk creating a small knot of gas which forms sub-stellar objects (Boffin *et al.* 1998). In the second, the gravitational interaction between the many objects in a cloud results in some of their number being ejected from the cloud and starved of further material (Reipurth & Clarke 2001).

Regardless of their formation, for our purposes we can treat BDs identically to planets. BDs are both brighter and more massive than planets, which makes them easier to detect, and any that are found around WDs are equally suited to exploring post main-sequence survival as planets.

1.4 Current surveys

Despite their success at planet detection around main sequence stars, radial velocity surveys are not appropriate for sub-stellar companion searches of WDs, mainly due to their faintness and paucity of absorption lines. Most searches have instead utilised the low luminosity of a white dwarf with respect to a companion. The first such search was started by Probst (1983). Zuckerman & Becklin (1987) started a much larger survey which was completed by Farihi *et al.* (2005a). It was a near-IR imaging survey of a total of 371 WDs and discovered two brown dwarf companions, for a BD companion fraction of approximately 0.5% equal to the main sequence close brown dwarf binary fraction. The first, GD165-b (Becklin & Zuckerman 1988) apparently sits on the threshold between brown dwarf and main sequence stars at $75 M_J$ (Kirkpatrick *et al.* 1999), while GD1400-b (Farihi & Christopher 2004; Farihi *et al.* 2005b) is slightly less massive.

A more sensitive imaging survey was suggested by Burleigh *et al.* (2002) who calculated that an 8m telescope could detect a $3 M_J$ planet at >5 AU from a WD in the near-IR. This survey is completed and should appear in Hogan *et al.* 2007 (in prep). In a similar vein, Debes *et al.* (2005a) used the coronagraphic imager NICMOS on the Hubble telescope to limit the mass of any companions around variable WD G29-38 to $6 M_J$ at angular separations greater than $0.9''$ or 15 AU. G29-38 was a particularly interesting target at the time because of an observed near-IR excess (Zuckerman & Becklin 1987) originally thought to be due to a companion. The true nature of the excess as emission from circumstellar dust was first suggested by Wickramasinghe *et al.* (1988) and confirmed by mid-IR spectroscopy by Reach *et al.* (2005a). Debes placed further limits on $\sim 7\text{--}18 M_J$ companions with angular separations $>0.9''$ to 6 other DAZs by a similar technique. Debes *et al.* (2006) completed the survey of another 13 WDs using the CFHT, achieving limits $\sim 15 M_J$ >19 AU.

The predictions of Livio & Soker (1984) regarding the fate of low-mass companions to WDs can be directly tested by the discovery of a brown dwarf around the white dwarf WD0137-349 (Maxted *et al.* 2006), although the results are inconclusive. The BD was found in an extremely short (90 minute) orbit around the white dwarf, in agreement with prediction. However, follow-up near-IR spectroscopy (Burleigh

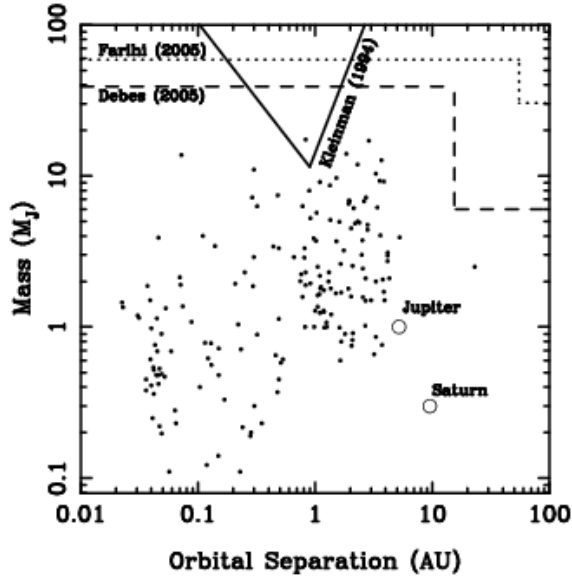


Figure 1.1 Limits on planetary companions to WDs based on other works. The filled dots are the positions of planets discovered around non WDs in the mass – orbital separation plane, mainly discovered with the radial velocity technique. For the most part, these masses are lower limits only. The open circles represent Jupiter and Saturn in our solar system. The solid line shows the limits on $m_p \sin i$ for companions around G29-38 placed by Kleinman *et al.* (1994) based on their Table 3. The dashed line is the best constraint on planet masses from Debes *et al.* (2005a, assuming an age of 1 Gyr) while the dotted line shows typical limits from the survey of Farihi *et al.* (2005a). The second two are direct-detection efforts and are significantly better than can be achieved for direction detection of companions to main sequence stars.

et al. 2006) found a temperature and spectral type more consistent with a cold BD as old as the system age (white dwarf cooling time plus progenitor lifetime). If the companion accreted mass while inside the AGB envelope it should have reheated and had a cooling age more consistent with the white dwarf cooling time alone. Silvotti *et al.* (2007) suggested that there may be a planet in a short period (or order years) around a sub dwarf star, an evolved object similar to a white dwarf. The orbital separation of the planet is again inconsistent with Livio & Soker (1984).

1.5 Finding planets around pulsating white dwarf stars

1.5.1 The pulsations of DAV stars

When DA stars cool to about 12,000 K (about half a billion years after formation) they become variable stars, or DAVs. The pulsations are multi-periodic, with periods between 100–1000s, amplitudes of a few percent, and continue until the star has cooled to about 11,000 K. The temperatures of DAs are most commonly measured by comparing optical spectra to atmosphere models and are typically trustworthy to within 200 K (Fontaine *et al.* 2003). The observed width of the pulsation instability strip varies between 950 K and 1050 K depending on models used (Mukadam *et al.* 2004a; Gianninas *et al.* 2006). DAVs have long been known to divide into two broad classes. Those near the blue (hot) end of the strip tend to have a smaller number of shorter period, lower amplitude modes and saw-tooth lightcurves while those nearer the red edge show more, larger amplitude shark-toothed pulse shapes (see Figure 1.2). The change in pulsation properties is most likely due to increasing depth of the convection layer near the surface of the star (Brickhill 1983, and subsequent articles). We observe that modes on 3 of the hotter hDAVs are stable in period and phase on human timescales, while modes on the cooler cDAVs oftentimes appear and disappear from observing season to season. The division between hot and cool DAVs is not strict and many stars exhibit characteristics of both sub-classes.

Although many known and unknown factors can influence the period of a pulsation mode on a hDAV, the fundamental limit on stability is due to the cooling of the star. At 12,000 K, the rate of temperature change of a DAV, $\dot{T} \sim 10^{-7}$ K/year (Wood 1992). The cooling of the star makes it more degenerate, decreasing the buoyancy frequency, and leading to an increase in the pulsation period, P , of a given mode. This increase is tiny, even on astronomical scales, with \dot{P} of a few times 10^{-15} . To put this into perspective, the published accuracy of the best state of the art atomic clock is 3.3×10^{-16} (see Table 1 of Wynands & Weyers 2005), and while highest frequency milli-second pulsar has a \dot{P} of $\lesssim 6 \times 10^{-19}$ (Hessels *et al.* 2006), the value for most milli-second pulsars is closer to 10^{-14} .

We plot the difference between the observed time of arrival of these stable pulses (or cycles) and those calculated based on the assumption of a constant period

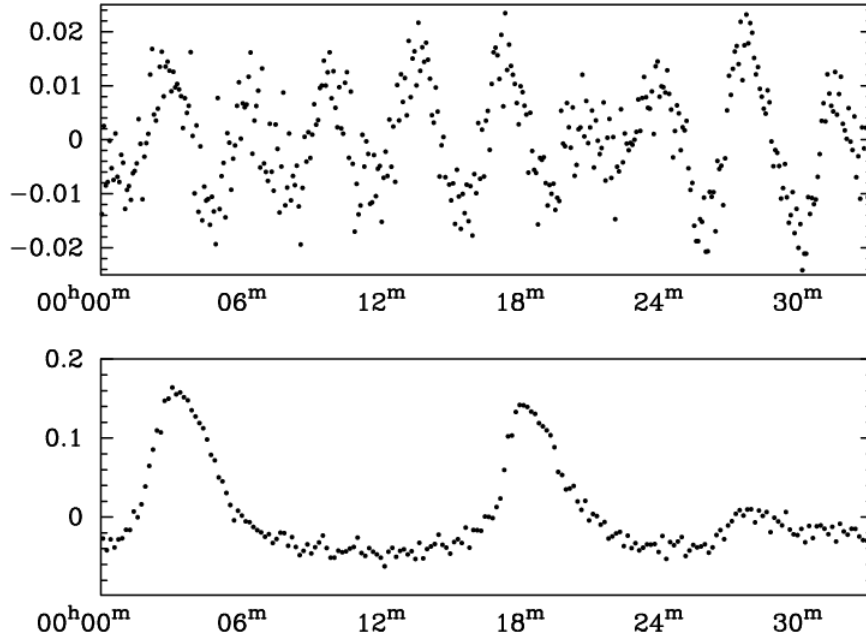


Figure 1.2 Typical pulse shapes for a hot and cold DAV pulsator. The time is given in minutes and the flux is in fractional amplitude. The hotter stars typically show short period, low amplitude, saw-tooth pulse shapes, while the cooler stars have longer period, larger amplitudes pulses characterised by a steep rise and a slower decline.

on an O-C diagram. If our best guess period is slightly larger than the true value by ΔP , the next pulse will arrive ΔP earlier than expected (giving an O-C value of $-\Delta P$), the next pulse will be $2\Delta P$ earlier, and the n^{th} pulse will arrive $n\Delta P$ seconds earlier than expected. The O-C diagram will then show a constant downward trend. Similarly, if our best guess period is too short, the O-C diagram will show an constant upward trend instead. If the period of pulsation is increasing due to cooling, each pulse will have a period slightly longer than the previous one, and the value of ΔP will increase with each pulse, resulting in a parabolic shape in the O-C diagram. Following Kepler *et al.* (1991), if we expand the observed time of arrival of the E^{th} pulse, T_E in a Taylor series,

$$T_E = T_0 + \frac{dT}{dE}(E - E_0) + \frac{1}{2} \frac{d^2T}{dE^2}(E - E_0)^2 + \dots \quad (1.6)$$

The change in arrival time with epoch, $\frac{dT}{dE}$, is just the period of pulsation, P . Similarly,

$$\frac{d^2T}{dE^2} = \frac{dP}{dE} = \frac{dP}{dt} \frac{dt}{dE} = \dot{P}P \quad (1.7)$$

Setting $E_0 = 0$, writing T_E as the observed time of arrival, O , and dropping terms of order higher than two, we get

$$O = T_0 + PE + \frac{1}{2}P\dot{P}E^2 \quad (1.8)$$

The expected time of arrival based on the assumption of a constant period can be written as

$$C = T'_0 + P'E \quad (1.9)$$

where the primes refer to estimated values. If we assign $\Delta x = x - x'$ the difference between the observed and calculated time,

$$O - C = \Delta T_0 + \Delta PE + \frac{1}{2}P\dot{P}E^2 \quad (1.10)$$

This approach has been used to measure temporal phenomena in many different astrophysical systems. Of particular interest, Kepler *et al.* (2005) used it to measure the rate of cooling of the white dwarf G117-B15A.

1.5.2 The effect of a planet on the observed pulsations

If a planet is in orbit around star, the star's distance from the Earth will change periodically as it orbits the center of mass of the planetary system. If the star is a stable pulsator like a hDAV, this will cause a periodic change in the observed arrival time of the otherwise stable pulsations compared to that expected based on the assumption of a constant period.

We can determine the semi-major axis of the planet's orbit, a_p , from Kepler's equations,

$$a_p = \left(\frac{GM_* P^2}{4\pi^2} \right)^{1/3} \quad (1.11)$$

where G is Newton's constant of Gravitation, P is the orbital period, and M_* is the stellar mass which can be determined by comparing the temperature and gravity of the WD to models. The semi-major axis of the star's orbit around the centre of mass of the system,

$$a_* = (a_p m_p) / M_* \quad (1.12)$$

where m_p is the mass of the planet. If the orbit of the planet is inclined at an angle i to the line of sight⁷, the projected axis size will be $a_* \sin i$. The change in distance corresponds to a change in light travel time from the star,

$$\tau = \frac{a_* \sin i}{c} \quad (1.13)$$

$$\tau = \frac{a_p m_p \sin i}{M_* c} \quad (1.14)$$

where c is the speed of light. In common with astrometric methods, the amplitude of the signal increases with the orbital separation of the planet, so for a given mass, planets in longer period orbits are easier to detect if given sufficient time.

It is standard practice to accumulate a full orbit of data on a planet before claiming a planet. However the presence of a planet with a given mass and orbital period can be ruled out with very much less than a full orbit if the observed O-C diagram is consistent with a straight line. Following Kepler *et al.* (1991), we measure the curvature of an O-C diagram in terms of the equivalent change in period that would produce that curvature,

$$\dot{P} = \frac{P}{c} \frac{GM_*}{a_p^2} \sin i \quad (1.15)$$

⁷By convention, i is defined so 0° is perpendicular to the line of sight and 90° toward the observer.

with \dot{P} measured from the O-C diagram according to Eqn 1.10. In practical terms, values of τ of about 1 second are routinely possible with enough data, and 3–4 years of observations constrains $\dot{P} \lesssim 10^{-13}$. Figure 1.3 shows the region of mass – orbital separation parameter space that can be probed with these limits. This approach breaks down if there is a planet present and the data set spans a significant fraction of the orbit. In this event, the assumption that \dot{P} is constant is no longer valid. As such Eqn 1.15 can be used to constrain the presence of planets, but not to measure the parameters of a planet once it is found. For that we must fit the orbital parameters directly.

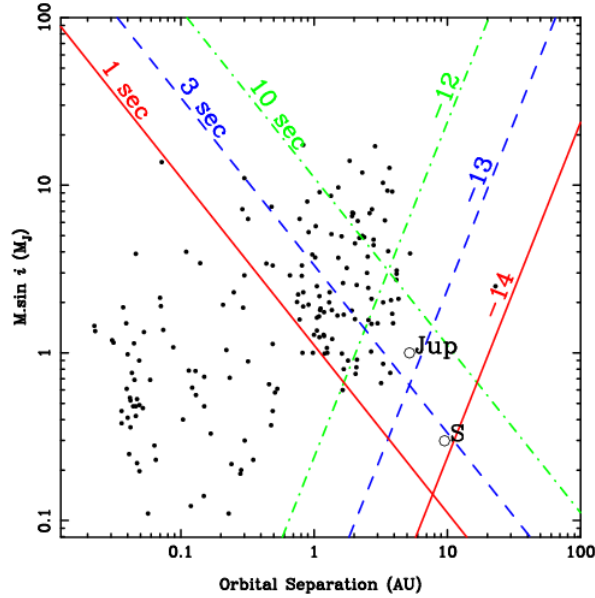


Figure 1.3 Graphical illustration of the limits on planets for three reasonable values of τ (Eqn 1.13) and \dot{P} (Eqn 1.15). The lines of positive slope (i.e. from lower left to upper right) are labeled with $\log_{10} \dot{P}$. The cooling of the star produces a \dot{P} of a few times 10^{-15} . These limits compare favourably to those from other techniques shown in Figure 1.1 and with good quality data can open a region of parameter space to study that is unavailable to the radial velocity method.

1.5.3 Doppler shift of pulsations

Although the spectra of DAVs are unsuitable for a doppler spectroscopic planet search, the frequency of the pulsations will also be periodically blue and redshifted as the star wobbles in its orbit due to the presence of a companion. Taking Kepler's equation (1.11) and the centre of mass equation (1.12), and noting that the velocity of the star in its orbit, v is given by $(2\pi a_*)/T$ we find after some algebra,

$$v = m_p \sqrt{\frac{G}{a_p M_*}} \quad (1.16)$$

The equation for doppler shift is

$$\frac{v}{c} = \frac{\Delta\lambda}{\lambda} = \frac{\Delta P}{P} \quad (1.17)$$

If we take a $1 M_J$ planet in a 1 AU orbit around a $0.6 M_\odot$ WD, we find a velocity amplitude of approximately 40 ms^{-1} , corresponding to a change in period of $0.13 \mu\text{s}$. While it is possible to measure the period with this accuracy, it would take far longer than the orbital period of the planet. It is therefore far easier to search for a change in the arrival times than directly measuring a change in the period.

1.6 Infrared Planet Limits with *Spitzer*

As previously discussed, WDs make popular targets for direct-detection planet searches. The advantages of this technique are enhanced by going into space, and to the mid-infrared. Companions are more difficult to spatially resolve at longer wavelengths because the resolution of a telescope decreases linearly with increasing wavelength. However, the flux from a WD decreases through this range while the flux from a planet or a BD generally increases, meaning that a companion can be detected as an excess flux from the star at certain wavelengths. Figure 1.4 shows a model spectrum from Finley *et al.* (1997) of a $12,000 \text{ K}$ DA at 10 pc between 1 and

$10\,\mu\text{m}$. Added to this spectrum is the flux from 1 Gyr old 5 and $10\,\text{M}_\text{J}$ planets from Burrows *et al.* (2003). A “bump” in the flux between 4 and $5\,\mu\text{m}$ is clearly visible in the combined spectrum. Also shown in this plot are filter transmission curves for the 4 cameras on *Spitzer*’s IRAC imager. An unresolved sub-stellar companion can be detected by comparing the observed flux at $4.5\,\mu\text{m}$ to one of the other 3 bands.

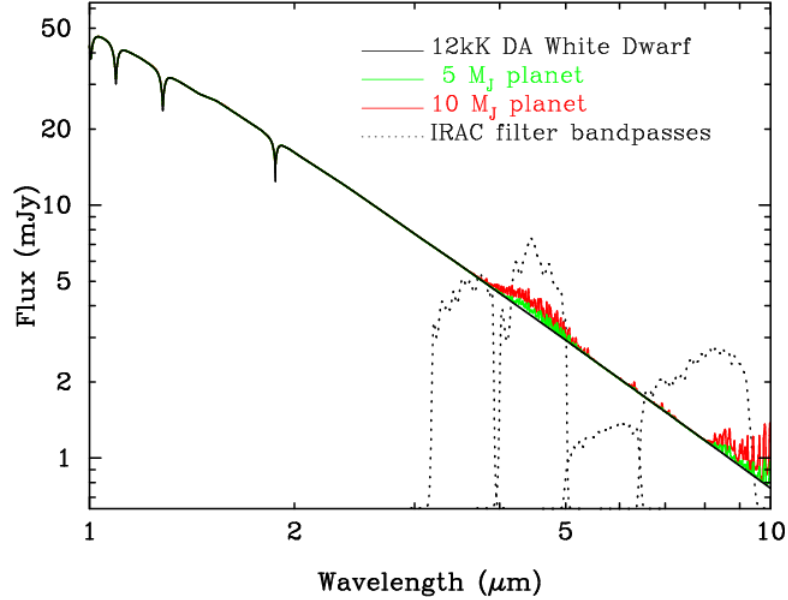


Figure 1.4 Combined model spectral energy distribution of a white dwarf and a planet. The solid line is a model atmosphere of a 12,000 K DA. The dark and light grey lines are the combined flux from the WD plus a 5 and $10\,\text{M}_\text{J}$ model planet atmosphere respectively. The dotted lines show the spectral response of the IRAC filters.

1.7 Summary

This dissertation describes two methods to find planets and brown dwarves around WDs. The efforts yielded two successes, a candidate planet detected using the O-C method, and a possible brown dwarf discovered as an infrared excess with *Spitzer*. In Chapter 2, I report on a search for suitable hDAV candidates from the Sloan Digital Sky Survey using time-series photometry. This work was previously published in

volume 625 of the *Astrophysical Journal*. Since then the number of known DAVs has increased to almost 150, and Chapter 3 describes the detection of a candidate planet with this method. Chapter 4 reports on limits on planets placed by this technique on other stars and discusses the successes and failures of the project.

In Chapter 5 we describe a Spitzer mid-infrared survey of 124 WDs which uncovered a potential WD+BD binary. In many cases this survey was sensitive to planetary-mass companions, although we found no strong evidence of any. The majority of this chapter appears in volume 171 of the *Astrophysical Journal's* supplement series. Finally, in Chapter 6 we place upper limits on the masses of any unresolved companions using the survey data in Chapter 5. The limits obtained disfavour the hypothesis that planets can form during or after the AGB phase of the progenitor star.

Chapter 2

Eleven New DAVs from the Sloan Survey

We report the discovery of eleven new variable DA white dwarf (ZZ Ceti) stars. Candidates were selected by deriving temperatures from model fits to spectra obtained from the Sloan Digital Sky Survey. We also find objects whose temperatures and gravities indicate they lie within the instability strip for pulsation, but which were not observed to vary. Although the temperatures are based on relatively low S/N spectra, an impure strip is unexpected, and if confirmed suggests that our knowledge of the pulsation mechanism is incomplete. This work brings the total number of published variable DA white dwarf stars to 82.

2.1 Introduction

The relatively simple structure and behavior of white dwarf stars (WDs) make them ideal objects for astrophysical study. For the variable WDs, asteroseismology allows a rare glimpse into the interior of a stellar object. WDs pulsate in three distinct instability strips along the HR diagram. The extremely high gravity of these objects makes non-radial gravity-modes energetically favorable (Winget 1998, and references therein). Of interest in this paper are the hydrogen atmosphere WDs (known as the

DAs) which pulsate at temperatures between approximately 11,000 K and 12,000 K (Mukadam *et al.* 2004a). We previously believed that variability was a normal part of the evolution of a cooling white dwarf (Fontaine *et al.* 1982; Bergeron *et al.* 2004), so these pulsating WDs (or DAVs) are otherwise normal stars caught during the brief period of evolution where their temperatures allow pulsation. However recent analysis by Mukadam *et al.* (2004b) has shown the presence of non-variable stars within the strip, indicating either that the models used for fitting temperatures need refinement, or the presence of an additional third parameter (surface gravity being the second) determining the pulsation properties of these objects. This is an important concern in the application of the conclusions of DA asteroseismology to other DAs.

A hot subset of the variable DAs (known as hDAVs) were discovered to exhibit extreme stability in the period and phase of their pulsations (Stover *et al.* 1980; Kepler *et al.* 1982). Kepler *et al.* (2005) showed that one such star, G117-B15A has a period stability of $\dot{P} = (4.12 \pm 0.83) \times 10^{-15}$, a stability that rivals that of atomic clocks. Mukadam *et al.* (2003) constrained the stability of ZZ Ceti to better than $(5.5 \pm 1.9) \times 10^{-15}$.

With such a stable signal the presence of an orbiting planet can be inferred from variations in the observed arrival time of pulsations due to the reflex orbital motion of the star. The first limits on planetary mass companions to white dwarf stars were placed by Kepler *et al.* (1988). For this paper, our search for new variables was biased toward the hot edge of the strip where these stable pulsators, suitable for searching for planets, are to be found.

A key constraint on both the prior progress of asteroseismology and the search for planetary companions was the limited number of suitable stars available for study. For that reason, Mukadam *et al.* (2004a) performed a photometric search and discovered 35 new DAVs. This search is on-going, and in this paper we report 11 new stars to make them available to the wider community. We refer the reader to Mukadam *et al.* (2004a) for a full description of this program.

2.2 Object Selection and Observation

The Sloan Digital Sky Survey (Fukugita *et al.* 1996; Gunn *et al.* 1998; York *et al.* 2000; Hogg *et al.* 2001; Smith *et al.* 2002; Stoughton *et al.* 2002; Pier *et al.* 2003) is proving to be an impressive source of new white dwarf stars (Kleinman *et al.* 2004). We obtained candidate DAVs from both the DR1 (Abazajian *et al.* 2003) and DR2 (Abazajian *et al.* 2004) samples. Objects from DR1 were selected from the catalogue of Kleinman *et al.* (2004) using temperature fits based on models published in Finley *et al.* (1997).

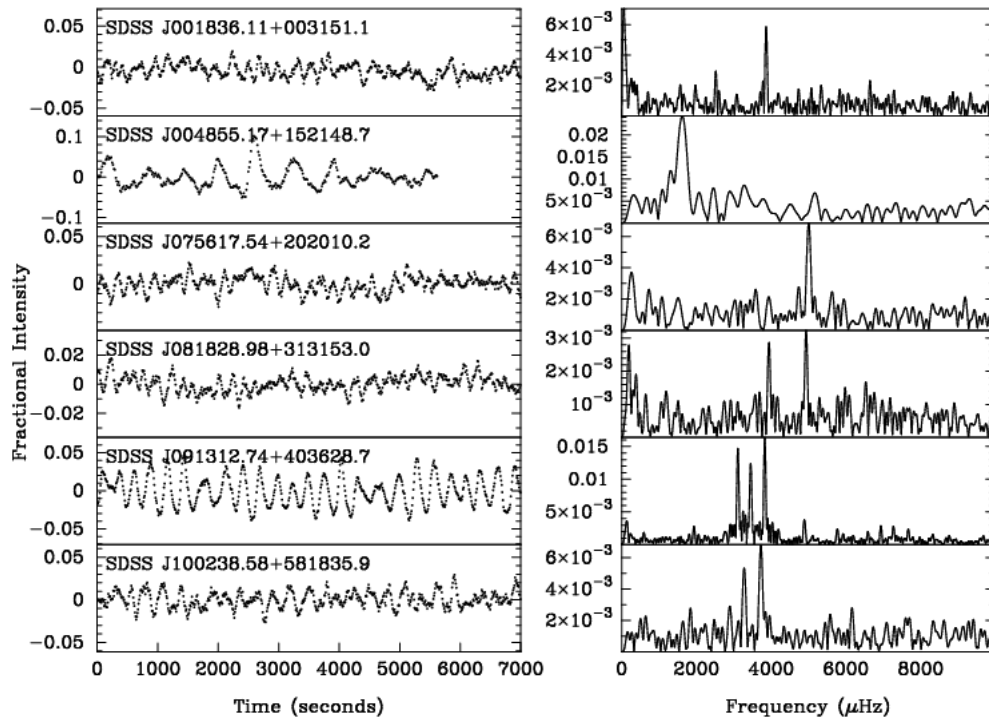


Figure 2.1 Two hour portions of lightcurves for the new pulsators. The lightcurves have been boxcar smoothed by seven points to emphasize the pulse shapes. The Fourier transforms in the right column are of the unsmoothed data and may be taken from longer data sets.

Objects from DR2 (which do not appear in Kleinman *et al.* 2004) with spectra were also selected. DA stars near the DA instability strip are easily identifiable due to their very broad Balmer lines caused by their very high surface gravity and

the fact that the Balmer lines are maximally broad near the temperature range of the instability strip (Fontaine *et al.* 2003). For each spectrum in the database we measured the equivalent widths of the H_β and H_γ lines over the wavelength region given in Table 2.1. Objects in the range $40\text{\AA} < H_\beta < 65\text{\AA}$ and $20\text{\AA} < H_\gamma < 45\text{\AA}$ were selected and a colour cut of $0.2 \leq (u - g) \leq 0.7$, $-0.4 \leq (g - r) \leq 0.05$ and $9.5(u - g) - (g - r) > 4.14$ was used to further trim the sample. The third cut removes DAs with Balmer lines of appropriate equivalent width but on the hotter side of the curve of growth ($\approx 15,000$ K). The temperatures and gravities of the selected DAVs were found by fitting to a grid of temperature models as described in Kleinman *et al.* (2004).

Table 2.1 Wavelengths used to calculate equivalent width of Balmer lines

Line	Center (\AA)	Width (\AA)
H_β	4861.3	324
H_γ	4340.5	214

Objects were observed and reduced as described in Mukadam *et al.* (2004a). Each object was observed for two hours on the 2.1m Otto Struve telescope at McDonald Observatory using the Argos prime focus CCD camera (Nather & Mukadam 2004). Individual exposure times were between 5 and 15 seconds depending on the brightness of the target and readout times were negligible due to the use of a frame transfer buffer. If an object showed signs of variability it was re-observed on a later night for confirmation. Faint objects or those observed under poor conditions may appear to show variability, so a second run is required to confirm variability. If an object did not appear to pulsate it was not re-observed. Many DAVs present closely spaced modes which can destructively interfere, effectively hiding a mode for periods longer than two hours. However the aim of this survey is to find as many pulsators as possible with the telescope time available, not to conduct a complete search of the sample, and so stars that did not appear to vary were not re-observed.

The CCD images were flat fielded and lightcurves extracted using IRAF's weighted aperture *apphot* package. We subtract the contribution from sky photons and divide by a combination of reference stars to remove small cloud variations.

We discovered 11 new DAVs and 26 stars that were not observed to vary. A

journal of observations appears in Table 2.2. Lightcurves and Fourier transforms of the new pulsators are shown in Figures 2.1 and 2.2. Table 2.3 lists the observed periods and amplitudes of pulsation. The high number of non-variables is due to an unsuccessful attempt to use a different method to measure the stellar temperatures. Our instability strip is similar to that discovered in Mukadam *et al.* (2004a), which is to be expected as we are using the same temperature fitting technique.

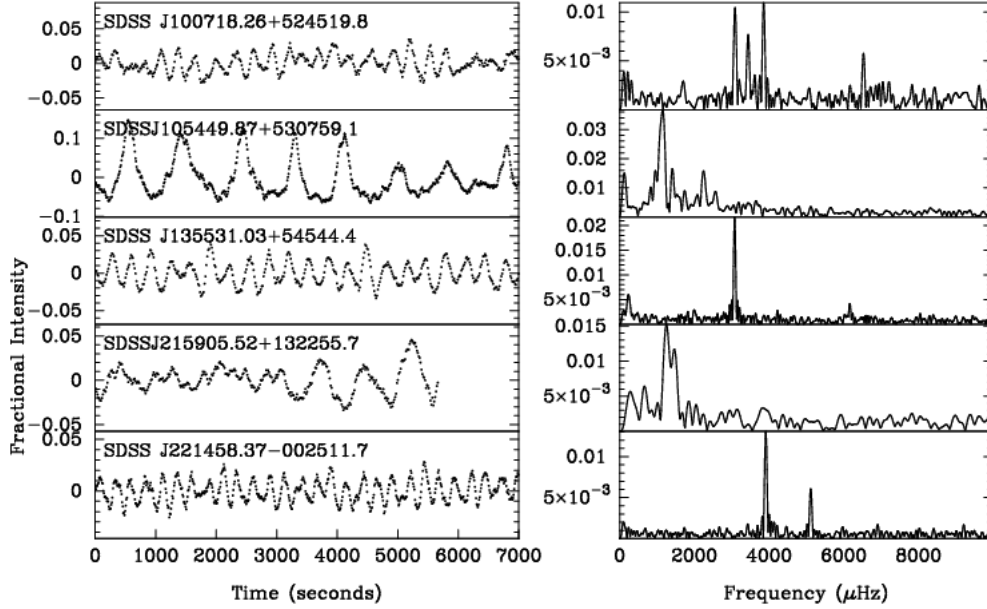


Figure 2.2 Same as Figure 2.1 for five additional pulsators.

2.3 Characteristics of the Instability Strip

A plot of the location of the new variables within the instability strip is shown in Figure 2.3. A table of the properties of the variables is presented in Table 2.4 and those stars not observed to vary in Table 2.5. The phrase non-variable is fraught with danger, as a star may be exhibiting destructive interference between two closely spaced modes while being observed, or merely be pulsating with too low an amplitude to be detected. For this reason, we prefer to use the term Not Observed to Vary (NOV).

The uncertainties in Figure 2.3 and Tables 2.4 and 2.5 are the formal least squares fit errors. In an effort to determine the extent of external errors in DAV temperature fits, Fontaine *et al.* (2003) compared the measured effective temperature of a number of DAs in the region of the instability strip as measured from two independently observed and reduced spectra of each object. They conclude that the external errors, due primarily to different flux calibrations, was ~ 200 K. It should be noted that that paper uses spectra with signal-to-noise ratios of greater than 80 per pixel, while our faintest star, SDSS J173712 ($g = 19.2$) has a S/N ratio of less than 8. Mukadam *et al.* (2004b), using similar spectra from the Sloan survey which are observed and reduced in a consistent manner, estimate an uncertainty in T_{eff} of less than 300 K for the fainter stars, and 200 K for the brighter stars.

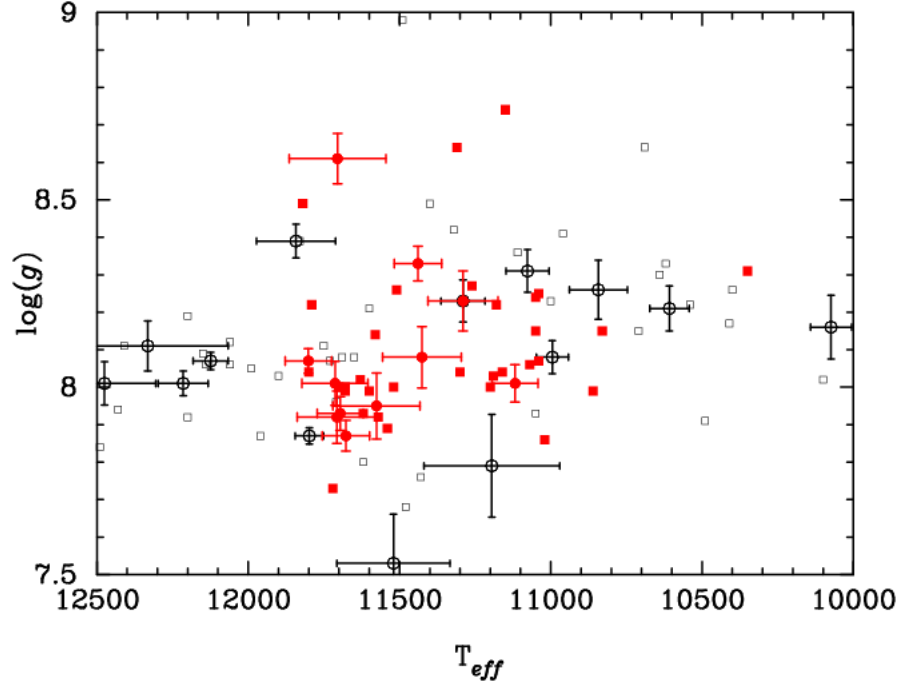


Figure 2.3 Distribution of effective temperatures and gravities of DAVs discovered in the Sloan survey. The filled shapes are pulsators, hollow shapes are NOVs. Circles are stars reported in this paper while squares are from Mukadam *et al.* (2004a). For clarity errorbars are only shown for objects reported in this paper, those in Mukadam *et al.* (2004a) are similar in size.

Our enlarged sample of DAVs has the same characteristics as the sample

Table 2.2. Journal of Observations

Run	ObjectName	UTC Date	Start time	Exp	Length
A0752	SDSS J001836.11+003151.1	2003-11-19	03:05:56	15	02:05:45
A0762	SDSS J001836.11+003151.1	2003-11-21	04:18:46	15	02:05:00
A0794	SDSS J001836.11+003151.1	2003-12-01	00:55:45	10	04:42:00
A0701	SDSS J004855.17+152148.7	2003-09-04	08:10:40	15	01:40:00
A0706	SDSS J004855.17+152148.7	2003-09-05	09:09:51	15	01:52:15
A0860	SDSS J075617.54+202010.2	2004-03-18	01:54:49	10	03:08:20
A0864	SDSS J075617.54+202010.2	2004-03-19	02:03:04	10	04:55:00
A0831	SDSS J081828.98+313153.0	2004-01-19	03:57:18	10	03:26:40
A0849	SDSS J081828.98+313153.0	2004-03-01	01:58:28	10	02:51:20
A0836	SDSS J091312.74+403628.7	2004-01-20	07:43:18	10	01:44:20
A0866	SDSS J091312.74+403628.7	2004-03-20	02:03:26	10	05:00:10
A0861	SDSS J100238.58+581835.9	2004-03-18	05:11:27	10	03:06:40
A0870	SDSS J100238.58+581835.9	2004-03-24	05:05:08	10	01:23:00
A0635	SDSS J100718.26+524519.8	2003-05-06	02:42:38	15	03:51:15
A0869	SDSS J100718.26+524519.8	2004-03-24	02:01:27	15	01:45:45
A0833	SDSS J105449.87+530759.1	2004-01-19	09:45:01	10	03:19:30
A0867	SDSS J105449.87+530759.1	2004-03-20	07:14:37	10	02:45:50
A0862	SDSS J135531.03+545404.5	2004-03-18	08:25:51	15	02:03:00
A0873	SDSS J135531.03+545404.5	2004-03-25	09:25:52	15	02:43:00
A0880	SDSS J135531.03+545404.5	2004-05-14	02:58:42	15	05:09:00
A0430	SDSS J215905.52+132255.7	2002-12-08	00:53:08	15	01:53:00
A0673	SDSS J215905.52+132255.7	2003-07-02	09:22:30	15	01:43:45
A0670	SDSS J221458.37−002511.7	2003-07-01	08:37:02	10	02:36:20
A0692	SDSS J221458.37−002511.7	2003-09-02	04:35:53	10	03:59:50
A0723	SDSS J221458.37−002511.7	2003-10-25	01:15:40	10	04:18:30
A0761	SDSS J221458.37−002511.7	2003-11-21	00:54:57	10	03:15:30
A0783	SDSS J221458.37−002511.7	2003-11-28	01:01:22	10	02:55:00

published in Mukadam *et al.* (2004a). Our survey emphasized the blue edge of the instability strip which is why we found more pulsators hotter than 11,500 K than cooler. With this bias in mind, our new sample still supports the narrower strip found in Mukadam *et al.* (2004b). We note that two stars not observed to vary, SDSS J143249 and SDSS J012234 lie within the strip. It is possible that these objects are complex pulsators whose modes were destructively interfering for the time they were observed, or simply that their amplitude was too low to be observed. If further observations address those concerns, these objects lend support to the arguments in Mukadam *et al.* (2004b) that the DA instability strip is impure.

Table 2.3. Observed Periods and Amplitudes

Object	Resolution (μ Hz)	Frequency (μ Hz)	Period (sec)	Amplitude (%)
SDSS J001836.11+003151.1	59	3876	257.9	0.58
SDSS J004855.17+152148.7	145	1625*	615.3	2.48
SDSS J075617.54+202010.2	56	5011	199.5	0.68
SDSS J081828.98+313153.0	81	3947*	253.3	0.29
		4942	202.3	0.33
SDSS J091312.74+403628.7	56	3119*	320.5	1.47
		3462	288.7	1.24
		3841*	260.3	1.65
		4903	203.9	0.38
SDSS J100238.58+581835.9	89	3282	304.6	0.53
		3728	268.2	0.68
SDSS J100718.26+524519.8	72	3094*	323.1	1.04
		3446	290.1	0.77
		3863*	258.8	1.10
		6540	152.8	0.58
SDSS J105449.87+530759.1	101	1150*	869.1	3.74
		2248	444.6	1.60
SDSS J135531.03+545404.4	54	3086	324.0	2.18
SDSS J215905.52+132255.7	147	1248	801.0	1.51
		1462*	683.7	1.17
SDSS J221458.37−002511.7	65	3917	255.2	1.31
		5122	195.2	0.61

Note. — We do not have the resolution in our data to resolve multiplets or closely spaced modes for most of these stars. Objects marked * show evidence of amplitude variability between runs. The resolution quoted is reciprocal of the length of the run.

Table 2.4 Properties of new DAVs

Mjd	Plate	Fiber	Designation	T _{eff} (K)	log(<i>g</i>)	<i>H</i> _β (Å)	<i>H</i> _γ (Å)	<i>u</i> − <i>g</i>	<i>g</i> − <i>r</i>	<i>g</i>
52203	0688	348	SDSS J001836.11+003151.1	11696±076	7.93±0.045	52.66±0.81	32.70±0.59	0.452	-0.160	17.360
51871	0420	388	SDSS J004855.17+152148.7	11290±116	8.23±0.080	52.51±1.58	37.41±1.13	0.401	-0.109	18.676
52941	1583	167	SDSS J075617.54+202010.2	11713±109	8.01±0.059	54.92±1.33	36.07±0.98	0.465	-0.150	18.240
52619	0931	321	SDSS J081828.98+313153.0	11801±077	8.07±0.033	55.25±0.80	38.65±0.57	0.382	-0.185	17.381
52668	1200	017	SDSS J091312.74+403628.8	11677±078	7.87±0.041	53.90±1.02	37.78±0.71	0.495	-0.224	17.635
52317	0558	573	SDSS J100238.58+581835.9	11707±131	7.92±0.070	54.82±1.32	36.83±0.95	0.480	-0.201	18.264
52400	0903	557	SDSS J100718.26+524519.8	11426±130	8.08±0.082	56.47±1.68	37.61±1.19	0.414	-0.162	18.872
52649	1010	629	SDSS J105449.87+530759.1	11118±076	8.01±0.050	50.81±1.02	37.85±0.71	0.451	-0.156	17.922
52797	1323	161	SDSS J135531.03+545404.5	11576±144	7.95±0.088	52.32±1.48	36.70±1.05	0.398	-0.146	18.583
52224	0734	419	SDSS J215905.52+132255.7	11705±160	8.61±0.067	54.86±1.75	37.52±1.28	0.381	-0.193	18.873
51791	0374	180	SDSS J221458.37−002511.7	11439±078	8.33±0.046	52.41±1.06	36.63±0.77	0.334	-0.099	17.909

Table 2.5 Table of Objects not Observed to Vary

Mjd	Plate	Fiber	Designation	T _{eff} (K)	log(<i>g</i>)	H_{β} (Å)	H_{γ} (Å)	$u - g$	$g - r$	g	Limit (mma)
51900	0390	455	SDSS J002049.39+004435.0	9160 ± 10	9.00±0.003	25.60±0.74	15.47±0.55	0.238	0.058	16.797	1
52203	0688	164	SDSS J002309.03−003342.0	15522 ± 81	8.01±0.016	55.56±0.49	38.94±0.34	0.242	-0.300	16.280	1
51879	0419	098	SDSS J004610.37+133910.2	11077 ± 71	8.31±0.057	52.31±1.24	33.07±0.90	0.404	-0.132	18.040	2
51871	0420	591	SDSS J005703.73+151014.6	10074 ± 68	8.16±0.085	43.11±1.76	23.76±1.32	0.546	-0.063	18.850	4
52209	0696	476	SDSS J012234.67+003026.3	11798 ± 47	7.87±0.022	55.66±0.61	34.94±0.42	0.355	-0.073	17.286	2
52178	0702	448	SDSS J020851.65+005332.4	13401 ± 150	7.77±0.024	58.75±0.64	38.40±0.44	0.386	-0.270	16.960	2
51869	0406	385	SDSS J022108.67+004924.7	10608 ± 65	8.21±0.060	46.24±1.57	35.73±1.11	0.457	-0.124	18.632	2
51816	0410	501	SDSS J025709.00+004628.0	12215 ± 83	8.01±0.033	57.51±0.84	38.97±0.60	0.418	-0.206	17.387	2
52203	0710	548	SDSS J031111.38−000344.4	14537 ± 197	8.32±0.040	63.66±0.93	37.63±0.66	0.295	-0.200	17.870	3
51929	0413	074	SDSS J032302.85+000559.6	13030 ± 158	7.98±0.041	59.63±0.89	42.24±0.62	0.785	-0.220	17.436	4
51901	0414	273	SDSS J032510.84−011114.1	18267 ± 86	7.59±0.017	46.27±0.74	30.97±0.55	0.446	-0.191	17.073	3
51901	0414	454	SDSS J032619.44+001817.5	12124 ± 58	8.07±0.023	58.08±0.87	38.25±0.61	0.387	-0.207	17.420	6
51810	0415	206	SDSS J033200.49−005752.5	17476 ± 109	7.77±0.023	45.24±0.78	32.68±0.54	0.227	-0.299	17.062	2
52370	0771	225	SDSS J101218.09+610818.9	11842 ± 131	8.39±0.045	55.39±1.01	36.78±0.74	0.399	-0.188	17.733	2
52378	0838	144	SDSS J114132.99+042028.8	11520 ± 187	7.53±0.131	49.85±1.31	36.37±0.94	0.524	-0.222	18.186	5
51984	0498	234	SDSS J140004.68+643128.3	10995 ± 53	8.08±0.044	48.85±1.05	36.05±0.74	0.467	-0.206	17.671	3
52024	0536	318	SDSS J143249.11+014615.5	11290 ± 73	8.23±0.056	52.60±0.96	38.12±0.70	0.540	-0.170	17.484	2
52045	0594	478	SDSS J154545.35+032150.0	15652 ± 272	7.97±0.054	54.98±1.67	36.45±1.19	0.329	-0.242	18.753	3
52395	0818	476	SDSS J164248.61+382411.1	18813 ± 204	8.40±0.035	51.50±1.20	34.64±0.83	0.076	-0.322	17.952	3
52438	0820	516	SDSS J165815.53+363816.0	10843 ± 96	8.26±0.079	50.22±1.98	30.05±1.46	0.455	-0.119	19.162	5
52017	0366	629	SDSS J173712.95+584428.7	11195 ± 224	7.79±0.137	49.37±2.14	37.36±1.50	0.517	-0.182	19.266	3
52224	0734	348	SDSS J215532.95+123801.5	12332 ± 266	8.11±0.067	55.03±1.34	38.07±0.97	0.376	-0.223	18.338	2
52518	0737	226	SDSS J222223.04+123824.7	13888 ± 142	7.58±0.030	53.84±0.87	40.60±0.59	0.388	-0.235	17.63	1
52263	0740	601	SDSS J225211.51+143610.5	17027 ± 219	7.86±0.044	49.09±1.25	32.85±0.87	0.213	-0.286	18.148	2
52251	0744	273	SDSS J231152.20+142417.2	12475 ± 170	8.01±0.058	57.03±1.30	39.03±0.95	0.448	-0.227	18.251	3
52553	0647	126	SDSS J233742.20−104144.0	16164 ± 109	7.89±0.024	52.29±0.79	36.73±0.54	0.168	-0.293	17.188	3

Chapter 3

A Candidate Planet around a White Dwarf

“Don’t tell me that he’s good. Tell me, is he lucky?”

Napoleon Bonaparte

3.1 Introduction

White dwarf stars (WDs) are attracting considerable attention recently as potential hosts for planetary systems. A WD is the end point of stellar evolution of 98% of all stars (e.g. Weidemann 2000) so WD surveys are representative of main sequence systems. Their chief attraction is their low luminosity – a 12,000 K white dwarf is $\sim 10^{-4}$ less luminous than an A star progenitor. This allows the possibility of direct detection of planetary mass companions within a few AU of the host star. A number of groups are pursuing this approach (e.g. Burleigh *et al.* 2002; Farihi *et al.* 2005a; Debes *et al.* 2006; Mullally *et al.* 2007) although no conclusive detections have been reported as yet.

We are pursuing a different approach by searching for the signal of orbital

motion in the arrival times of pulsations of variable WDs. Hydrogen atmosphere WDs with temperatures of approximately 11-12,000 K are variable stars and are known as DAVs. They are otherwise normal DAs cooling through the temperature range of the instability strip (Fontaine *et al.* 1982; Gianninas *et al.* 2006). DAVs exhibit multi-periodic oscillations with periods around 100 to 1000s and amplitudes of a few percent. A subset of these stars, the hDAVs, have stable modes with rates of period change (\dot{P}) measured or constrained to better than a few parts in 10^{-15} (Kepler *et al.* 2005; Mukadam *et al.* 2003).

These stable pulsations allow the orbital motion of the WD around the center of mass of a planetary system to be detected as a periodic change in the observed arrival time of the pulses compared to that calculated based on the assumption of a constant period (O-C), similar to how planets were discovered around pulsars (Wolszczan & Frail 1992). More recently, Silvotti *et al.* (2007) suggested that the O-C diagram of a sub-dwarf B star indicated the presence of a companion planet in a 3 year orbit. The most attractive feature of this method is that for a given mass, planets in long-period orbits will produce a larger effect on arrival times and are therefore easier to detect. The low luminosity of the WD makes follow-up by direct detection of the flux from the planet possible with current instruments (e.g. *Spitzer*).

With this in mind we initiated a survey of 15 DAVs in the hope of detecting the signal of a planetary or brown dwarf companion. We report here on the detection of a candidate planet around one of our survey DAVs, GD66. We present these results to encourage other observations of this star both with time series photometry and other techniques. GD66 (WD0517+307) was first reported as a potential white dwarf by Giclas *et al.* (1965), and as a DAV by Dolez *et al.* (1983). It is an 11,980 K, $\log g=8.05$ hDAV (Bergeron *et al.* 2004) with a V magnitude of 15.6 (Eggen 1968) corresponding to a distance of about 51pc (Mullally & de Graff 2005). Models from Wood (1992) estimate a mass of $0.64(03) M_{\odot}$ and a cooling age of 500 Myr. Using the initial final mass relations of Ferrario *et al.* (2005) and Willams (2006) we find a progenitor mass of $2.05 - 2.43 M_{\odot}$, corresponding to a progenitor age of between 0.9 and 1.4 Gyr (Pols *et al.* 1998), or a total lifetime of less than 2 Gyr.

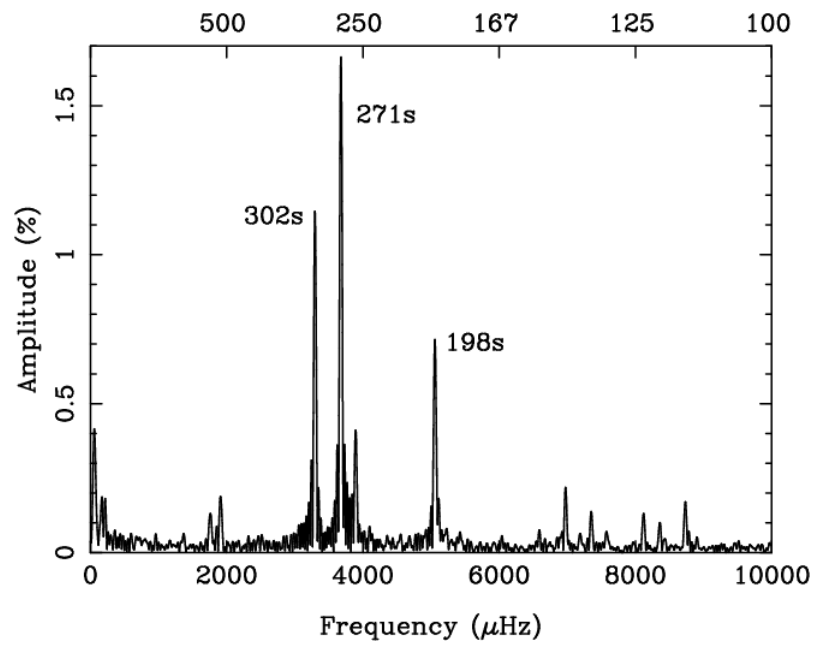


Figure 3.1 Sample Fourier transform of GD66 from a single 6 hour run, A1397. The modes discussed in the text are labeled with their periods.

3.2 Observations and Reductions

We have been observing GD66 since October 2003 using the Argos photometer designed for this project (Nather & Mukadam 2004) on the 2.1m Otto Struve telescope at McDonald Observatory. We take continuous sequences of exposures, 5 to 10 seconds in duration, for between 2 and 8 hours. Because Argos is a frame transfer camera no time is lost to chip readout, maximizing our use of telescope time.

We reduce our data in the manner described in Mullally *et al.* (2005) with one improvement. Argos suffers from a fluctuating bias level but does not have an overscan region. To account for this we measure the bias from a dead column and subtract this value from both our science and dark frames before flatfielding. This is clearly not ideal, but the best approach to measuring the bias available given that the level can vary on timescales shorter than the exposure time. We perform weighted aperture photometry with a variety of apertures using the IRAF package *wphot*, choosing the aperture that gives the best signal-to-noise by eye. In poor conditions the effect of clouds dominates the signal and is difficult to model and remove. Designing an algorithm that can competently select suitable regions of a lightcurve from which to determine the aperture that gives the least scatter is not simple, however it is a nearly trivial task for the human eye.

We divide the light curve by a combination of one or more reference stars, remove points affected by cloud, fit a second-order polynomial to remove the long term trend caused by differential extinction, and correct our timings for the motion of the Earth around the barycenter of the solar system using the method of Stumpff (1980). We show a journal of observations in Table 3.4.

We show an example Fourier transform (FT) of the lightcurve of this star in Figure 3.1 and list the detected modes in Table 3.1. The FT is dominated by a single mode at 302s, triplets of modes separated by $\approx 6.4\mu\text{Hz}$ at 271 and 198 seconds and a handful of other lower amplitude modes. There are also some combination and harmonic peaks present. We measure the period and amplitude of each mode by fitting a sine curve to the entire data set using the Levenberg-Marquart method (Bevington 1969). Where necessary, we refine the period by fitting and removing a linear trend in the O-C diagram. Having established an accurate period we then

perform a linear least squares fit to each run to measure the arrival times for that mode. The scatter between individual runs is often greater than the signal we intend to measure, so we use the arrival times of combinations of runs from a given month for analysis.

3.3 Analysis

3.3.1 The 302s mode

We simultaneously fit the two largest amplitude modes in this star, the 302 and 271.7s, and show the O-C values for their respective phases in Figures 3.2 and 3.5. The curvature in the phase of the 302s mode is unmistakable. O-C diagrams of hDAVs are expected to show parabolic behavior as the cooling of the star produces a monotonic increase in the period of pulsation (see Kepler *et al.* 1991). However, based on observations of other DAVs and models of white dwarf interiors (Bradley 1998; Benvenuto *et al.* 2004) we expect the cooling to cause a $\dot{P} \sim 10^{-15}$. If we fit a parabola to our data we find a $\dot{P} = 1.409(86) \times 10^{-12}$, three orders of magnitude larger than expected from cooling alone.

The tangential motion of the star with respect to the line of sight also causes a parabolic curvature in the O-C diagram. As the star moves linearly in space perpendicular to our line of sight, its distance to us changes parabolically (Pajdosz 1995). The USNO-B1 catalogue (Monet *et al.* 2003) quotes a proper motion of 131.6(5.0) mas/yr corresponding to a \dot{P} of 6.4×10^{-16} , again too small to explain the observed data.

The possibility that the star’s behavior has some unknown internal cause cannot be ignored. For example, a closely spaced mode of low amplitude would produce a sinusoidal phase variation. To reproduce the observed period of 4.62 years the hidden mode would have to be separated by $0.0068 \mu\text{Hz}$ from the observed mode. If the mode was a rotationally split multiplet the frequency splitting would be of the same order of magnitude seen in the other two triplets, implying that any such mode has to be an independent mode with an accidental degeneracy in frequency. However, to have a large enough amplitude to affect the measured phase

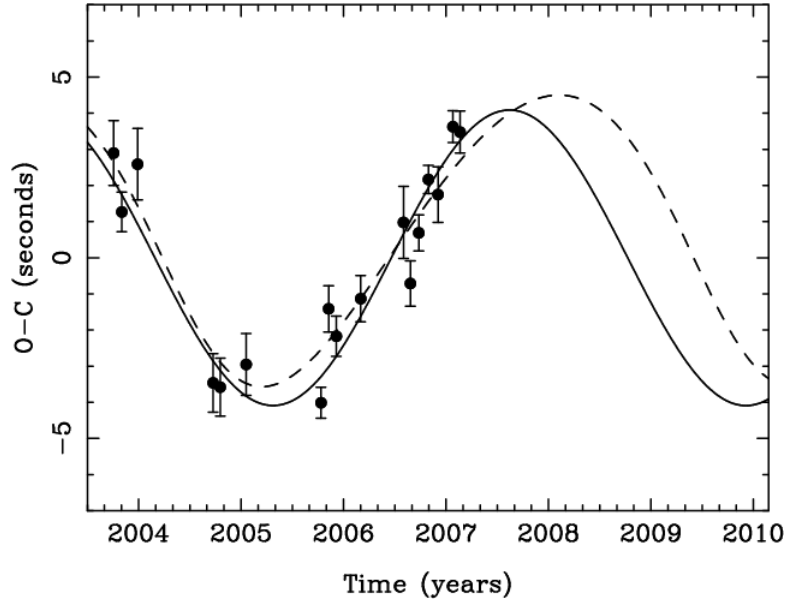


Figure 3.2 O-C diagram of the 302s mode. The solid line is a sinusoidal fit to the data, while the dashed line is a fit of an eccentric orbit. The parameters of the eccentric fit are poorly constrained, but a range of reasonable values are given in Table 3.2.

requires a low spherical harmonic degree ($\ell \leq 4$). The density of low ℓ modes in this frequency range makes such a chance agreement in period highly unlikely (Kumar & Goodman 1996).

Time series observations of another DAV, G29-38, showed a variation in the phase of one mode consistent with an $0.5M_{\odot}$ object in an eccentric 109 day orbit (Winget *et al.* 1990) before the amplitude of the mode dropped below the limits of detectability the following year. However, analysis of other modes on the same star failed to reproduce this behavior (Kleinman *et al.* 1994) and near-infrared imaging (Kuchner *et al.* 1998; Debes *et al.* 2005b) did not detect any sub-stellar companions. It is possible that the same internal effect that mimicked a companion to G29-38 is also present in GD66 albeit with a much smaller amplitude and considerably longer period. The amplitude of the mode also changes considerably in G29-38 on timescales of months, but this is not true for GD66 as Figure 3.3 shows. Modes on other DAVs demonstrated to be stable in phase, G117-B15A (Kepler *et al.* 2005),

Table 3.1. List of Observed Periods in GD66

Freq (μHz)	Period (sec)	Amplitude (%)
1916.64550(19)	521.744892(53)	0.1499
3302.888454(26)	302.7652959(24)	1.1021
3673.735619(100)	272.2024946(74)	0.2261
3680.335200(14)	271.7143808(10)	1.6859
3686.926392(97)	271.2286316(71)	0.2347
3896.67941(10)	256.6287588(67)	0.2819
5060.688277(77)	197.6015801(30)	0.3763
5066.929387(95)	197.3581875(37)	0.3053
5073.16899(10)	197.1154521(39)	0.2905
6605.77673(96)	151.382652(22)	0.0308
6983.22397(37)	143.2003332(76)	0.0785
7360.67011(17)	135.8571958(32)	0.169
7588.1074(22)	131.785167(39)	0.0129
8127.84068(23)	123.0339077(35)	0.1234
8369.81774(60)	119.4769147(85)	0.0485
10286.4284(22)	97.215473(21)	0.0129
10663.16620(64)	93.7807759(56)	0.0456

Note. — The 123s mode is close to the drive frequency of the telescope (at 120s) and should be considered highly suspect. All other peaks shorter than 151 seconds are harmonics or combinations of lower frequency modes.

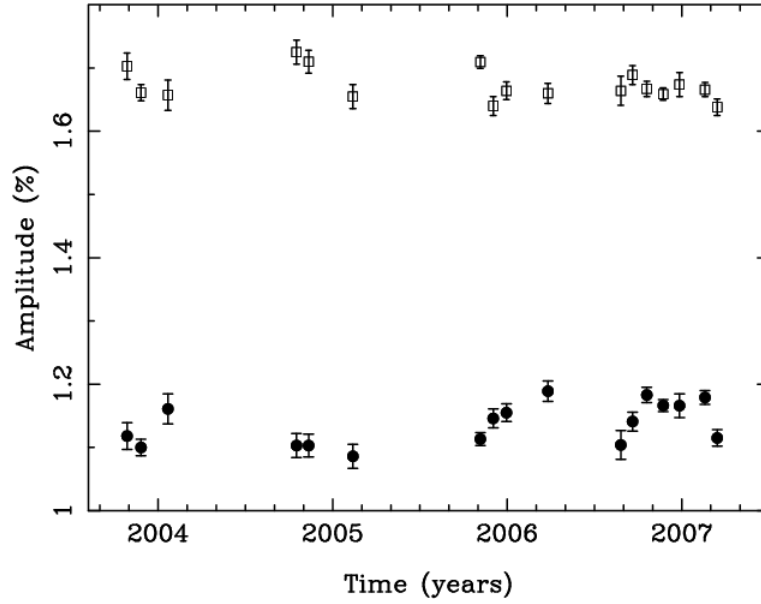


Figure 3.3 Amplitude of 302s (filled circles) and 271.7s modes (open squares). The error bars are the formal least square errors. Changes in sky brightness and amount of sky included in the software aperture during image extraction can easily explain the observed variation in amplitude.

R548 (Mukadam *et al.* 2003) and L19-2 (O'Donoghue & Warner 1987) are also stable in amplitude, suggesting that whatever effect was present in G29-38 does not apply to GD66.

We can not explain the observed curvature in this star with any known physical process, and conclude that it is caused either by the presence of a companion planet, or by another unknown effect. If we assume the curvature is caused by a planet in a circular orbit, the best fit period is 4.62(23) years and we can use Kepler's laws to determine an orbital separation, $a_p = 2.389(88)$ AU. The amplitude of the sine curve, $\tau = 4.09(40)$ s and is related to the semi-major axis of the star's orbit, a_* , by $\tau c = a_* \sin i$ where i is the inclination of the orbit to the line of sight and c is the speed of light. The mass of the planet, m_p , is equal to $(M_* a_*)/a_p$, where M_* is the mass of the star. Using these two equations we find an $m_p \sin i$ of 2.22(16) M_J . Figure 3.4 shows the χ^2 value for a range of orbital periods. Figure 3.2 shows the best fit to the 302s mode of an eccentric orbit, although without a full orbit of

	Circular	Eccentric
Period (years)	4.62(23)	5.9(0.7)
Orbital Separation (AU)	2.389(88)	2.8(0.2)
$m_p \sin i$ (M_J)	2.22(16)	2.09(04)
Eccentricity		0.25(05)

Table 3.2 Parameters of the planet for a circular or eccentric orbit. Error bars on the circular orbit are formal errors of the fit, while for the eccentric orbit the errors give an informal estimate of the range of acceptable parameters.

data the fit is poorly constrained. The parameters of the plotted fits are given in Table 3.2.

Apparently periodic signals in O-C diagrams can be caused by random jitter or drift in the period of the pulsator. A likelihood statistic, \mathcal{L} , that a given data set was caused by different combinations of observational error, period jitter and drift can be calculated according to Koen (2006). We expand his methodology to determine the likelihood that the data shown in Figure 3.2 is the signature of a companion, or the result of stochastic changes in the pulsation period. We first calculate \mathcal{L} for a model of the data that seeks to explain the data by invoking jitter or drift in the period and find values for $\log \mathcal{L}$ of -15.1673 and -15.0918 respectively. A model including both jitter and drift gives a similar value. Next, we calculate a log likelihood of -11.5549 that the residuals of the planet fit can be explained by observational error alone, strongly disfavoring the hypothesis that the observations can be explained by small random changes in the pulsation period.

3.3.2 The 271.7s mode

Detection of other modes on GD66 exhibiting the same behavior as the 302s mode would eliminate the possibility of an internal cause for the signal. It is almost impossible to conceive of any effect which would cause the same O-C behavior in two modes of different periods, while motion of the star will affect the time of arrival of all modes equally. Unfortunately, this test is complicated by the observed period structure. The two large peaks in the Fourier transform at 271 and 198 seconds are both triplets with modes separated by $\approx 6.4 \mu\text{Hz}$. A data span of 42 hours is

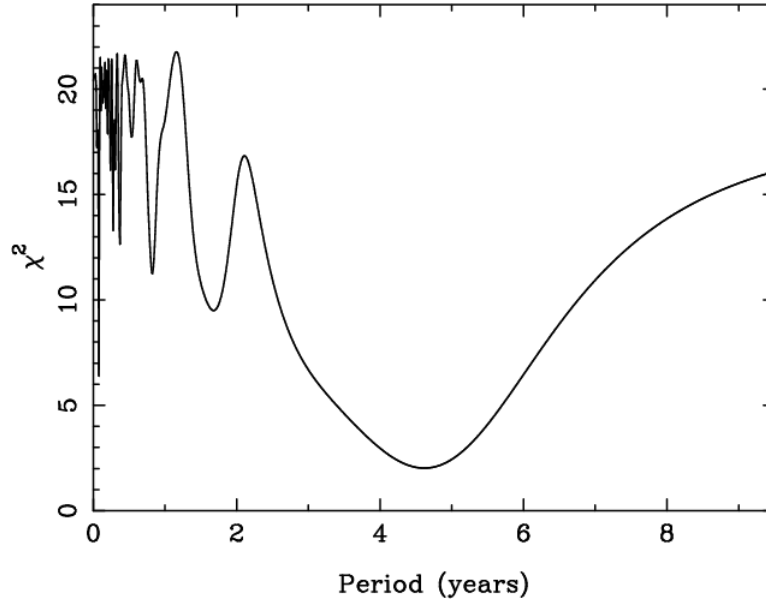


Figure 3.4 χ^2 against orbital period for the 302s mode for a range of orbital periods. χ^2 rises steeply for periods longer than the best fit. Because this statistic is calculated using a linear least squares fit at each period, the values of χ^2 do not agree with those of the non-linear fits used to fit the best period. For periods longer than 10 years, the value of χ^2 converges on a value slightly larger than 15.

required to resolve modes with this separation in frequency. While this can be achieved by combining runs over many nights, the measured phase in an individual run can be heavily affected by the unresolved nearby frequencies. The measured phase of combined runs is similarly affected and the scatter in the arrival times is significantly larger than predicted by the formal errors of the least squares fit.

We considered the possibility that the power at 256s ($3900\mu\text{Hz}$) could be influencing scatter. We compared the O-C values for the 271.7s mode measured by simultaneously fitting the 302 and 271.7s modes with that found from simultaneously fitting these two plus a mode at 256s. We found that, in the worst case, the measured phase differed by 1σ and conclude the effect of this nearby mode is insignificant.

The 271s triplet is composed of a large (1.7%) amplitude central peak at 271.7s and two smaller (0.2%) companion modes. We perform a Monte Carlo simulation to estimate the size of the scatter and hence the uncertainty in the phase

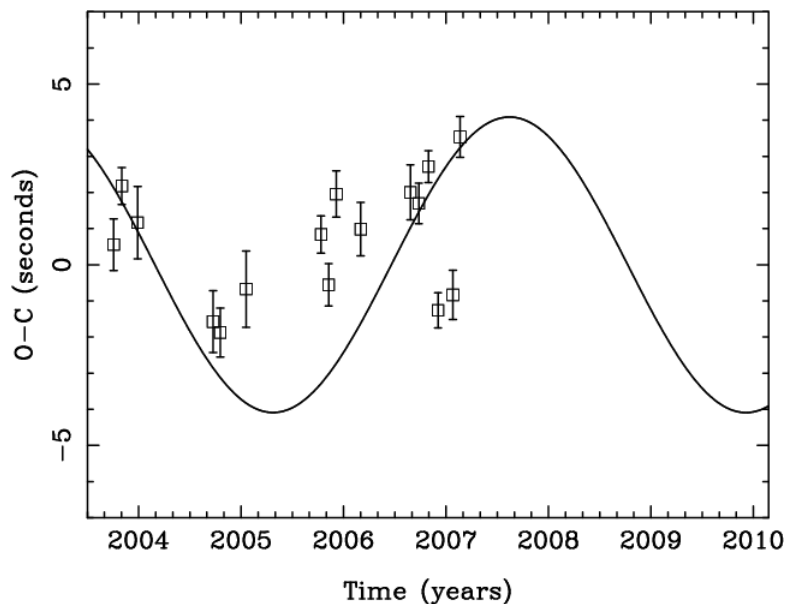


Figure 3.5 O-C diagram for the 271.7 second mode. The solid curve is the fit to the 302s mode in Figure 3.2. See text for discussion.

Model	Mode	
	302s	271.7s
Sine Curve	2.17	23.40
Parabola	1.98	22.83
Straight Line	19.23	15.93

Table 3.3 Reduced Chi squares, χ_r^2 for fits of various models to the data. In each case, the model was fit to the data on the 302s mode, and χ_r^2 calculated as $\chi^2/(\text{\#data points} - \text{\#parameters})$. χ_r^2 was calculated for the 271.7s with these same parameters as $\chi^2/(\text{\#data points})$. This means the entries in the second column are tests of how well the 271.7s mode agrees with the 302s mode. The straight line model consists of the line $y = 0$ and is not fit to the 302s mode. As we have yet to observe a full orbit, the 302s mode can still be well fit with both a sine curve and a parabola, but is clearly inconsistent with a straight line. The 271.7s mode is inconsistent both with the 302s mode and with a straight line.

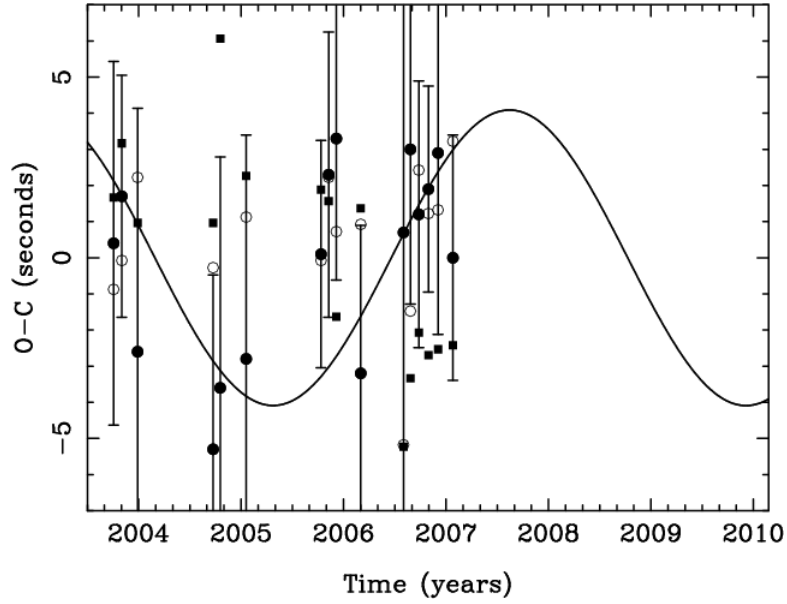


Figure 3.6 Same as Figure 3.5 but for the 198s triplet. The solid squares are for the 197.6s mode, solid circles are the 197.3s mode, while open circles are the 197.1s mode. For clarity, error bars are only shown for the 197.3s mode, but are similar for the other two. The uncertainty in these values is too large to distinguish between a planet and a straight line.

of the central mode. We randomize the phase of all but the 271.7s mode and measure the phase of that mode in 3,000 lightcurves and integrate to determine the central 68% of area under the resulting histogram of measured phase. We show an O-C diagram for the 271.7s mode with error bars calculated in this manner in Figure 3.5, with the fit to the 302s mode overplotted. The data do not match the planet model in many places, but are also inconsistent with scatter around zero, as would be expected from the null hypothesis. Quantitatively, the value of χ_r^2 for each model is 23.4 and 15.9 respectively. Assuming the sizes of the error bars are reasonable, we conclude that some other effect, most likely related to the presence of the other nearby modes of the triplet is affecting the intrinsic phase of this mode at the level of a few seconds. Intriguingly, many of the points do lie close to their predicted values, but currently we can not use this mode to support or refute the planet hypothesis. A table of χ_r^2 for different models is shown in Table 3.3.

In contrast to the 271s triplet, the 198s triplet is composed of three peaks of roughly equal amplitude. We fit these three modes simultaneously, and compute uncertainties with the same method as described above. However, as Figure 3.6 shows, the uncertainty in the phase of each mode is too great to distinguish between the planet model and a straight line indicative of no planet. The other modes on this star are of lower amplitude and therefore not suitable for phase analysis.

3.4 Discussion

Analysis of this star eludes a definitive conclusion. The 302s large amplitude, isolated, easy to measure mode shows a phase variation consistent with the presence of a planetary companion and inconsistent with any other known effect. However, a large number of points in the 271.7s triplet member mode scatter away from their predicted values, presumably due to interference from the observed nearby small amplitude modes. Our claim of detecting a planet is therefore still provisional, and as such we refer to it only as a candidate planet. For brevity in the following discussion we assign the label Maeve to this candidate planet. Further observations will determine whether the O-C diagram is periodic as predicted, while multi-site coverage over a number of nights will provide sufficient temporal resolution to independently measure the phase of each mode in the triplets and better study their behavior.

Any planet around GD66 was either formed from the proto-stellar disk of the main sequence progenitor or created from AGB ejecta that did not escape the system. Livio *et al.* (2005) suggest that planets could form during a binary white dwarf merger, but the low mass of this WD ($0.64 M_{\odot}$) makes this scenario unlikely. If Maeve is coeval with the progenitor star, it must have survived the AGB phase that preceded the white dwarf. Livio & Soker (1984) predict that any planet engulfed in the AGB will either spiral onto the core and be destroyed, or accrete matter and form a close-in brown dwarf companion to the eventual white dwarf. However, at a distance of 2.4 AU the current orbital separation is significantly smaller than the maximum extent of the AGB progenitor of 4–4.5 AU (Pols *et al.* 1998). Similarly, Silvotti *et al.* (2007) quote a separation of only 1.7 AU for the possible planet

around the sub-dwarf star HS2201+2610. For the right range of initial separations planetary migration may be a competition between conservation of angular momentum causing the planet to drift outwards with stellar mass loss (Jeans 1924), and gas drag causing the planet to spiral inward during relatively short periods when the planet is engulfed by the star during a thermal pulse, explaining Maeve’s current position. Alternatively, if this was a multi-planet system the planetary orbits may have become unstable during the mass loss phase (Debes & Sigurdsson 2002) causing Maeve to be scattered into its current small orbit while a second planet was boosted into a higher orbit or ejected from the system.

Although our technique does not provide a measure of the inclination of the orbit to the line of sight, we can use the pulsation properties of the star to guess a value. If we assume the triplets are rotationally split, that the pulsation axis is aligned with the rotation axis, and that the intrinsic power in each mode of the triplet is equal, we can determine the inclination of the rotation axis to the line of sight by comparing the observed relative amplitudes of the peaks in the triplet. This last assumption is the weakest; the two distinct triplets in the data do not have the same relative amplitudes (see Table 3.1). Nevertheless, this is a useful exercise as studies of transiting planets (e.g. Winn *et al.* 2005, 2006) as well as our own solar system agree with the prediction that the orbital plane of a planet is aligned with the plane of rotation of a star to within a few degrees. Comparing the relative amplitudes of the modes in the 271s triplet to the model of Pesnell (1985), Yeates *et al.* (2005) determined an inclination of the pulsation axis to the line of sight of 13° , although their confidence in this value was low and the uncertainty is about 10° . If the plane of rotation of GD66 is aligned with the planetary orbit then the inclination is $\sim 13^\circ$ and the implied mass is $\sim 9.8 M_J$. In contrast, the nearly equal amplitudes of the 198s triplet imply an inclination near 45° and a mass of $4.4 M_J$. The true mass of the planet probably lies between these two values.

3.4.1 Confirmation by Direct Detection

The low luminosity of the WD means that the flux from the planet is comparable with the star in the mid-infrared. Fig. 1.4 shows a simulated spectrum of this system. In the wavelength region covered by Channel 2 of the IRAC photometer

the contrast between the star and a planet can be as low as 10, allowing the flux from the planet to be directly detected with *Spitzer*. Directly detecting the planet is an independent confirmation of the existence of the planet and the information gleaned from comparing this measurement to models will be complementary to that learned from observing the secondary eclipses of transiting planets. In particular, this planet did not experience significant heating from the star (at least for most of its life).

The fundamental limit on the accuracy of IRAC observations is found by taking repeat observations of the primary standards, and is at the level of 1%. This limit is probably due to our uncertainty in the detailed shape of the pixels. The absolute calibration of the photometry is based on comparing the flux in each channel to that predicted based on models of main sequence A stars and is good to better than 2% (Reach *et al.* 2005b). The relative calibration between channels has not been fully assessed but lies somewhere between these two values. We can achieve a lower systematic uncertainty than the relative calibration error by comparing our photometry to that of DAVs with similar temperatures, gravities and surface composition. We will be able to reference the excess in GD66 to the SEDs of a sample of nearly identical stars¹ thus bypassing the uncertainties in the calibration process and approaching the repeatability limit.

There is always the chance that our comparison stars possess undetected planetary companions, spoiling their usefulness as calibrators. To minimize this potential we can select reference WDs with strong planet limits based on extensive O-C monitoring as a comparison², ZZ Ceti (Mukadam *et al.* 2003) and L19-2 (O'Donoghue & Warner 1987).

¹WD atmospheres are well understood and well behaved in the optical and near infrared and are blackbodies in the spectral region of interest. Collisionally Induced Absorption (CIA) is not yet modeled in the infrared (see e.g. Kilic *et al.* 2006a) but the IRAC survey of Mullally *et al.* (2007) shows that this effect is not a concern for WD temperatures above 6000 K.

²Another DAV, G117-B15A, has even better planet limits based on this same technique, but unfortunately is too close to a 10th magnitude star which would saturate the detector in the required frame time.

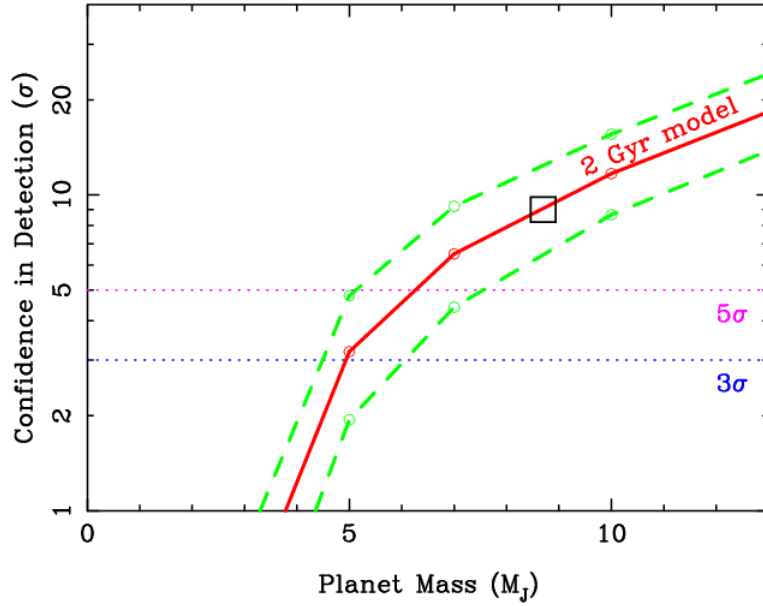


Figure 3.7 Ability to detect excess flux in Channel 2 as a function of mass assuming 1% photometry. The minimum mass of the planet is $2 M_J$, while the mass based on the inclination argument (see text) would be $\approx 9 M_J$ (large square). The uncertainty in the model predictions is shown by the dashed lines. The dotted lines indicate 3σ and 5σ confidence levels.

Model Uncertainties

We can determine the mass of the planet by comparing the magnitude of the excess to planet models. The luminosity of a planet is a function of both its mass and age. The age of the system is simply the cooling age of the white dwarf plus the progenitor lifetime, ≈ 2 Gyr. Despite the success of models (Burrows *et al.* 2003) they still have considerable uncertainties, partly due to the paucity of observational tests.

For brown dwarf stars (BDs), Patten *et al.* (2006) found that models over-estimated the flux in the $4.5 \mu\text{m}$ band by a factor of 1.5–3.0 and attributed the observed deficit to a stronger than expected CO feature. We expect this deficit to decline with decreasing temperature and be small for the mass region of interest. Burrows *et al.* (2006a) found good agreement between observations of secondary transits of planets from IRAC, IRS and MIPS (Charbonneau *et al.* 2005; Deming

et al. 2006, 2005) and atmosphere models incorporating redistribution of flux from the day to night side of the planet. Models accurately predict the planetary flux for these unusual systems in the mass region of interest, indicating the flux overestimate for BDs is not applicable to planets.

The maximum radius of the progenitor AGB was ≈ 4.5 AU and it is possible that the planet was engulfed in the stellar envelope during some portion of the late stages of stellar evolution approximately 500 Myr ago, and reheating of the outer planetary atmosphere is a concern. A hotter planet would lead to a larger flux and an overestimate of the planetary mass. However it is likely that heat flux did not penetrate deeply into the envelope (a medium-rare planet), and the planet probably cooled rapidly after the AGB dissipated. It is of course possible that the planet was formed from stellar material that was not dissipated into the planetary nebula (Jura & Turner 1998), in which case the planet would be < 500 Myr old and therefore considerably hotter and brighter.

Assuming, as above, that the age of the system is 2 Gyr, and taking into account the concerns listed above, the flux from the planet can be expected to be somewhere in the range of what is predicted for a 1.5 and 2.5 Gyr old planet. For Fig. 3.7 we use these models to calculate the excess flux over the WD atmosphere that different planets would produce and our confidence level in that detection. For example we could detect a $6 M_J$ planet with between 3 and 7σ or a $9 M_J$ planet with $7\text{--}13\sigma$. The uncertainty in the mass of the detected planet due to the models will be $\sim 2 M_J$.

3.5 Conclusion

We present evidence of a candidate planet around the white dwarf GD66. The changing arrival times of the 302s mode of this pulsator cannot be explained by any known effect except the presence of a planet in a 4.62 year orbit with $m_p \sin i = 2.22 M_J$. Our confidence in the detection of this planet is tempered by the absence of a second, isolated, independent pulsation mode which would confirm the hypothesis. Confirmation will come from either observing a full orbit of the planet, or by direct detection in the infrared.

Table 3.4. Journal of Observations

Run	Month	Date	Start time	Exp	Run Length
A0726	Oct03	25 Oct 03	09:04:23	10	3hr 32m 40s
A0729		27 Oct 03	09:42:27	10	0hr 31m 20s
A0730		27 Oct 03	10:58:12	10	1hr 30m 30s
A0733		28 Oct 03	06:52:39	10	5hr 25m 40s
A0738		29 Oct 03	11:08:30	10	1hr 16m 10s
A0742		31 Oct 03	09:32:33	10	2hr 58m 50s
A0746		1 Nov 03	08:17:12	10	1hr 06m 20s
A0755	Nov03	19 Nov 03	07:29:14	5	3hr 11m 20s
A0767		22 Nov 03	05:11:34	5	4hr 06m 30s
A0789		29 Nov 03	06:08:55	5	3hr 20m 50s
A0793		30 Nov 03	06:49:05	5	5hr 59m 50s
A0795		1 Dec 03	05:44:42	5	3hr 19m 05s
A0835	Jan04	20 Jan 04	03:26:37	5	3hr 15m 20s
A0838		21 Jan 04	03:09:07	5	3hr 32m 50s
A0843		26 Jan 04	03:00:45	5	1hr 57m 15s
A0935	Oct04	15 Oct 04	09:10:52	5	3hr 15m 35s
A0937		16 Oct 04	07:31:23	5	4hr 51m 50s
A0943		18 Oct 04	09:14:29	5	2hr 35m 35s
A0946	Nov04	19 Oct 04	08:29:49	5	3hr 42m 45s
A0948		9 Nov 04	05:44:47	5	4hr 14m 00s
A0951		10 Nov 04	06:38:03	5	5hr 45m 15s
A0953		11 Nov 04	05:33:30	5	2hr 23m 20s
A0957		20 Nov 04	09:36:40	5	2hr 44m 25s
A0985	Feb05	7 Feb 05	01:45:43	5	4hr 09m 00s
A0991		13 Feb 05	01:35:11	5	4hr 02m 25s
A0992		14 Feb 05	01:28:34	5	3hr 17m 00s
A1104	Aug05	31 Aug 05	10:12:31	5	1hr 28m 40s
A1109		2 Sep 05	10:44:11	10	1hr 20m 30s
A1126	Oct05	30 Oct 05	07:23:36	5	5hr 10m 10s
A1129		31 Oct 05	09:57:13	5	2hr 29m 40s
A1132		1 Nov 05	07:13:27	5	5hr 11m 45s
A1141		4 Nov 05	09:29:57	5	1hr 24m 50s
A1143		5 Nov 05	06:16:13	10	6hr 31m 20s

Table 3.4—Continued

Run	Month	Date	Start time	Exp	Run Length
A1148		7 Nov 05	07:33:14	10	5hr 08m 20s
A1152		9 Nov 05	07:08:37	5	2hr 30m 05s
A1155		10 Nov 05	08:58:19	10	0hr 33m 30s
A1157		11 Nov 05	07:02:17	10	5hr 41m 00s
A1160		12 Nov 05	05:53:19	10	6hr 21m 10s
A1161		13 Nov 05	06:14:02	10	2hr 57m 30s
A1162		14 Nov 05	09:36:40	10	3hr 09m 50s
A1164	Nov05	29 Nov 05	05:30:51	5	4hr 19m 05s
A1173		2 Dec 05	05:04:36	5	4hr 17m 35s
A1182		5 Dec 05	07:00:46	5	3hr 40m 15s
A1185		6 Dec 05	06:32:07	5	3hr 02m 55s
A1199	Dec05	28 Dec 05	03:21:45	5	4hr 00m 35s
A1202		29 Dec 05	03:26:21	5	4hr 09m 50s
A1206		30 Dec 05	05:22:53	5	2hr 54m 30s
A1208		31 Dec 05	04:26:36	5	3hr 41m 00s
A1212		3 Jan 06	04:18:29	5	3hr 50m 20s
A1280	Feb06	6 Mar 06	02:16:02	5	2hr 33m 25s
A1283	Mar06	25 Mar 06	02:32:46	5	3hr 09m 45s
A1287		26 Mar 06	02:18:55	5	2hr 27m 15s
A1293		30 Mar 06	02:00:21	10	2hr 59m 20s
A1296		31 Mar 06	01:48:17	10	3hr 30m 10s
A1354	Aug06	24 Aug 06	10:04:43	5	1hr 36m 50s
A1357		26 Aug 06	10:07:52	10	1hr 43m 40s
A1362		29 Aug 06	09:45:40	5	2hr 03m 35s
A1367	Sep06	18 Sep 06	09:17:53	5	2hr 48m 45s
A1371		19 Sep 06	08:41:07	5	3hr 27m 20s
A1373		20 Sep 06	08:45:03	5	3hr 19m 55s
A1378		21 Sep 06	08:39:05	5	2hr 48m 45s
A1381		22 Sep 06	08:43:06	5	3hr 18m 35s
A1383	Oct06	17 Oct 06	06:45:07	5	5hr 35m 10s
A1385		18 Oct 06	06:35:20	5	5hr 57m 00s
A1388		20 Oct 06	06:34:10	5	5hr 52m 00s
A1390		21 Oct 06	06:32:37	5	5hr 57m 45s

Table 3.4—Continued

Run	Month	Date	Start time	Exp	Run Length
A1393		23 Oct 06	06:33:09	5	5hr 55m 00s
A1395		24 Oct 06	06:34:43	5	2hr 02m 00s
A1397	Nov06	21 Nov 06	04:55:45	5	7hr 49m 50s
A1399		22 Nov 06	05:14:51	5	7hr 23m 50s
A1402		23 Nov 06	08:11:39	5	4hr 30m 50s
A1405		24 Nov 06	08:51:05	5	3hr 56m 10s
A1407		25 Nov 06	07:07:26	5	5hr 46m 10s
A1409		26 Nov 06	05:31:19	5	1hr 48m 00s
A1410		26 Nov 06	07:41:24	5	4hr 46m 25s
A1413	Dec06	20 Dec 06	08:20:19	10	3hr 08m 00s
A1422		23 Dec 06	04:53:13	10	1hr 59m 00s
A1424		26 Dec 06	04:50:26	5	4hr 00m 50s
A1427		27 Dec 06	06:03:28	5	3hr 06m 25s
A1430		28 Dec 06	03:31:07	5	1hr 37m 05s
A1434		1 Jan 07	04:42:10	5	4hr 38m 25s
A1450	Feb07	15 Feb 07	02:04:39	10	2hr 13m 10s
A1452		16 Feb 07	01:48:09	5	0hr 34m 50s
A1453		16 Feb 07	02:27:52	5	4hr 14m 05s
A1459		18 Feb 07	01:16:48	5	4hr 59m 55s
A1461		19 Feb 07	01:37:32	5	4hr 25m 20s
A1464		21 Feb 07	01:39:56	5	5hr 05m 30s
A1467		22 Feb 07	01:24:22	5	4hr 02m 25s
A1472	Mar07	15 Mar 07	01:44:13	5	5hr 36m 25s
A1474		16 Mar 07	01:45:01	5	3hr 05m 10s
A1476		17 Mar 07	01:42:47	5	5hr 15m 55s
A1480		18 Mar 07	01:46:56	5	4hr 47m 40s

Note. — Runs Aug05 and Feb06 are very short, do a poor job of resolving the modes and are excluded from our analysis.

Chapter 4

Limits on Planets around Other White Dwarves

4.1 Motivation

In chapter 3, we present evidence for a candidate planet around one of our WDs, GD66. Here we present limits on the presence of companions around the other stars in our sample. Over the 4 years of monitoring GD66, we also observed a group of similar stars with a range of magnitudes, pulsational properties and data coverage. We present these limits not as an exercise in extracting the last possible value from our data, but because the absence of detectable planets is as scientifically interesting as their discovery. These results will help us test theoretical predictions of the fate of planets after the star dies.

Surveys for planets around WDs offer insight into planetary behaviour unavailable through other searches. Despite forming from a wide mass-range of main sequence stars, WDs are a remarkably homogeneous group in terms of mass and composition. Our method of searching for evidence of companions in changing arrival times of pulsations is sensitive to planets not currently detectable with other techniques (§1.5 has a full discussion). The existence, frequency, and orbital parameters of planets around WDs will provide clues on the fate of planets (including the

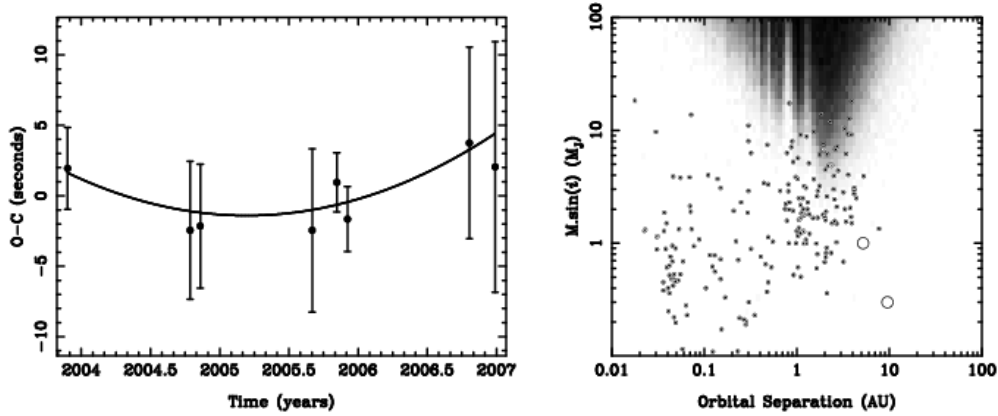


Figure 4.1 **Left:** O-C diagram for one star in our sample, WD0018+0031. Each point is the measured phase of the mode listed in Table 4.1 for the combination of runs from a given month. The value shown is the difference between the observed and expected arrival time of the pulse (i.e. the phase) for that month. The solid line is the best fit parabola to the data. As the table shows, the curvature is zero within the measured uncertainties for many of these stars. **Right:** Limits on planets that can be placed around this star using the O-C diagram at left as calculated by the Monte Carlo technique discussed in the text. The filled circles are planets (and presumably some BDs) discovered with the radial velocity method, while the open circles indicate the location of Jupiter and Saturn in our own solar system. The shaded area indicates the region of parameter space where planets would have been detected had they existed around this star, with the white area indicating a near zero probability of detecting a planet and progressively darker shades of grey indicating increasing probability of planet detection.

Earth) when their parent star dies as a red giant.

Livio & Soker (1984, and references therein) looked at what would happen to a hypothetical gas giant planet engulfed in the envelope of the evolved star. They found that gas drag causes the planet to spiral inward toward the core. Below a critical mass, the outer layers of the planet are stripped of material causing the planet to evaporate. However, above this threshold accretion processes win out over evaporation and the planet mass increases. The end state of the system is then a white dwarf and a low mass companion (either a brown dwarf or a low mass star) in a very short-period orbit (\sim hours). They suggested that this process might explain cataclysmic variables, WDs that accrete from low mass companions with

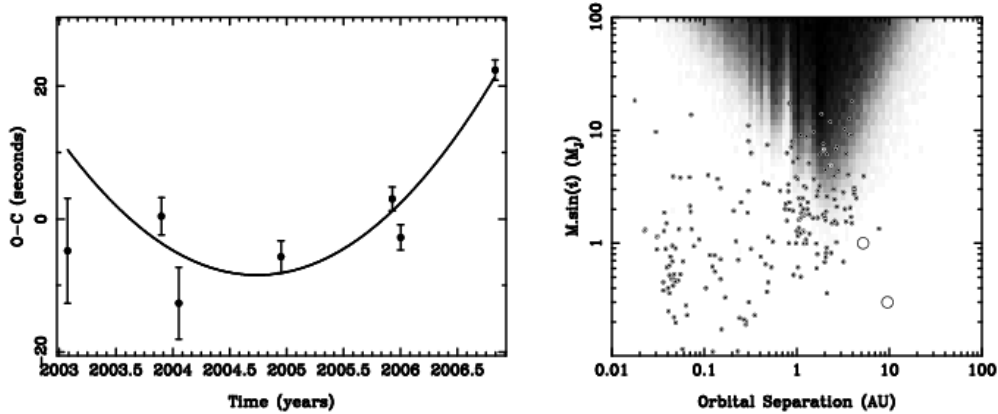


Figure 4.2 Same as Figure 4.1 for another white dwarf, WD0111+0018. These data is considerably sparser because WD0111 is a 19th magnitude object and can only be observed in excellent conditions.

short-period orbits.

A planet just outside the radius of the red giant will raise large tides on the surface of the star, bleeding energy from the planet's orbit and causing it to spiral in towards the star (Rasio *et al.* 1996). The effect of this interaction falls off with radius to the 8th power and has an insignificant effect on planets at greater distance. For these stars the planet must drift outward with mass loss in order to conserve angular momentum as described in §1.2.2. Gas drag caused by interaction with the strong stellar wind will act to counter this outward drift. However, Duncan & Lissauer (1998) show that in our own solar system, the amount of eject solar material that the outer planets will interact with is less than 1% of their (the planets') mass, and will have a very small effect on their final orbital separation. Burleigh *et al.* (2002) showed that planetary orbits do not become unbound due to mass loss, and Duncan & Lissauer demonstrated that the outer planets of our solar system would not develop instability due to orbital interaction on timescales of a billion years after the sun becomes a white dwarf. However instability can occur in systems with a larger mass progenitor that loses more than half its mass on becoming a WD.

The picture painted by this brief review of theory (and as first suggested by Farihi *et al.* 2005a) is that the distribution of companions to WDs bifurcates into a population of close-in BDs, and a more distant population of relatively unscathed

planets. This picture is consistent with the properties of known WD plus BD binaries, GD165-b is 120 AU away from GD165-a (Becklin & Zuckerman 1988) while WD0137-349-b (Maxted *et al.* 2006) is separated by 0.002 AU. (The other confirmed binary, GD1400-b (Farihi & Christopher 2004) has an unknown separation but constrained to be less than 12 AU). Many cataclysmic variable systems are believed to consist of a WD and a sub-stellar mass companion in very short (~ 1 hour) orbits, however, it is difficult to place an upper mass of the companion in these systems. Moreover, the companion is losing mass by accretion onto the primary, and so is possibly the remnant of a main sequence star and less interesting from a planetary perspective.

However, nature need not be bound to this simple scenario. As Debes & Sigurdsson (2002) suggest, the orbits of multi-planet systems could become unstable during mass loss. As the mass of the central star decreases, and the orbits drift outward, the orbital periods of two planets will pass through resonances where the ratio of the periods can be expressed as the ratio of small integers. In resonance, the gravitational influence of interplanetary forces is amplified and can perturb the orbits resulting in a close encounter between the planets which would likely eject one planet from the system, while pushing the other closer to the parent star. Also, as suggested in the previous chapter, for a planet with the right initial separation the evolution of its orbit could be a competition between outward drift to conserve angular momentum and inward spiral due to gas drag during the relatively brief times when the star engulfs the planet during a short-lived thermal pulse.

Predicting the fate of planets is at best speculative, mainly because the final stages of stellar evolution occur rapidly, are difficult to study, and hence poorly understood. Mass loss may be a slow gentle affair, or more turbulent, erratic and dangerous for planets. Previously unthought-of effects may also play a dominant role. For example, although the migratory influence of a proto-planetary disk was first calculated by Goldreich & Tremaine (1980), the effect of orbital migration (Lin *et al.* 1996) in producing hot Jupiters was not widely anticipated.

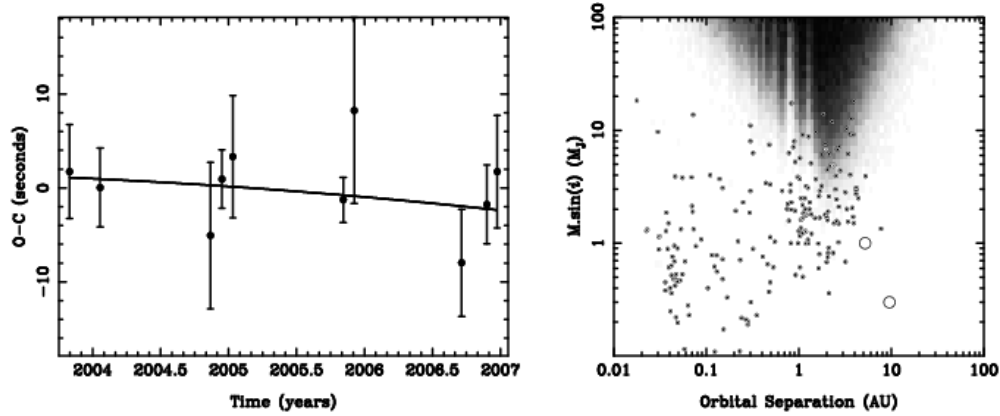


Figure 4.3 WD0214–0823

4.2 The Survey

Kleinman *et al.* (2004) published a number of candidate DAVs with spectra taken by the Sloan Digital Sky Survey (Adelman-McCarthy *et al.* 2006). A follow up survey by Mukadam *et al.* (2004a) and as presented in Chapter 2 confirmed 46 of these candidates to be pulsators, although not all were of the stable hDAV variety. We selected our targets from these two papers as well as known DAVs published in the literature (see Fontaine *et al.* (2003) and Bergeron *et al.* (1995) for a list of DAVs known at the start of this survey). The ideal DAV for this survey would exhibit a number of isolated, relatively low amplitude (0.5–2%) modes. Multiplet, or otherwise closely-spaced modes are difficult to resolve in single-site data and interference between the unresolved modes makes accurately measuring the phase difficult. However, the ideal DAV is difficult to find, and most of our stars only exhibited one isolated mode with amplitude $\gtrsim 0.5\%$.

Our observations were conducted using the Argos frame-transfer CCD photometer (Nather & Mukadam 2004) on the 2.1m Otto Struve telescope at McDonald Observatory. We observed each star with exposure times between 5 and 15 seconds for periods of between 2 and 8 hours. Because Argos is a frame transfer camera, no time is lost to chip readout. Lightcurves were extracted from the images as described in Chapter 3. Briefly, we dark subtracted and flat-fielded our images before performing aperture photometry on the white dwarf and one or more reference stars

Table 4.1. Modes used to construct O-C diagrams

Starname	Period (sec)	Amplitude %	T ₀ (bjed)	\dot{P}
G117–B15A	215.1973888(12)	1.9	2442397.9194943(28)	$-1.07(49) \times 10^{-13}$
G185–32	370.2203552(55)	0.1	2453589.6557652(39)	$-0.5(1.0) \times 10^{-13}$
G238–53	122.1733598(38)	0.2	2453168.6334690(37)	$-5.1(2.4) \times 10^{-13}$
GD244	202.9735114(40)	0.4	2452884.8712551(31)	$-0.7(2.3) \times 10^{-13}$
WD0018+0031	257.777859(13)	0.6	2452962.6358455(41)	$9.4(9.2) \times 10^{-13}$
WD0111+0018	292.9445269(90)	1.9	2452963.7174240(44)	$4.01(50) \times 10^{-12}$
WD0214–0823	262.277793(12)	0.6	2452941.7929372(37)	$-0.8(7.5) \times 10^{-13}$
WD0913+4036	172.605159(15)	0.3	2453024.8275265(47)	$9.6(9.8) \times 10^{-13}$
WD1015+0306	254.9184466(73)	0.6	2453065.6152126(47)	$8.5(4.4) \times 10^{-13}$
WD1354+0108	198.3077098(14)	0.6	2452665.9507137(33)	$-5.3(7.8) \times 10^{-14}$
WD1355+5454	323.9518703(72)	2.2	2453082.8582370(41)	$1.06(51) \times 10^{-12}$
WD1724+5835	335.536871(16)	0.6	2453139.8477229(37)	$1.41(97) \times 10^{-12}$
WD2214–0025	255.1524057(36)	1.3	2452821.8521780(35)	$-0.4(2.1) \times 10^{-13}$
WD2214–0025	195.1406388(65)	0.4	2452821.8513303(35)	$3.2(3.4) \times 10^{-13}$
R548	212.76842927(51)	0.4	2446679.833986	$1.2(4.0) \times 10^{-15}$

Note. — T₀ is the time of the arbitrarily defined zeroth pulse and is given in units of barycentric corrected day. Data on R548 comes from Mukadam *et al.* (2003) who do not provide a value for uncertainty in T₀. We do not claim statistical significance for the measurement of \dot{P} for any star.

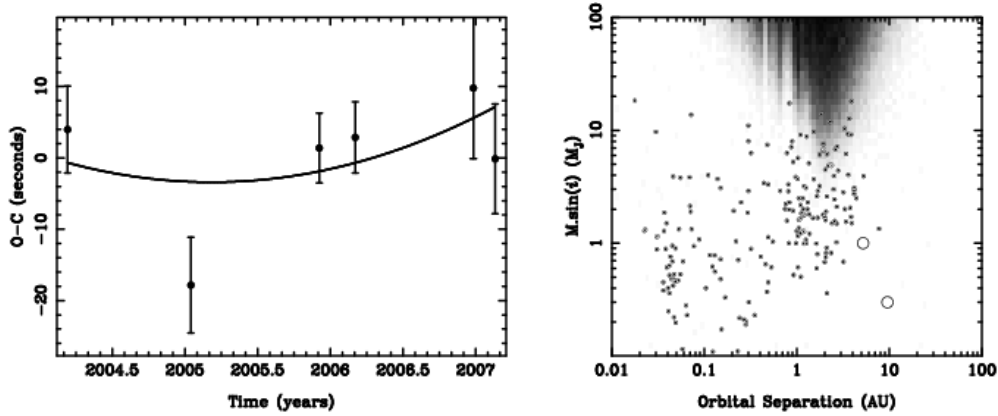


Figure 4.4 WD0913+4036. The second data point consists of 3 short, widely spaced datasets and should be considered untrustworthy.

using *wphot* in IRAF. We next divided the flux from the target in each frame by the flux from the reference stars to remove that effects of cloud or other transparency variations. Points heavily affected by cloud were removed by hand, and we fitted and removed a 2nd order polynomial to account for differential extinction. Finally, we converted our times of observation from UTC to barycentric Julian ephemeris date using the method of Stumpff (1980).

Before measuring the phase we must first accurately determine the period. We proceed by fitting a sine curve at the appropriate period using the Levenberg-Marquardt non-linear least squares technique (Bevington 1969). The measured period, P_o , will differ from the true period, P , by an amount δP , that will hopefully be $\lesssim \Delta P$, the measured uncertainty in P_o . If we project sine curves with periods P and P_o into the future they will slowly fall out of phase, and then back into phase again. When the phases match up, the shorter period will have completed one more extra cycle than the longer period. When measuring the period of a lightcurve with large gaps it is easy to measure the wrong period simply because one doesn't see what the signal is doing during the gaps and choose an incorrect period which fits the available data well.

In Fourier space, this problem manifests itself as the alias pattern. The Fourier Transform (\mathcal{FT}) of an uninterrupted finite lightcurve of a single sine curve

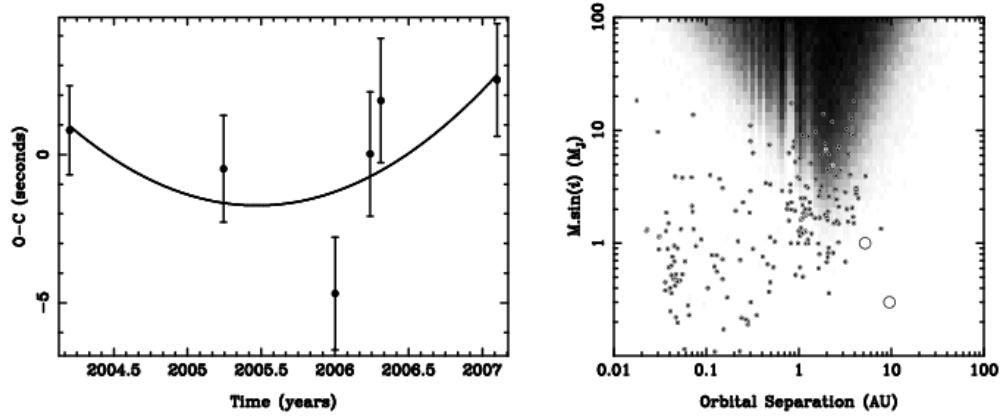


Figure 4.5 WD1015+0306

is a sinc function¹. Two finite lightcurves separated by a gap will show a series of narrower alias peaks inside the envelope of the sinc envelope. Each alias peak corresponds to periods that give an integer difference in the number of cycles in the gap (see Figure 4.6).

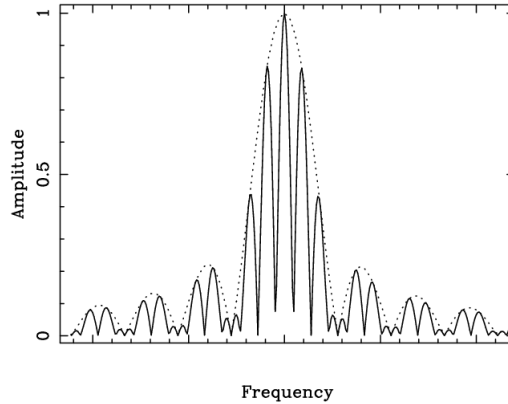


Figure 4.6 Aliases in an \mathcal{FT} . The dotted line shows the \mathcal{FT} of a 1 hour run. The solid line is the \mathcal{FT} of two similar data sets 30 hours apart. To reliably bridge the gap in this data set, the uncertainty in period (or frequency) of the mode based in a single data set must be less than the spacing between alias peaks.

To avoid mis-measuring the period we endeavoured to keep the gap between

¹A sinc function is defined as 1 for $\theta = 0$ and $\frac{\sin \theta}{\theta}$ otherwise.

data sets very much shorter than the “single cycle error time”, or the time it would take the period $P_o - \Delta P$ to accumulate an extra cycle over P_o . If we label the epoch (the number of cycles of a sine curve of period P since some arbitrary time), E , then the single cycle error time is the time taken until

$$E_{P_o - \Delta P} = E_{P_o} + 1 \quad (4.1)$$

If the the number of cycles since a time t , is $E_P = t/P$, then the above equation becomes

$$\frac{t}{P_o - \Delta P} = \frac{t}{P_o} + 1 \quad (4.2)$$

$$\Rightarrow t \left(\frac{1}{P_o - \Delta P} - \frac{1}{P_o} \right) = 1 \quad (4.3)$$

$$\Rightarrow t = \frac{P_o(P_o - \Delta P)}{\Delta P} \quad (4.4)$$

To avoid fitting the wrong alias we design our observational strategy such that the gap between observations is always less than this value. In Fourier space, the uncertainty in period (or frequency) must be less than the spacing between alias peaks in the transform.

For the hDAVs observed with Argos, 8 uninterrupted hours of data are typically enough that a gap of 24 hours introduces an uncertainty of $\lesssim 10\%$ of a cycle. A second run the following (or indeed the previous) night gives a single cycle error time of ~ 1 week, a third run within that week extends the window to a month. By ensuring our observations are sufficiently close together we can be confident of always measuring the period of the correct alias.

Having established the period we next measure the phase of each lightcurve by performing a least squares fit at the best fit period and measuring the time of first positive crossing of a sine curve. The phase is expressed in seconds between 0 and P_o . The assumption of a least squares fit is that points are scattered in a

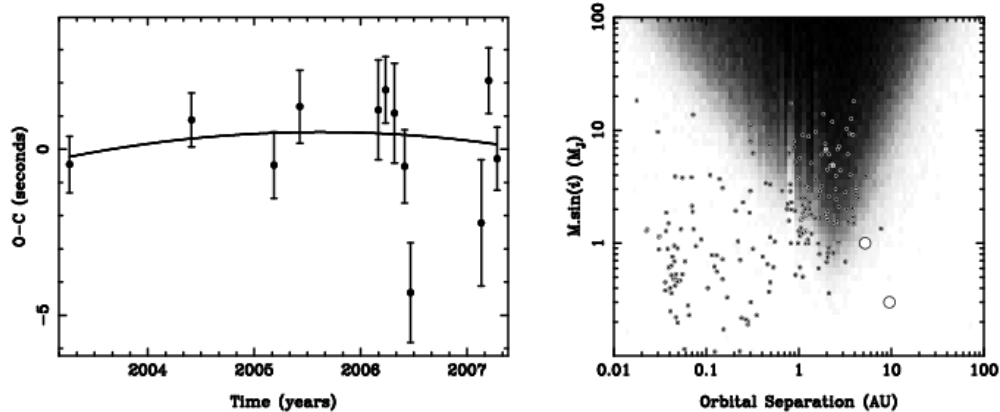


Figure 4.7 WD1354+0108

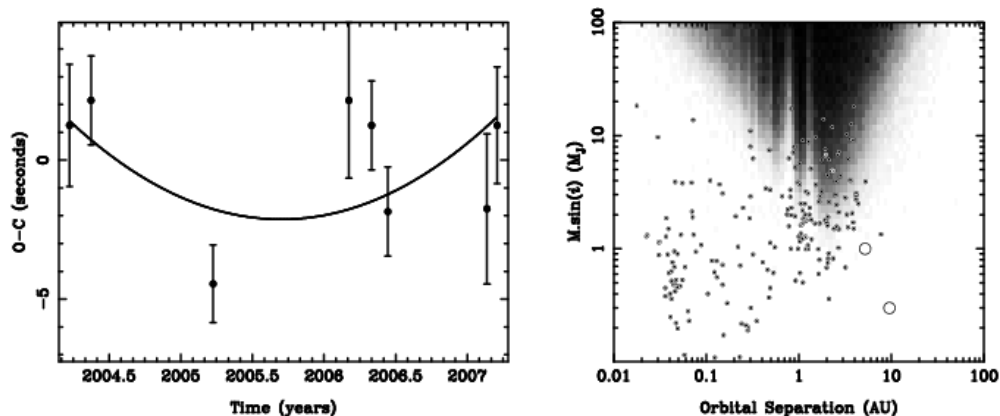


Figure 4.8 WD1355+5454

Gaussian distribution² about their true value so the uncertainty in any measured parameter declines with the square of the number of data points. By combining data from different nights in a given month we can decrease the uncertainty at the expense of temporal resolution. As we are looking for signals with timescales of years, this is an acceptable trade off. As the amount of data increases, we repeat

²This assumption is a valid one. The uncorrelated noise in a lightcurve is well described by a Gaussian distribution, while correlated noise (mostly due to cloud or transparency variations) is not. However, the joy of differential photometry is that most atmospheric effects are removed by dividing by a comparison star. Thus while the assumption is not strictly true (and no assumption ever is), it passes the more important test of being *useful*.

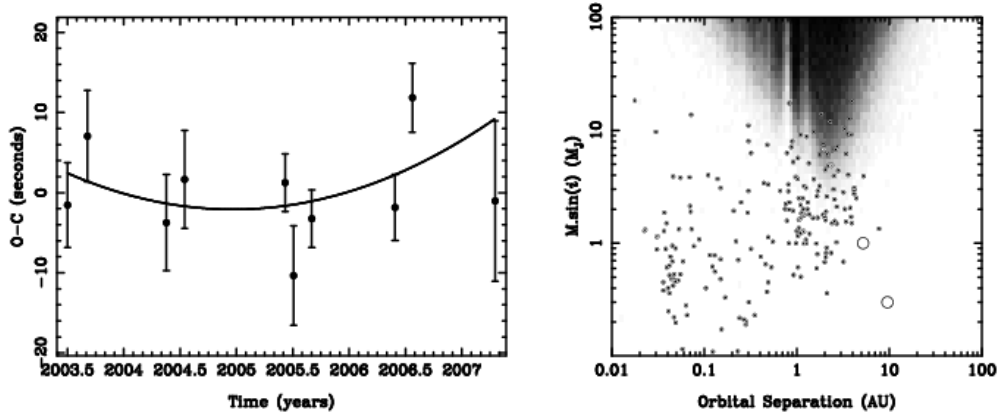


Figure 4.9 WD1724+5835

the procedure, refitting the best period to the enlarged data set and performing a least squares fit at that period.

4.3 Results

Chapter 3 presents a candidate planet discovered in this survey. In this chapter, we present limits on companions to the other survey stars. The fundamental limit on our ability to detect planets is set by the scatter in the O-C diagram. Other factors which affect this limit include the timespan and sampling pattern of the data. We perform a Monte Carlo analysis to estimate the region of the mass–orbital separation plane in which planets are actually detectable around each star. We randomly choose a planet mass, orbital separation, eccentricity, and other orbital parameters and calculate the effect this planet would induce on the O-C diagram of a $0.55 M_{\odot}$ white dwarf. We then sampled this O-C diagram with the same observing pattern and error bars as our actual data for each star and fit the resulting O-C diagram with a sine curve and a parabola. If either the amplitude of the sine curve or the curvature of the parabola were measured with 3σ confidence, the hypothetical planet was determined to be detected. We repeated this process 10^6 times for each star and drew a shaded relief map indicating the percentage of the time a planet with a given mass and orbital separation was detected with either technique to 3σ ,

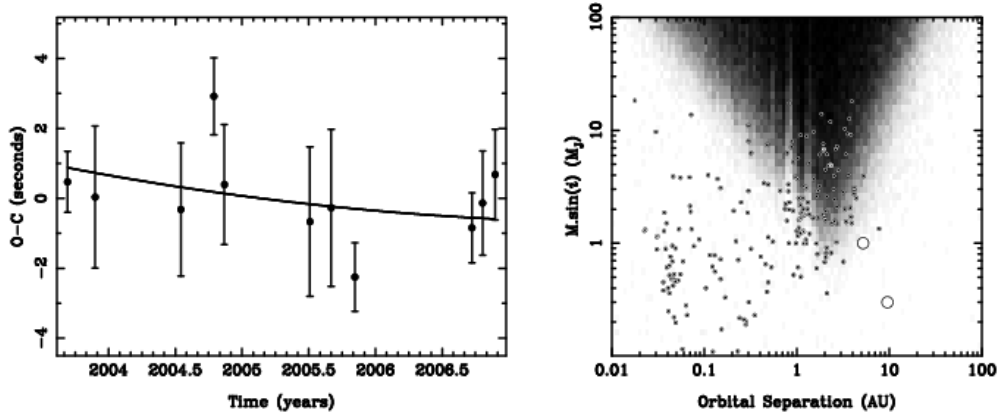


Figure 4.10 WD2214–0025

with dark shades indicating near 100% detection efficiency, and white indicating regions where planets were unlikely to be detected. As can be seen in the figures, the annual sampling pattern means that planets with orbital periods of 1 (Earth) year are difficult to detect, resulting in the weak limits for planets at separations of slightly less than 1 AU. Table 4.2 shows the estimated progenitor masses for this sample.

4.3.1 Notes on Individual Stars

WD0111+0018.— At $g = 18.6^{\text{th}}$ magnitude³, this is our faintest target and correspondingly has our weakest limits. Also, because it could only be observed under the best conditions the data coverage is quite low. The apparently impressive curvature in this O-C diagram is entirely due to the last data point, which is probably spurious and should be treated with considerable skepticism. See Figure 4.2.

WD1354+0108.— This bright (16.4^{th} magnitude) star has a baseline stretching back to early 2003 and some of the highest accuracy time measurements, and as a result has the best limits on planets for stars without archival data. A Jupiter-mass planet at 5 AU is likely detectable. See Figure 4.7.

WD2214-0025.— This is the only star in the sample for which reasonable O-C

³Magnitudes in this chapter are based on the SDSS system unless otherwise noted.

Table 4.2. Initial and Final Masses

Star	Initial Mass (M_{\odot})	Final Mass (M_{\odot})	Age (Gyr)
G117–B15A	1.69(30)	0.595(29)	3.2(1.7)
G185–32	2.10(32)	0.638(32)	2.40(65)
G238–53	1.36(26)	0.562(25)	5.0(4.6)
GD244	1.85(32)	0.611(32)	2.7(1.2)
R548	1.65(29)	0.591(28)	3.3(1.9)
WD0018+0031	1.45(27)	0.571(25)	4.3(3.2)
WD0111+0018	3.33(34)	0.769(32)	1.86(69)
WD0214–0823	1.40(27)	0.566(25)	4.8(4.0)
WD0913+4036	1.17(26)	0.542(25)	7.7(6.1)
WD1015+0306	2.62(33)	0.693(32)	2.02(63)
WD1354+0108	1.79(32)	0.605(32)	2.9(1.4)
WD1355+5454	1.54(27)	0.580(25)	3.8(2.4)
WD1724+5835	1.26(26)	0.551(25)	6.3(4.2)
WD2214–0025	3.75(35)	0.814(32)	1.91(76)

Note. — Estimated ages, initial and final masses for the sample. The algorithm used is discussed in § 6.2.4, and the various caveats are noted there.

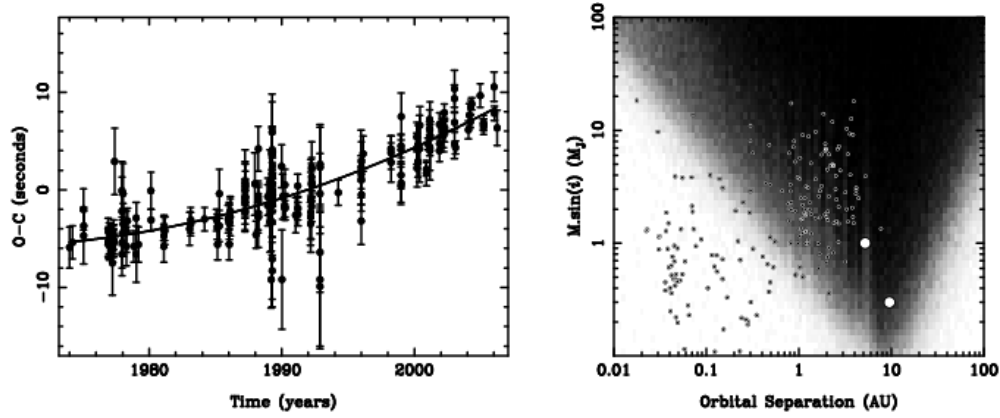


Figure 4.11 G117–B15A

diagrams were obtained for two modes. The O-C diagram shown is the weighted sum of the O-C values for these two individual modes. See Figure 4.10.

G117-B15A.— Also known as WD0921+354. 30 years of archival data comes from Kepler *et al.* (2005), although some of the more recent data in that work was taken in conjunction with this project. Where data did not come from our observations we used the O-C value quoted in their Table 1. With this timebase, the curvature caused by the change in period due to cooling becomes evident. This cooling effect is removed from the data before performing the Monte Carlo simulation. The limits on long-period planets placed around this star are among the best constraints placed around any stellar object by any technique. See Figure 4.11.

G185-32.— Also known as WD1935+279. The point from the early 90’s comes from archival data from the Whole Earth Telescope (Xcov8, Castanheira *et al.* 2004). This extra point gives a long baseline, but the poor coverage in our survey reduces the sensitivity. See Figure 4.12.

R548.— Also known as ZZ Ceti and WD0133-116. The entire data set comes from Mukadam *et al.* (2003). See Figure 4.15.

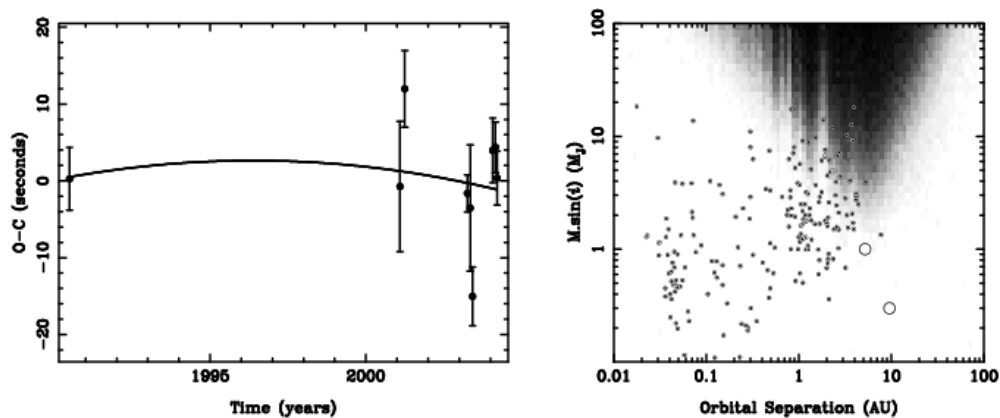


Figure 4.12 G185-32

4.4 Discussion and Conclusion

Mullally (2003) discussed the projected success of this project. We expected scatter of between 0.1 – 1.0 seconds and limits on \dot{P} corresponding to Jupiter-mass analogues around a sample of 30 stars. As can be seen from the figures in this chapter, we fell short in all three predictions. The sample size is only 15 stars, uncertainties of 1s were achieved for only a very small number of points, and while the lowest mass planet detectable is typically of the order of a Jupiter mass, for most stars the upper mass limit on planets at 5 AU (Jupiter’s distance from the sun) are typically 5–10 M_J .

The standard bearer of blame for an observational project is the weather. Anecdotally however, conditions over the extended period of this project were not significantly worse than normal for McDonald Observatory. A number of runs suffered from exceptionally cloudy conditions, but others were unusually clear.

The original plan⁴ was to spend just 9 hours per star per year for 30 stars. The reality is that we devoted many more hours to fewer stars and yet the uncertainties in our measurements were still much greater than predicted. To understand the discrepancy between predicted and actual success, it is informative to look at our timing measurements of a sample star, WD1354+0108. At 16.4th magnitude

⁴As described in §4.2.1 of the 2002 proposal to the NASA Research on Solar Systems grant.

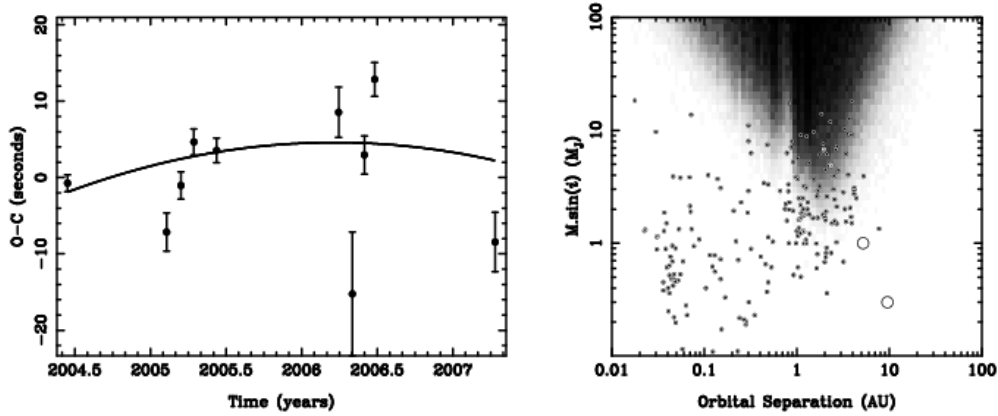


Figure 4.13 G238-53

this star is one of the brightest in our sample. Its pulsation spectrum is nearly mono-periodic, with a single short-period mode at 198s of amplitude 0.5%. A single 4 hour run on this star yields an average uncertainty in the measured time of arrival of the pulsation of approximately 1.4s, depending on the observing conditions. The uncertainty scales inversely with the square of the observing time, so 8 hours of data is required to reduce the uncertainty to 1.0s. This can easily be achieved by combining runs from separate nights (although the scaling breaks down for short runs less than ≈ 90 minutes). However, to achieve the projected 0.3s uncertainty requires an unfeasible 84 hours of data. Our practical limits on short-period planets around one of our best candidates is set close to our most conservative predictions at the start of the project. With larger uncertainty in each point, our ability to detect or constrain \dot{P} also declines, explaining our larger than expected limits on long-period companions.

For fainter stars, the flux declines by a factor of 2.5 per magnitude decrease in brightness, increasing the root mean squared (rms) scatter by 0.63 and a corresponding increase in the timing uncertainty. Another mono-periodic pulsator, WD1355+5454, is 2.2 magnitudes fainter so we would expect a timing uncertainty of 3.8s for a mode of similar amplitude in a four hour run. The mode on WD1355 is approximately 4 times larger in amplitude, reducing our expected uncertainty by a factor of two to 1.9s, in close agreement with the typical 2.1s observed uncertainty. 16 hours of data is therefore required on this object to reduced the timing uncer-

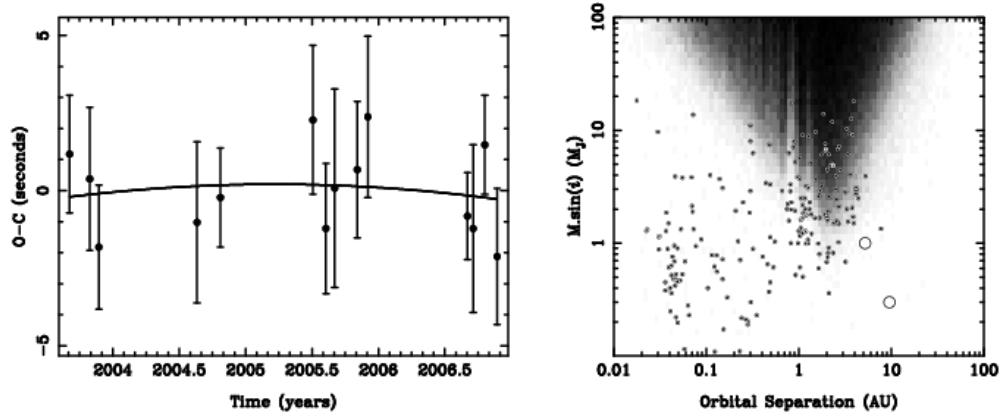


Figure 4.14 GD244

tainty to 1.0s. We therefore need more than 9 hours per data point per year to even approach the conservative limit on timing accuracy. Worse, this simple scaling relation underestimates the uncertainty for stars where the studied mode does not dominate over other peaks in the transform, as is the case for most of our stars. Nor does it apply in the faint star limit where the flux from the star is dominated by the flux from the sky.

The second question is why the number of stars in the sample was so much smaller than expected. As described above, the projected 9 hours per object per

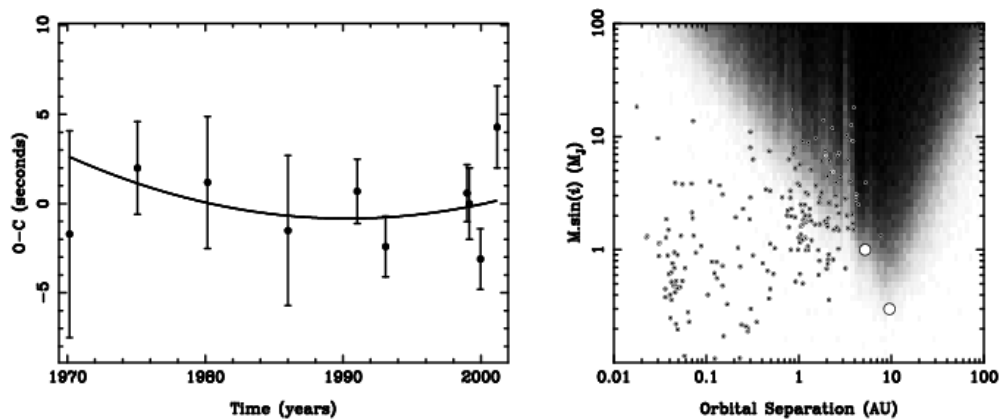


Figure 4.15 R548

year is insufficient to get the desired timing accuracy, but was also unfeasible for the amount of observing time granted. The project was successful in obtaining 30 nights per trimester at McDonald Observatory, or 90 nights per year. The accepted proportion of “clear” nights at McDonald is $1/3$ nights suitable for photometry, and $2/3$ for spectroscopy. As differential photometry is less sensitive to cloud, we found that the spectroscopic value was more appropriate for our observations, giving 60 clear nights per year. With an average of 10 hours of darkness per night, and assuming 1 hour per night devoting to changing and acquiring targets (2 or 3 changes per night taking 20–30 minutes each) this gives 540 hours of data per year. With 30 stars, this corresponds to 18 hours per star per year, or 36 hours per star with a sample of only 15 stars.

We further adopted a strategy of attempting 3 monthly points on a target per year instead of two to give better coverage and to better identify outlier points, yielding 6 hours per month for each of 30 objects, or 12 hours for each of 15. Six, or even 9 hours is insufficient data for reasonable accuracy of a data point. Add to this calculation the fact that the first year included time devoted to discovering new targets (as discussed in Chapter 2) and the extra time in the last year was devoted to the candidate planet host star GD66 (Chapter 3), and it is clear that 30 stars was an unfeasible goal.

However despite falling short of its goals, this project should still be considered a success. For the stars presented in this work, the limits placed on planets are more rigorous than those placed on WDs using other methods (see Figure 1.1 in the Introduction). And while a null result around a sample of 15 stars would not have been interesting (the frequency of detected planets around main sequence stars is somewhere between 5-10%, so if the probability of detecting a planet has a Poisson distribution then the probability of detecting no companions due to bad luck is between 50% and 22%), fortune favoured the bold and we discovered exactly the signal we were searching for around one of our objects. The fact that we do discover an object in our smallish survey suggests that planets around WDs are indeed common, although it is folly to estimate their frequency based on one data point. While one object in 15 suggests a frequency of 6%, this figure does not account for the different sampling sensitivities for the different stars.

Our survey is sensitive to BDs at a wide range of orbital separations. Farihi *et al.* (2005a) determined the BD binary fraction for WDs to be $\lesssim 0.5\%$, consistent with the value obtained in Chapter 5. This value is also consistent with the small number of BDs discovered in radial velocity surveys (Marcy & Butler 2000; Grether & Lineweaver 2006), so the lack of BDs in this small sample is entirely unsurprising.

Our limits on the rate of period change (\dot{P}) are currently $\sim 10^{-12}$ to 10^{-13} . All other effects being equal, our constraint on \dot{P} scales with the square of the time base and with 3 more years of observation we will begin to constrain this value to a few parts in 10^{-15} , of the order of the cooling rate of the star. With limits of this magnitude currently set for only 2 stars, these results will open a new window into the interiors of WDs. Cooling rates can be used to assess core composition, test models of stellar structure and even to constrain the effect on cooling of hypothesized sub-atomic particles like axions created in the hot core (Raffelt 1986).

After only 3–4 years of observations we are already placing limits on planetary companions comparable to those placed on long-period planets by the radial velocity method. As our observations continue and our time base increases, our limits will extend to longer periods and lower masses, probing a region of parameter space unlikely to be accessible to other methods in the near future. Within the next 3 years we should be able to constrain the presence of Saturn analogues. At that time our constraint on \dot{P} will be $\sim 10^{-15}$ and close to measuring the period change caused by the cooling of the star. Our survey suggests that planets around WDs may be common, and closer to the WD than expected. Continued observations will increase the sample space and potentially find a population of more distant planets.

Chapter 5

A *Spitzer* White Dwarf Infrared Survey

We present mid-infrared photometry of 124 white dwarf stars with the *Spitzer Space Telescope*. Objects were observed simultaneously at 4.5 and 8.0 μm with sensitivities better than 0.1 mJy. This data set can be used to test models of white dwarf atmospheres in a new wavelength regime, as well as to search for planetary companions and debris disks.

5.1 Introduction

White dwarf stars (WDs) are the evolutionary end point of stellar evolution for all main sequence stars with a mass $\lesssim 8M_{\odot}$ (Weidemann 2000). The mass of an isolated WD is believed to be uniquely determined by the progenitor mass; hence the progenitor lifetime for a WD can be estimated. Nuclear burning has ceased, so its evolution is one of monotonic and predictable cooling. From the mass and temperature of a WD its cooling age can be calculated. A WD is a stellar gravestone with a date of birth and death carved upon it.

Previous WD infrared surveys have concentrated on the near-infrared. Zuckerman & Becklin (1992) surveyed 200 stars down to K=16 while Farihi *et al.* (2005a)

surveyed 371 WDs (including 82 for which data came from Zuckerman & Becklin 1992) using several different telescopes. In the mid-infrared Chary *et al.* (1998) surveyed 11 WDs (and one sub-dwarf) with ISOCAM at 7 and 15 μm . Our survey significantly extends these previous works by looking at a large (124) sample of stars at 4.5 and 8.0 μm with a limiting sensitivity of better than 0.1 mJy. This data set allows us to study the behavior of WD atmospheres in this wavelength range and to search for companion planets and disks. Such a large data set will also undoubtedly be useful to other researchers for unanticipated reasons.

The primary purpose of our survey was to search for the presence of planets and brown dwarf companions. With radii $\sim 1 R_{\oplus}$, WDs are orders of magnitude less luminous than their progenitor stars. This dramatically reduces the contrast between the host star and any orbiting daughter planets. Probst (1983) reported on the first infrared search for sub-stellar companions around WDs while Burleigh *et al.* (2002) suggested using near-infrared imaging to detect $\gtrsim 3M_J$ planets in orbits > 5 AU with 8m telescopes. Recent attempts to directly detect a companion to a WD include Debes *et al.* (2005a, 2006) and Farihi *et al.* (2005a). Theoretical spectra of brown dwarf stars and massive planets show a distinctive bump around 4-5 μm between absorption bands of methane and water (Sudarsky *et al.* 2003; Burrows *et al.* 2003). By comparing the observed flux in this passband with that of a nearby passband we can hope to directly detect the companion as an excess to the WD flux. Limits on planets around WDs based on this survey will be published in a later work.

Excess mid-infrared flux around a WD can also be caused by a warm disk of circumstellar material. Fortunately, the spectral signature of a disk is markedly different from that of a planet or brown dwarf, showing a mostly flat continuum over a broad wavelength range. Zuckerman & Becklin (1987) discovered the first WD with an infrared excess, G29-38, and Wickramasinghe *et al.* (1988) first suggested that the excess was due to a circumstellar disk. Reach *et al.* (2005a) detected emission features of silicates at 10 μm from this disk using a *Spitzer* IRS spectrum (Houck *et al.* 2004).

Jura (2003) suggested that the metals in the atmosphere of G29-38 were accreted from the debris disk of a disrupted asteroid. Disks have also been detected

around GD362 (Kilic *et al.* 2005; Becklin *et al.* 2005), GD56 (Kilic *et al.* 2006b), and WD2115-560 (this work). Von Hippel *et al.* (2006, submitted, hereafter HKK06) proposed that debris disks may be the source of the metals observed in the photospheres of approximately 25% of WDs (Zuckerman *et al.* 2003) and suggested that debris disks are therefore very common. Mid-infrared observations are sensitive to cooler dust at larger orbital separations and will be important in determining the origin and lifetimes of these disks.

Our survey has also uncovered some unusual behavior of the spectral energy distributions (SEDs) of cool WDs. Kilic *et al.* (2006a) published an SED of WD0038-226 showing a dramatic flux deficit and noted that DAs below 7000 K consistently showed a small flux deficit (although see Tremblay & Bergeron 2007). These results provide an opportunity to investigate the properties of matter in extreme conditions, but uncertainty in the infrared luminosity of the coolest WDs is an obstacle to their use in WD cosmochemistry to measure the age of the Galaxy.

5.2 Target Selection, Observations and Reductions

Drawing from the McCook & Sion Catalogue (McCook & Sion 1999), we cross-referenced with the 2MASS survey (Skrutskie *et al.* 2006), selecting all stars brighter than $K_s = 15$, rejecting known binaries and planetary nebulae, for a total of 135 objects. We removed one object to avoid conflict with the Reserved Observations Catalogue, and the TAC removed three other WDs awarded to a different program. In total we observed 131 objects and successfully measured the flux for 124 of these. The remaining objects were too heavily blended with other, brighter objects. A breakdown of the spectral type of each object is given in Table 5.1. In the course of a more detailed literature search we discovered, for a small number of stars, differences between the temperature and spectral type quoted in McCook & Sion compared to more recently published values. Where applicable, references are listed in the notes to Table 5.2.

Each object was observed simultaneously in channels 2 and 4 (4.5 and 8.0 μm) with the IRAC camera (Fazio *et al.* 2004) on *Spitzer* (Werner *et al.* 2004). Five 30s exposures were taken of each object using a Gaussian dither pattern. The data were

processed with version S11.4.0 of the IRAC pipeline, which removes well-understood instrumental signatures, to produce the basic calibration data (BCD) files

We performed aperture photometry on these BCD files using the *astrolib* package in IDL. For most stars, we chose a 5 pixel aperture, although for a number of objects we used 2 or 3 pixels instead to avoid contaminating flux from nearby objects. We measured sky in an annulus of 10-20 pixels centered on the star. We made the appropriate aperture correction suggested by the IRAC data handbook. For channel 2 we multiplied the flux by 1.221, 1.113 and 1.050 for apertures of 2, 3, and 5, while the values for channel 4 were 1.571, 1.218, and 1.068 respectively.

The recorded flux for a stellar object is dependent on the location on the array where it was observed. This is because of both a variation in pixel solid angle (due to distortion) and a variation of the spectral response (due to varying filter response with incidence angle over the wide field of view). We accounted for these effects by multiplying the measured flux by the appropriate location dependent correction factor as described in Reach *et al.* (2005b). We do not apply a correction to our photometry to account for variation in the flux as a function of location of the stellar centroid within the pixel, as this correction only applies to data taken in channel 1.

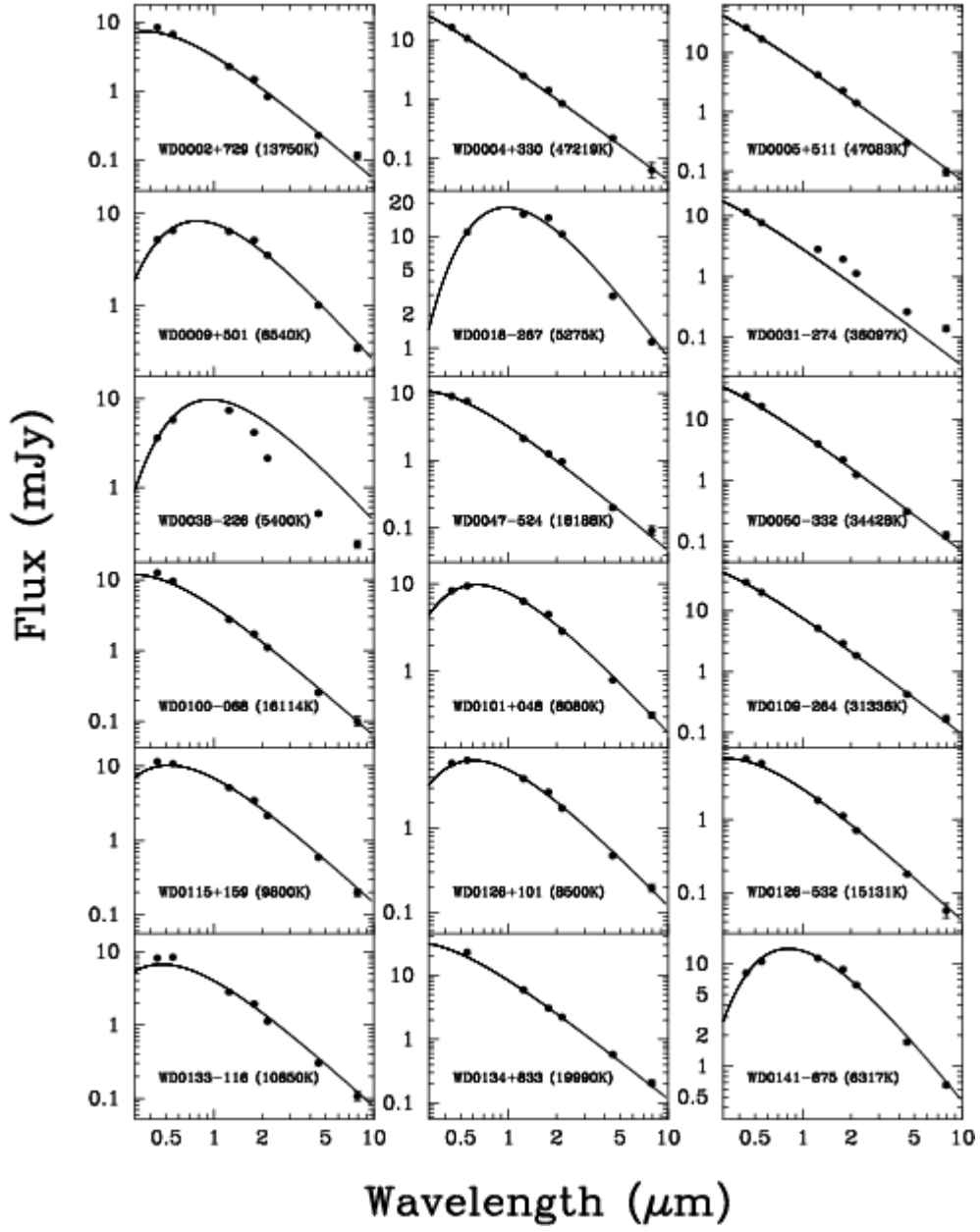
Because the sensitivity of the IRAC sensors is wavelength dependent, the recorded flux differs from the true flux in a manner that depends on the source's spectral shape. Fortunately this effect is small (of order the systematic uncertainty) and, as a WD spectrum is dominated by a Rayleigh-Jeans tail in the mid-infrared, easily corrected. We used the values suggested in Reach *et al.* (2005b) of 1.011 at $4.5\ \mu\text{m}$ and 1.034 at $8\ \mu\text{m}$. We did not apply color correction to objects whose SEDs were inconsistent with a single blackbody source (see Table 5.2). The IRAC pipeline removes some but not all cosmic rays. To clean our data of remaining artifacts we removed frames where the flux deviated by more than 3.5σ from the median and calculated the weighted average flux of the remaining frames.

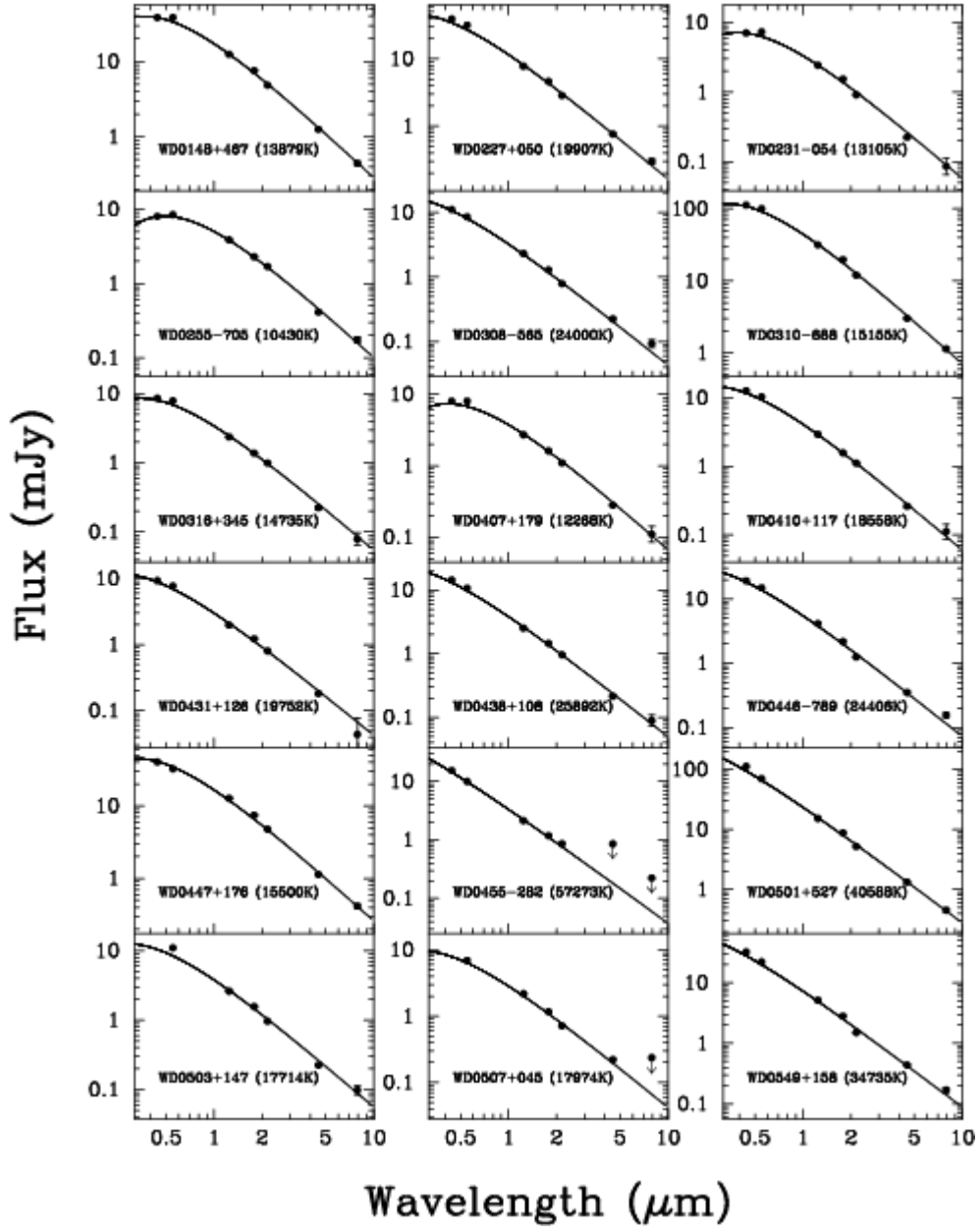
5.3 Results

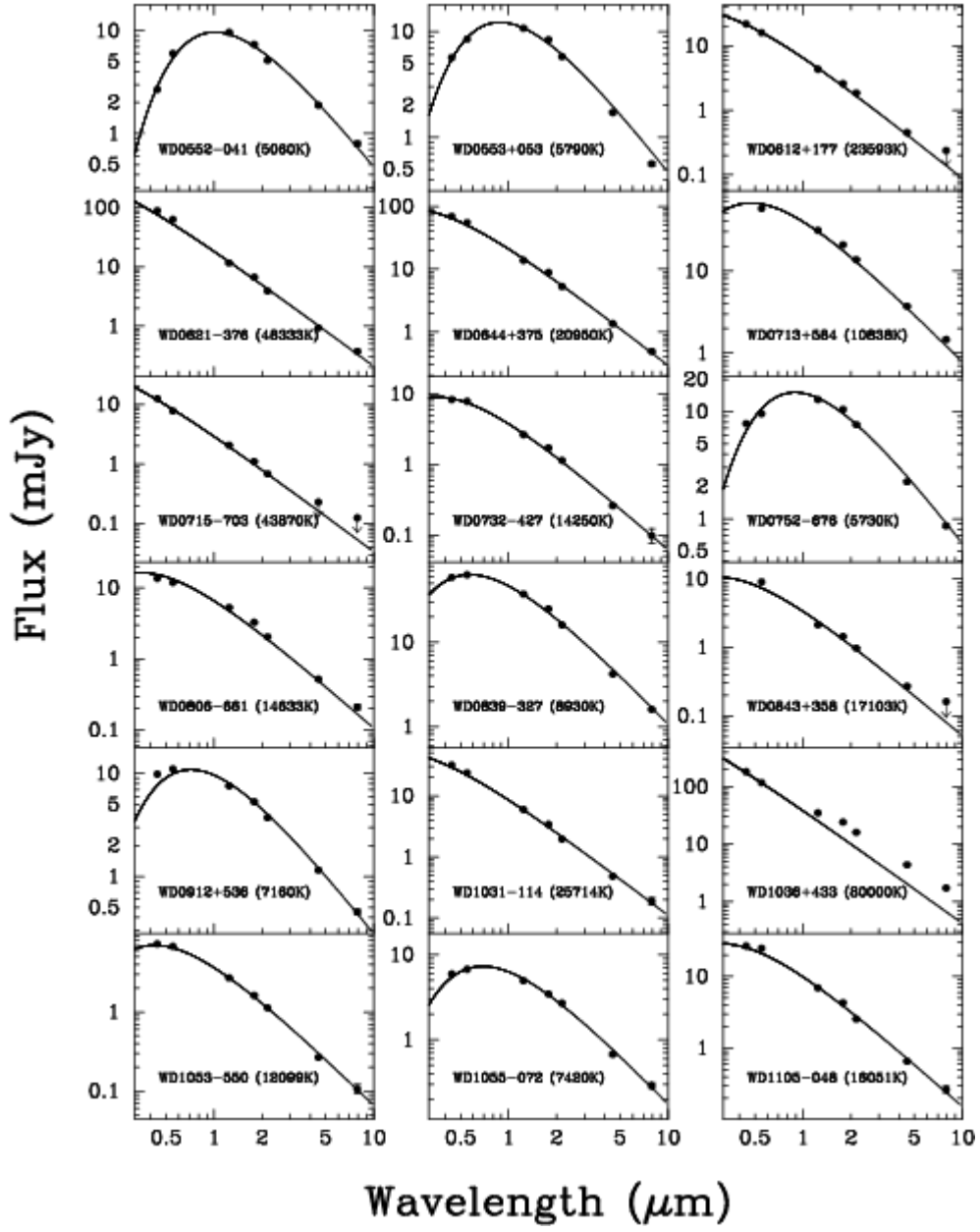
We present the fluxes for each WD in the two IRAC bands in Table 5.2. For comparison, we also list the flux for each object in J, H and K as measured by the 2MASS survey. An SED for each object, with optical photometry from the McCook & Sion catalogue is presented in Figure 5.1. A blackbody at the quoted temperature and fit to the optical and near-infrared data is also shown to guide the eye. A subset of objects in this sample have been previously published in Reach *et al.* (2005a) and Kilic *et al.* (2006a); we present photometry for these stars here for completeness. Note that as these papers used an earlier version of the IRAC pipeline their published fluxes differ slightly from those presented here.

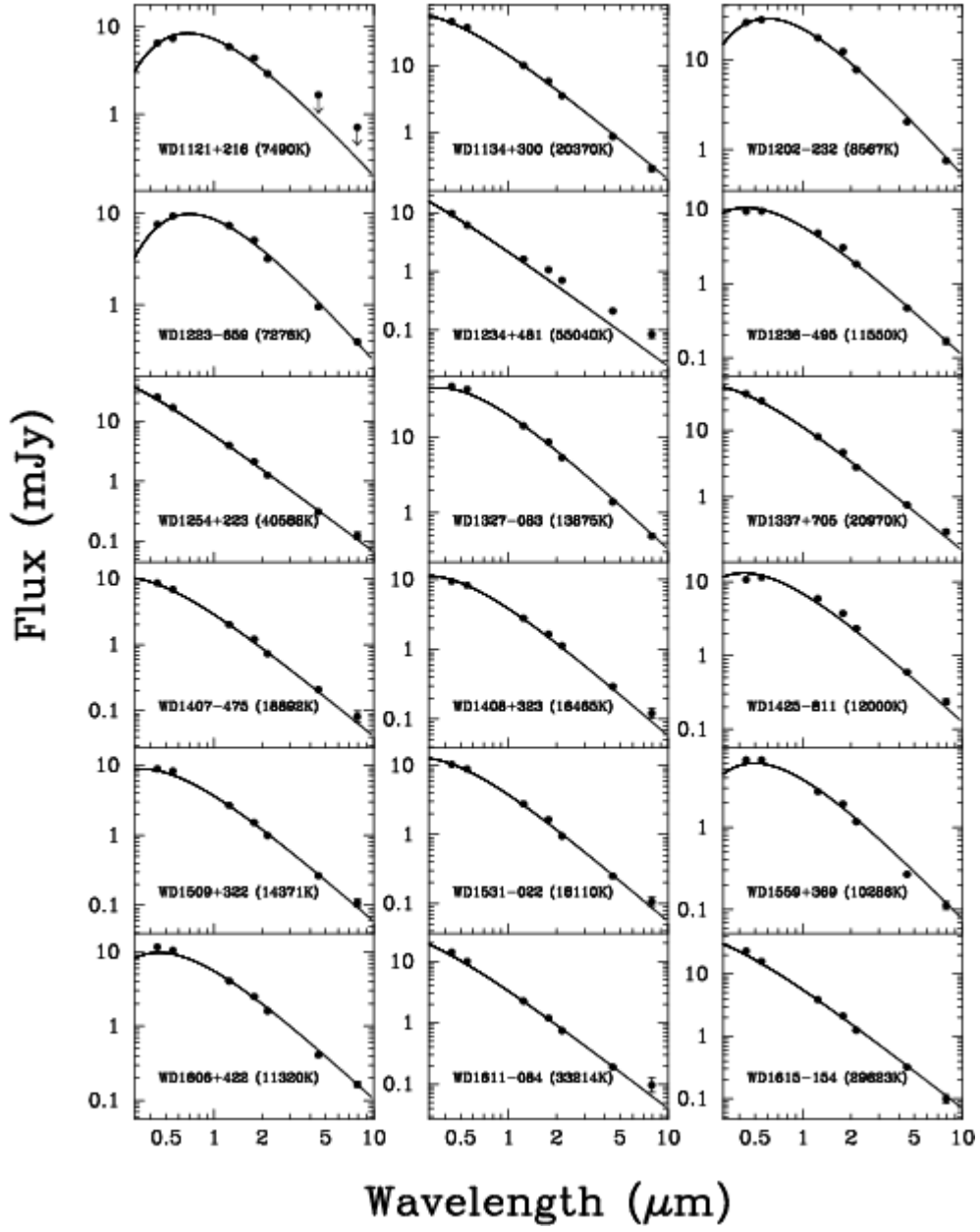
5.3.1 Notes on Individual Objects

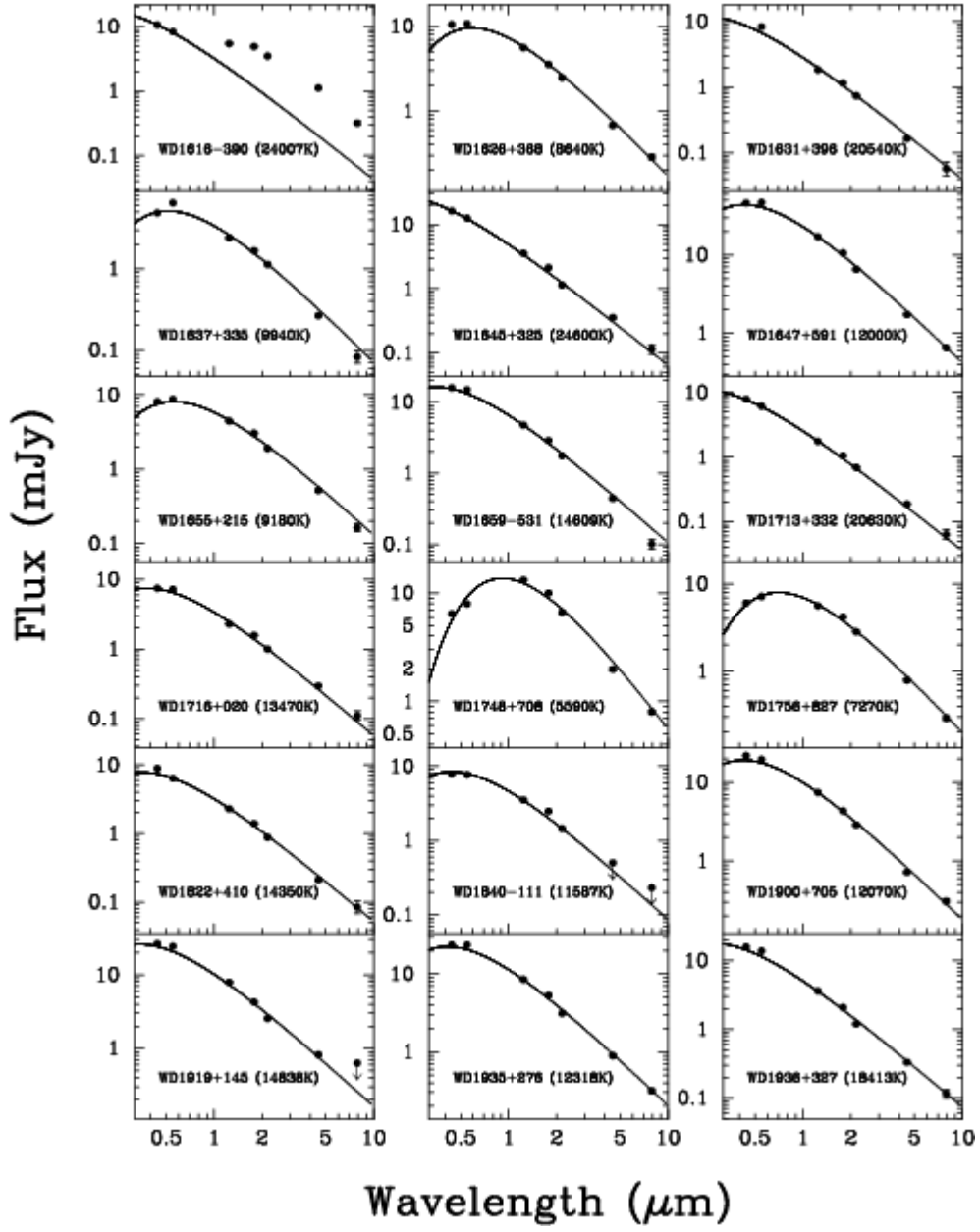
WD0002+729.— A handful of stars show a small excess at $8\mu\text{m}$; we discuss this star as an example object. The atmosphere of WD0002+729 is contaminated with small amounts of metals (Wolff *et al.* 2002) which may increase the probability of the existence of a disk. However, the flux is close to our sensitivity limits ($\approx 0.1\text{ mJy}$) and our error bar may be underestimated; our confidence in this excess is low. By fitting models to this excess we can determine that if this excess is due to a disk, its maximum temperature must be less than about 300 K.

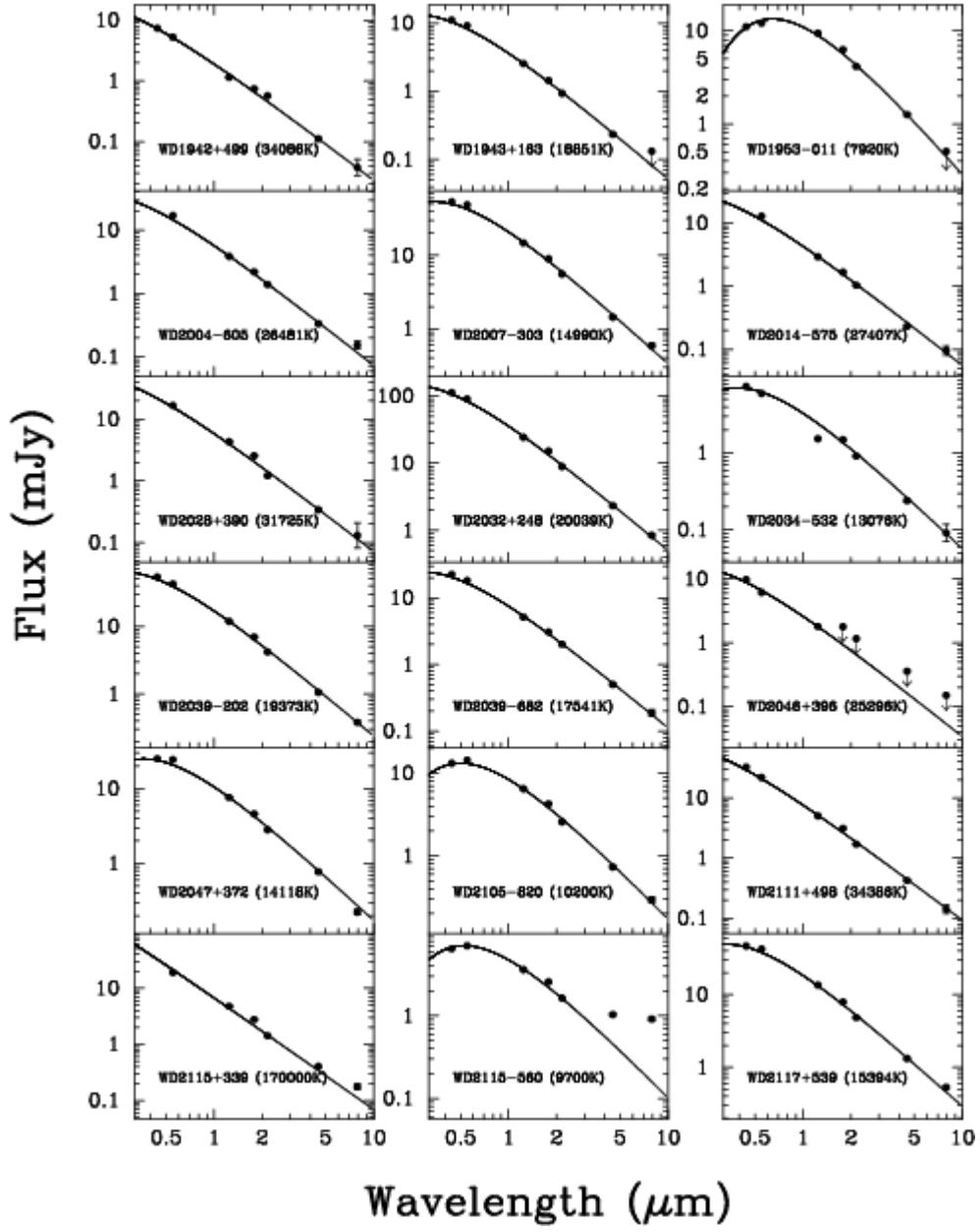












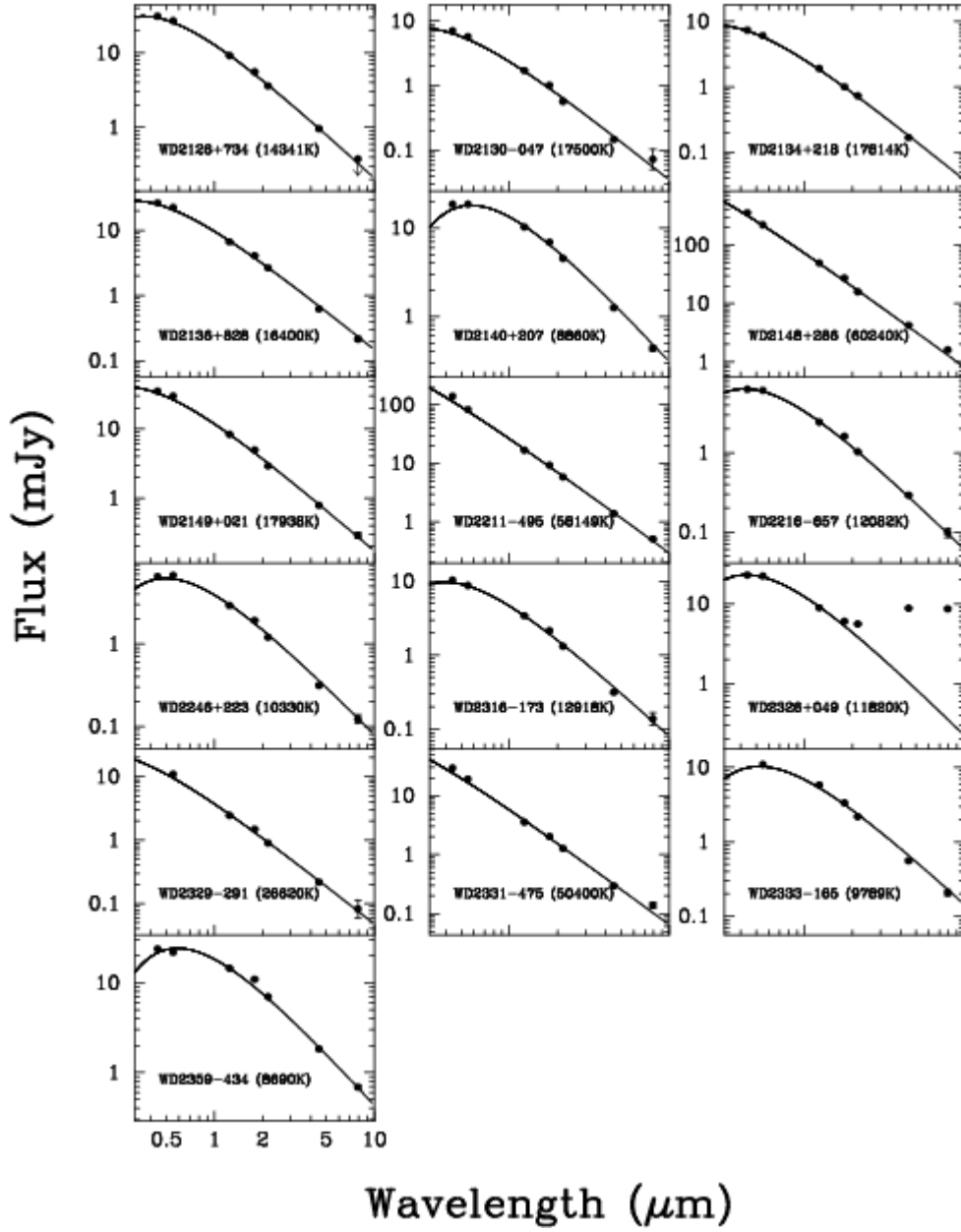


Figure 5.1 SEDs for the 124 WD stars in this survey. Our IRAC photometry points are at 4.5 and $8\,\mu\text{m}$. Also shown for comparison are near-IR fluxes from 2MASS, and B and V photometry from the McCook & Sion catalogue where available. Points with arrows indicate upper limits on the flux, not measurements (see Table 5.2). Where errorbars are not shown they are smaller than the size of the points. The solid line represents a blackbody at the temperature listed in Table 5.2 fit to the optical and near IR data. A blackbody is a good, but not perfect, model of a WD photosphere, and this accounts for much of the deviation in the photometry. A better fit can be achieved with atmosphere models, however as these fits are intended only to guide the eye a blackbody does an adequate job.

WD0031-274.— McCook & Sion incorrectly classified this object as a DA. Kilkenny *et al.* (1988) classified it to be an sdOB star with their criterion “dominated by HeI and HeII lines; often Balmer absorption present”. Lisker *et al.* (2005) measure a temperature of $36,097\text{ K}$ and a distance of 900 pc . They refer to it as an sdB. Our photometry shows a clear excess from J onward relative to the visible photometry. Close examination of the images does not reveal any irregularities in the point response function. At this distance, the flux from a sub-stellar companion would be negligible. We fail to find a good fit for a low-mass main-sequence star nor does the excess show the broad flat shape of a circumstellar dust spectrum. The excess is best fit with a blackbody temperature of $18,300\text{ K}$, however a circumstellar object of this temperature would be detectable in the visible flux. Cyclotron emission has been suggested as a source of infrared emission in WDs, but this object is not known to have a strong magnetic field. Further study is necessary to determine the true nature of this object.

WD0038-226.— WD0038 has been known to have a near-IR flux deficit for some time now (Wickramasinghe *et al.* 1982) which had been explained by Bergeron *et al.* (1994) as Collisionally Induced Absorption. At cooler surface temperatures (WD0038 is $5,400\text{ K}$), the hydrogen in the atmosphere combines to form molecular H_2 . Collisions between these molecules causes them to vibrate and rotate providing a rich spectrum of allowed absorption energies. However, absorption from CIA is expected to be negligible beyond about $3\,\mu\text{m}$ and cannot explain the flux deficit at 4.5 and $8.0\,\mu\text{m}$. See Kilic *et al.* (2006a) for a further discussion of this object’s

dramatic flux deficit.

WD0447+176.— McCook & Sion incorrectly quote Wegner & Swanson (1990) giving a V magnitude of 13.4 instead of 12.65. Kilkenny *et al.* (1988) report $V=12.62$ and a temperature of 33.8 kK. This temperature does not fit the SED well, and we instead plot the best fit blackbody temperature of 15.5 kK.

WD0843+358.— This object partially resolves into two objects separated by 2.2 pixels at $8\,\mu\text{m}$, causing the observed excess at that band. The companion object is not seen at any bluer wavelengths. Were the companion sub-stellar in nature the excess would be greater at $4.5\,\mu\text{m}$ than at 8; we therefore conclude that the excess is due to a background object. Examination of POSS 1 plates from 1953 shows no evidence of an object at the current position of the WD.

WD1036+433.— Also known as Feige 34. Thejll *et al.* (1991) determine it to be an 80 kK sdO. Maxted *et al.* (2000) note that they observed $\text{H}\alpha$ in emission from this object, but the emission is intermittent as other observers make no mention of it (Oke 1990; Bohlin *et al.* 2001). Chu *et al.* (2001), who also observe emission, suggest this emission could be caused by photoionization of the atmosphere of a hot Jupiter companion.

Our photometry shows a clear excess from H onward. Examination of the individual images shows that the WD is the brightest object in the vicinity, and no evidence of a line-of-sight companion. This excess was first observed in J, H and K by Probst (1983). Thejll *et al.* (1991) summarized the available photometry at that time and concluded that the colors were “marginally consistent” with a companion K7-M0 dwarf. We find that the excess is well fit in color and magnitude by a 3750 K Kurucz model (Kurucz 1979), corresponding to a spectral type of M0 or M1.

WD1234+481.— Liebert *et al.* (2005) measure a temperature for this star of $55,040 \pm 975$ K, $\log g$ of 7.78 ± 0.06 and derive a distance of 144 pc. Holberg *et al.* (1998) measure 56,400 K, 7.67 and 129 pc respectively based on an *International Ultraviolet Explorer* (IUE) spectrum. Other authors measure similar values. Based on white dwarf interior models we determine a mass of 0.57(02) solar masses and a cooling time of approximately 4.7 million years. According to Weidemann (2000), this corresponds to a main sequence progenitor mass between 1 and 1.8 solar masses

Table 5.1. Classifications of Observed Stars

Type	Number
DA	98
DB	10
DC	3
DO	2
DQ	2
sd	2
Other	7

and hence a poorly constrained main sequence life time between 1.2 and 12 Gyr (Girardi 2000).

Debes *et al.* (2005a) noticed an excess in the near-infrared and assigned a preliminary spectral type to the companion of M8 V. As shown in Figure 5.2, we observe an infrared excess in all five bands. The IRAC images are round and isolated. The measured flux values in apertures of 2, 3 and 5 pixels yield consistent values, ruling out the possibility that the excess is caused by contamination from a nearby bright star. We note that the excess can be fit by a model of a brown dwarf with $T_{\text{eff}} \approx 2000$ K corresponding to a spectral type of early L. If planned follow-up observations confirm the sub-stellar nature of this companion it would be the fourth WD – brown dwarf binary known.

WD1616-390.— Sion *et al.* (1988) list this star as a $0.61M_{\odot}$ DA with T_{eff} of 24,007 K. We notice a clear excess from J onward. The colors of the excess are well fit with a 4000 K Kurucz model of a main sequence star, corresponding to a late K spectral type. However the magnitude of the excess is too large to be consistent with a K dwarf companion. We conclude that the excess is either from a foreground dwarf star or a background giant.

WD2115-560.— This object has an infrared excess consistent with a dust debris disk. See HKK06 for further details.

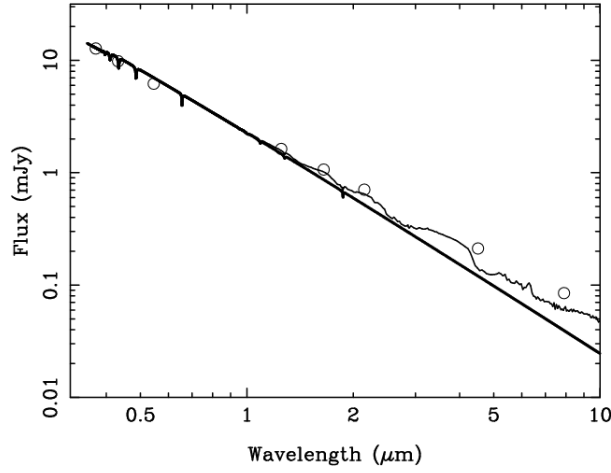


Figure 5.2 SED of WD1234+481. The open circles are the observed photometry. The thick solid line is a 55,040 K DA model atmosphere representing the flux from the white dwarf and fitted to the optical photometry. The thin line represents a brown dwarf model atmosphere with T_{eff} of 2000 K and $\log g$ of 5.0.

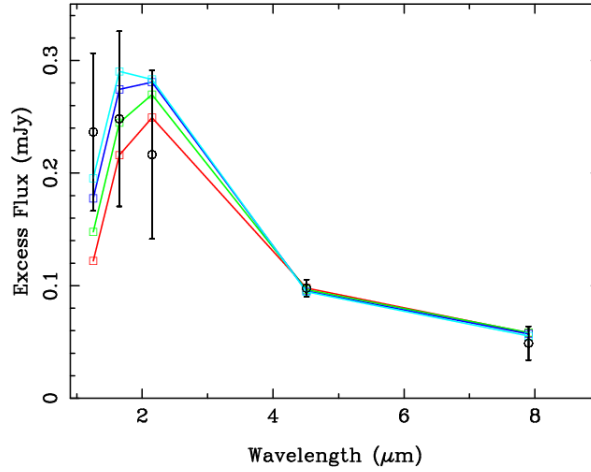


Figure 5.3 Fit of BD models with temperatures ranging from 1700–2000 K and $\log g$ of 5.0 from Burrows *et al.* (2006b) to the excess flux from WD1234+481.

WD2134+218 This object was too faint to be detected at 8 μm . The expected flux according to a blackbody model was 0.05 mJy, less than our nominal detection limit of about 0.1 mJy with the 150s exposure time used.

WD2326+049.— This object, also known as G29-38, has an infrared excess consistent with circumstellar dust. This excess was first reported by Zuckerman & Becklin (1987). Reach *et al.* (2005a) fit a *Spitzer* IRS spectrum of the disk with a mixture of olivine, forsterite and carbon dust.

5.4 Discussion

We fit the observed SEDs of DA stars between 6 and 60 kK in the optical and near-infrared with synthetic photometry derived from models kindly supplied by D. Koester. Details of the input physics and methods are described in Finley *et al.* (1997), Homeier *et al.* (1998) and Koester *et al.* (2001). We then compared the observed excess (or deficit) over the fitted model in the mid-infrared to the uncertainty in the observation. Objects with disks (WD2326, WD2115), probable companions (e.g. WD1234) or contaminated photometry are not included. We expect the distribution of this excess/deficit for the sample to be well described by a Gaussian distribution with mean 0 and standard deviation of 1. We plot this distribution in Figure 5.4. The grey histogram corresponds to IRAC channel 4 photometry and the fitted Gaussian is plotted with a dashed line. The outlined histogram corresponds to channel 2 and the Gaussian is shown as a solid line. The dispersion in channel 2 is measurably greater than expected, indicating that our error bars may be underestimated. The measured flux in channel 4 is on average 1σ higher than expected. This may be because the majority of stars have excess flux in this band (possibly due to a disk), or because of a poor match of our models to reality. As these models are well tested only in the optical regime for which they were originally intended, it is possible that this result points to new and unexpected physical processes affecting the mid-infrared portion of the spectrum.

Three brown dwarf companions to WDs are known (Becklin & Zuckerman 1988; Farihi & Christopher 2004; Maxted *et al.* 2006). In our survey we find one object with an SED consistent with a brown dwarf companion, or a detection frequency of $\lesssim 1\%$. The survey of Farihi *et al.* (2005a) set the observed brown dwarf companion fraction at $0.4\% \pm 0.1\%$, consistent with our result. Our selection of targets deliberately excluded stars with known main sequence binary companions explain-

ing the dearth of such companions in our sample. Both sub-dwarf stars in our survey show an infrared excess. This is consistent with the survey of Allard *et al.* (1994), who determined that 54%–66% of sub-dwarf stars have a main sequence companion.

Table 5.3 lists the 20 objects in our survey with measured abundances of metal in their photospheres. Two of these objects (WD2115 and WD2326) have debris disks. HKK06 suggest that all DAZs are accreting from debris disks. The small fraction of DAZs with disks initially appears to refute this claim. It should be noted that for stars with temperatures $\gtrsim 19\text{kK}$, dust from any debris disk inside the Roche limit is expected to sublimate quickly and will not produce a noticeable infrared signature. For the cooler stars, the metal abundances are significantly lower and the flux from the debris disk is expected to be correspondingly dimmer. Deeper observations will be required to confirm or refute this hypothesis.

5.5 Conclusion

We have conducted a large mid-infrared WD photometric survey, obtaining images of 124 WDs with a limiting sensitivity better than 0.1mJy. This survey has already found an unexplained flux deficit in the SED of a cool WD, and a debris disk around another star. This data set can be used to constrain the presence of planets around these stars as well as test and refine model WD atmospheres.

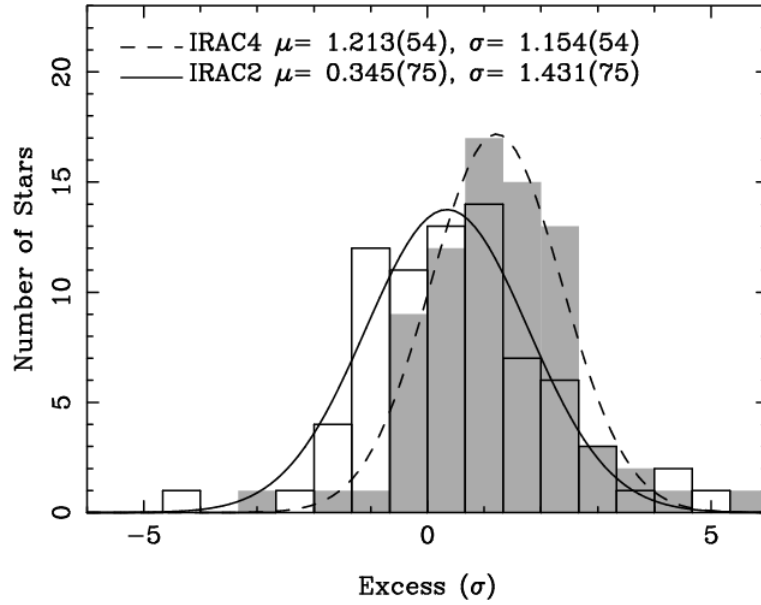


Figure 5.4 Histogram of excesses and deficits for a selection of the DAs observed in this survey. Each bin represents the difference between the observed flux and that predicted by models from Finley *et al.* (1997) as a fraction of the size of the measured photometric error. If no stars show unusual behavior, we expect this histogram to be well fit by a Gaussian with mean 0 and a standard deviation of 1. IRAC 2 is shown as white bars fit with the solid line while IRAC 4 is shown as a grey histogram fit with the dashed line. The mean of each distribution is given by μ while the standard deviation is given by σ . See text for discussion.

Table 5.2. Infrared Fluxes for Stars in this Sample

Name	Type	T_{eff}	J	H	K	IRAC 2	IRAC 4	Ap	Notes
WD0002+729	DBZ	13750	2.272(40)	1.484(29)	0.833(16)	0.2277(79)	0.116(16)	3	1
WD0004+330	DA	47219	2.503(44)	1.416(28)	0.857(16)	0.2212(86)	0.064(21)	5	
WD0005+511	DO	47083	4.200(73)	2.271(44)	1.411(27)	0.2975(99)	0.096(14)	3	
WD0009+501	DAP	6540	6.41(11)	5.14(10)	3.528(67)	1.006(31)	0.343(23)	5	2
WD0018-267	DA	5275	15.88(28)	14.72(29)	10.51(20)	2.923(88)	1.134(42)	5	
WD0031-274	sdB	36097	2.816(49)	1.937(38)	1.124(21)	0.2634(89)	0.138(16)	3	3
WD0038-226	C_2H	5400	7.34(13)	4.141(81)	2.132(40)	0.507(16)	0.229(23)	5	2,4
WD0047-524	DA	18188	2.117(37)	1.257(25)	0.961(18)	0.1982(73)	0.091(15)	3	
WD0050-332	DA	34428	3.989(70)	2.191(43)	1.249(24)	0.312(10)	0.127(17)	3	
WD0100-068	DB	16114	2.742(48)	1.710(33)	1.102(21)	0.256(11)	0.100(17)	3	
WD0101+048	DA	8080	6.32(11)	4.486(88)	2.862(54)	0.792(25)	0.315(26)	5	
WD0109-264	DA	31336	5.125(89)	2.899(57)	1.835(35)	0.422(14)	0.168(22)	5	
WD0115+159	DC	9800	5.149(90)	3.454(68)	2.155(41)	0.594(19)	0.197(22)	3	
WD0126+101	DA	8500	3.888(68)	2.688(52)	1.731(33)	0.472(15)	0.194(20)	3	
WD0126-532	DA	15131	1.828(32)	1.122(22)	0.710(13)	0.1801(66)	0.057(14)	3	
WD0133-116	DAV	10850	2.816(49)	1.937(38)	1.124(21)	0.303(10)	0.107(16)	3	
WD0134+833	DA	19990	5.88(10)	3.058(60)	2.212(42)	0.576(19)	0.205(21)	5	
WD0141-675	DA	6317	11.37(20)	8.85(17)	6.20(12)	1.722(52)	0.658(29)	5	5
WD0148+467	DA	13879	12.45(22)	7.58(15)	4.848(92)	1.257(39)	0.444(29)	5	
WD0227+050	DA	19907	7.76(14)	4.608(90)	2.844(54)	0.764(24)	0.297(27)	5	
WD0231-054	DA	13105	2.435(42)	1.539(30)	0.913(17)	0.2249(87)	0.086(27)	5	
WD0255-705	DA	10430	3.873(68)	2.292(45)	1.695(32)	0.412(13)	0.174(16)	3	6
WD0308-565	DB	24000	2.308(40)	1.286(25)	0.787(15)	0.2243(80)	0.093(14)	3	
WD0310-688	DA	15155	31.57(55)	19.69(38)	12.01(23)	3.030(92)	1.142(41)	5	
WD0316+345	DA	14735	2.375(41)	1.381(27)	0.993(19)	0.2234(80)	0.079(18)	3	
WD0407+179	DA	12268	2.709(47)	1.610(31)	1.097(21)	0.280(10)	0.110(31)	5	
WD0410+117	DA	18558	2.941(51)	1.577(31)	1.115(21)	0.2626(97)	0.112(32)	5	
WD0431+126	DA	19752	1.972(34)	1.227(24)	0.801(15)	0.1815(76)	0.044(34)	5	
WD0438+108	DA	25892	2.522(44)	1.448(28)	0.962(18)	0.2143(76)	0.089(20)	3	
WD0446-789	DA	24406	4.135(72)	2.173(42)	1.252(24)	0.350(12)	0.156(14)	3	
WD0447+176	DB	15500	12.71(22)	7.43(14)	4.764(90)	1.135(35)	0.415(24)	3	
WD0455-282	DA	57273	2.134(37)	1.181(23)	0.863(16)	0.857(27)	0.223(26)	5	7
WD0501+527	DA	40588	15.32(27)	8.76(17)	5.228(99)	1.327(41)	0.454(32)	5	

Table 5.2—Continued

Name	Type	T_{eff}	J	H	K	IRAC 2	IRAC 4	Ap	Notes
WD0503+147	DB	17714	2.614(46)	1.569(31)	0.966(18)	0.2247(77)	0.099(17)	2	
WD0507+045	DA	17974	2.180(38)	1.167(23)	0.714(14)	0.2213(76)	0.236(20)	2	7
WD0549+158	DA	34735	5.144(90)	2.818(55)	1.506(28)	0.437(14)	0.169(19)	2	
WD0552−041	DZ	5060	9.63(17)	7.35(14)	5.166(98)	1.892(58)	0.799(34)	5	
WD0553+053	DAP	5790	10.73(19)	8.36(16)	5.79(11)	1.717(52)	0.561(26)	3	
WD0612+177	DA	23593	4.342(76)	2.594(51)	1.853(35)	0.450(15)	0.236(24)	2	8,5
WD0621−376	DA	48333	11.56(20)	6.68(13)	3.879(73)	0.922(29)	0.370(23)	5	
WD0644+375	DA	20950	13.79(24)	8.82(17)	5.271(100)	1.350(42)	0.487(30)	5	
WD0713+584	DA	10838	31.14(54)	20.75(40)	13.66(26)	3.71(11)	1.461(50)	5	
WD0715−703	DA	43870	2.055(36)	1.095(21)	0.683(13)	0.2281(93)	0.124(22)	5	9
WD0732−427	DAE	14250	2.660(46)	1.720(34)	1.148(22)	0.2620(92)	0.098(25)	3	
WD0752−676	DAZ	5730	12.94(23)	10.47(20)	7.57(14)	2.219(67)	0.859(30)	3	2
WD0806−661	DQ	14633	5.259(92)	3.271(64)	2.049(39)	0.519(16)	0.209(17)	3	10
WD0839−327	DA	8930	37.26(65)	24.81(48)	16.04(30)	4.20(13)	1.598(52)	3	
WD0843+358	DZ	17103	2.144(37)	1.442(28)	0.971(18)	0.2704(100)	0.161(24)	5	7
WD0912+536	DCP	7160	7.57(13)	5.32(10)	3.722(70)	1.150(35)	0.454(25)	5	
WD1031−114	DA	25714	5.94(10)	3.406(66)	1.953(37)	0.482(16)	0.188(26)	5	
WD1036+433	sdO	80000	35.10(61)	24.27(47)	16.14(30)	4.37(13)	1.723(57)	5	4,11
WD1053−550	DA	12099	2.702(47)	1.621(32)	1.129(21)	0.2666(93)	0.106(15)	3	
WD1055−072	DC	7420	4.949(86)	3.454(68)	2.691(51)	0.674(21)	0.289(23)	3	2
WD1105−048	DA	16051	6.93(12)	4.288(84)	2.549(48)	0.655(21)	0.266(30)	5	
WD1121+216	DAZ	7490	5.93(10)	4.388(86)	2.913(55)	1.660(51)	0.709(27)	2	7,5
WD1134+300	DA	20370	10.12(18)	5.87(12)	3.554(67)	0.873(27)	0.291(30)	5	5
WD1202−232	DAZ	8567	17.45(30)	12.30(24)	7.71(15)	2.038(62)	0.753(31)	3	
WD1223−659	DA	7276	7.39(13)	5.099(100)	3.200(60)	0.953(30)	0.394(18)	2	5
WD1234+481	DA	55040	1.628(28)	1.067(21)	0.707(13)	0.2116(75)	0.085(15)	3	4,12
WD1236−495	DAV	11550	4.787(84)	3.050(60)	1.824(34)	0.468(15)	0.167(15)	3	
WD1254+223	DA	40588	3.960(69)	2.122(41)	1.261(24)	0.310(10)	0.123(18)	3	5
WD1327−083	DA	13875	14.26(25)	8.70(17)	5.37(10)	1.386(42)	0.488(26)	3	5
WD1337+705	DAZ	20970	8.00(14)	4.651(91)	2.777(52)	0.753(24)	0.296(22)	5	
WD1407−475	DA	18892	2.022(35)	1.208(24)	0.728(14)	0.2093(77)	0.082(17)	2	
WD1408+323	DA	16465	2.780(48)	1.647(32)	1.126(21)	0.293(10)	0.121(21)	5	5
WD1425−811	DAV	12000	5.91(10)	3.708(72)	2.322(44)	0.594(20)	0.234(21)	5	

Table 5.2—Continued

Name	Type	T_{eff}	J	H	K	IRAC 2	IRAC 4	Ap	Notes
WD1509+322	DA	14371	2.680(47)	1.516(30)	0.989(19)	0.2640(89)	0.108(14)	3	
WD1531−022	DA	18110	2.783(48)	1.647(32)	0.948(18)	0.2487(85)	0.106(17)	3	
WD1559+369	DAV	10286	2.705(47)	1.916(37)	1.169(22)	0.2680(89)	0.112(13)	2	9
WD1606+422	DA	11320	4.063(71)	2.511(49)	1.599(30)	0.409(13)	0.165(13)	2	
WD1611−084	DA	33214	2.258(39)	1.192(23)	0.745(14)	0.1903(79)	0.096(29)	5	9
WD1615−154	DA	29623	3.863(67)	2.120(41)	1.249(24)	0.319(11)	0.099(18)	3	
WD1616−390	DA	24007	5.446(95)	4.901(96)	3.489(66)	1.117(35)	0.319(22)	3	4,13
WD1626+368	DBZ	8640	5.594(98)	3.544(69)	2.477(47)	0.680(21)	0.286(17)	3	
WD1631+396	DA	20540	1.835(32)	1.150(22)	0.737(14)	0.1651(61)	0.057(15)	3	
WD1637+335	DA	9940	2.410(42)	1.673(33)	1.133(21)	0.2648(90)	0.082(16)	2	
WD1645+325	DBV	24600	3.559(62)	2.128(42)	1.144(22)	0.356(12)	0.115(21)	5	
WD1647+591	DAV	12000	17.08(30)	10.59(21)	6.53(12)	1.724(52)	0.652(28)	5	
WD1655+215	DA	9180	4.447(78)	3.047(59)	1.900(36)	0.518(16)	0.163(20)	3	
WD1659−531	DA	14609	4.726(82)	2.873(56)	1.750(33)	0.441(15)	0.100(17)	2	
WD1713+332	DA	20630	1.748(30)	1.052(20)	0.689(13)	0.1882(66)	0.064(12)	2	
WD1716+020	DA	13470	2.298(40)	1.573(31)	0.998(19)	0.296(10)	0.110(18)	2	
WD1748+708	DXP	5590	13.15(23)	9.98(20)	6.62(12)	1.981(60)	0.802(31)	5	
WD1756+827	DA	7270	5.609(98)	4.183(82)	2.828(54)	0.787(25)	0.290(21)	5	5
WD1822+410	DZ	14350	2.285(40)	1.395(27)	0.877(17)	0.2108(74)	0.085(19)	3	
WD1840−111	DA	11587	3.526(62)	2.481(48)	1.449(27)	0.501(20)	0.231(24)	2	7
WD1900+705	DXP	12070	7.39(13)	4.312(84)	2.865(54)	0.720(23)	0.309(23)	5	
WD1919+145	DA	14838	7.91(14)	4.261(83)	2.544(48)	0.818(34)	0.631(73)	2	7
WD1935+276	DAV	12318	8.50(15)	5.31(10)	3.107(59)	0.890(28)	0.315(20)	3	5
WD1936+327	DA	18413	3.608(63)	2.079(41)	1.199(23)	0.332(11)	0.115(18)	3	
WD1942+499	DA	34086	1.136(20)	0.737(14)	0.565(11)	0.1113(50)	0.037(13)	3	
WD1943+163	DA	18851	2.550(44)	1.441(28)	0.936(18)	0.2341(90)	0.133(15)	2	7
WD1953−011	DAP	7920	9.43(16)	6.29(12)	4.153(78)	1.259(39)	0.505(24)	3	7,2
WD2004−605	DA	26481	3.845(67)	2.193(43)	1.384(26)	0.334(12)	0.154(24)	5	
WD2007−303	DA	14990	14.77(26)	8.99(18)	5.56(10)	1.433(44)	0.589(34)	5	
WD2014−575	DA	27407	2.936(51)	1.667(33)	1.040(20)	0.2314(80)	0.095(18)	3	
WD2028+390	DA	31725	4.314(75)	2.556(50)	1.215(23)	0.341(12)	0.131(77)	2	9
WD2032+248	DA	20039	24.37(42)	15.19(30)	8.90(17)	2.336(71)	0.842(35)	5	
WD2034−532	DB	13076	1.532(27)	1.490(29)	0.915(17)	0.2409(95)	0.091(26)	5	

Table 5.2—Continued

Name	Type	T_{eff}	J	H	K	IRAC 2	IRAC 4	Ap	Notes
WD2039–202	DA	19373	11.82(21)	6.95(14)	4.191(79)	1.058(33)	0.382(23)	3	
WD2039–682	DA	17541	5.139(90)	3.075(60)	2.013(38)	0.499(16)	0.187(21)	5	
WD2046+396	DA	25296	1.792(31)	1.781(35)	1.161(22)	0.358(12)	0.150(21)	2	7
WD2047+372	DA	14118	7.61(13)	4.595(90)	2.826(53)	0.774(25)	0.224(18)	2	
WD2105–820	DAZ	10200	6.48(11)	4.265(83)	2.575(49)	0.736(23)	0.295(28)	5	5
WD2111+498	DA	34386	5.018(87)	3.118(61)	1.703(32)	0.426(14)	0.142(26)	2	
WD2115+339	DOV	170000	4.739(83)	2.761(54)	1.418(27)	0.404(14)	0.175(22)	5	14
WD2115–560	DAZ	9700	3.618(63)	2.582(50)	1.641(31)	1.034(32)	0.913(35)	5	4,15
WD2117+539	DA	15394	13.49(23)	7.88(15)	4.830(91)	1.320(40)	0.532(26)	3	5
WD2126+734	DA	14341	9.21(16)	5.55(11)	3.610(68)	0.963(30)	0.377(17)	2	5,7
WD2130–047	DB	17500	1.717(30)	1.016(20)	0.573(11)	0.1477(78)	0.073(32)	5	16
WD2134+218	DA	17814	1.909(33)	1.006(20)	0.729(14)	0.1672(75)	...	5	17
WD2136+828	DA	16400	6.64(12)	4.107(80)	2.662(50)	0.622(20)	0.215(20)	5	
WD2140+207	DQ	8860	10.24(18)	6.90(14)	4.520(85)	1.252(39)	0.434(26)	5	
WD2148+286	DA	60240	49.26(86)	27.23(53)	15.90(30)	4.22(13)	1.599(51)	3	
WD2149+021	DAZ	17938	8.34(14)	4.965(97)	2.918(55)	0.788(25)	0.288(28)	5	5
WD2211–495	DA	58149	16.83(29)	9.24(18)	5.85(11)	1.384(42)	0.507(29)	5	
WD2216–657	DZ	12082	2.439(42)	1.617(32)	1.031(20)	0.2913(96)	0.098(14)	3	
WD2246+223	DA	10330	2.925(51)	1.921(38)	1.202(23)	0.313(10)	0.122(16)	3	
WD2316–173	DB	12918	3.417(60)	2.151(42)	1.324(25)	0.316(12)	0.138(29)	5	
WD2326+049	DAV	11820	8.91(16)	6.03(12)	5.60(11)	8.80(26)	8.64(26)	5	4
WD2329–291	DAWK	26620	2.451(43)	1.481(29)	0.895(17)	0.2173(89)	0.082(32)	5	
WD2331–475	DAZ	50400	3.562(62)	2.038(40)	1.275(24)	0.2974(99)	0.138(16)	3	
WD2333–165	DA	9789	5.83(10)	3.344(65)	2.181(41)	0.558(18)	0.207(19)	3	
WD2359–434	DAP	8690	14.58(25)	10.97(21)	7.01(13)	1.841(56)	0.692(34)	5	

Note. — Infrared fluxes for stars in this survey. Fluxes are in units of mJy. Values in parentheses are uncertainties for the two least significant digits for each measurement. Ap refers to the aperture size in pixels used in the photometry. Temperatures and spectral types are taken from McCook & Sion (1999) or Table 5.3, unless otherwise noted. JHK photometry taken from the 2MASS survey and is presented here for convenience. Notes are as follows: (1) Also known as GD408. Spectral type and temperature from Wolff *et al.* (2002). (2) Spectral type taken from Kilic *et al.* (2006a). (3) Also GD619. Spectral type and temperature from Kilkenny *et al.* (1988). (4) No colour correction applied to this photometry. (5) Spectral type taken from Simbad. (6) Temperature from Giovannini *et al.* (1998). (7) Photometry of this star is contaminated by the flux from a nearby object and is not trustworthy. (8) Photometry of this object is affected by the diffraction spike of a bright foreground object. (9) Temperature from Finley *et al.* (1997). (10) 8 μ m photometry slightly contaminated by background nebulosity. (11) Spectral type and temperature from Thejll *et al.* (1991). (12) Spectral type and temperature from Liebert *et al.* (2005). (13) Temperature from Sion *et al.* (1988). (14) Temperature from Werner *et al.* (1996). (15) Temperature from Koester & Wilken (2006). (16) Temperature from Oke *et al.* (1984). (17) Object not detected at 8 μ m.

Table 5.3. Survey Objects with Detected Photospheric Metals

Name	[Ca/H]	T_{eff}	Type	Ref
WD0002+729	-11.4	13750	DBZ	D93
WD0005+511	...	47083	DO	H03
WD0455-282	...	57273	DA	H03
WD0501+527	...	40588	DA	H03
WD0552-041	...	5060	DZ	E65
WD0621-376	...	48333	DA	H03
WD0843+358	-9.6	17103	DBZ	D93
WD1202-232	-9.8	8567	DAZ	K06
WD1337+705	-6.7	20970	DAZ	K06
WD1626+368	-8.65	8640	DBZ	W02
WD1645+325	...	24600	DB	H03
WD1822+410	-8.15	14350	DZ	W02
WD2032+248	...	20039	DA	H03
WD2105-820	-8.6	10200	DAZ	K05
WD2111+498	...	34386	DA	H03
WD2115-560	-7.6	9700	DAZ	K06
WD2149+021	-7.7	17938	DAZ	K06
WD2216-657	-9.1	12082	DZ	K05
WD2326+049	-6.4	13003	DAZ	K06
WD2331-475	...	50400	DA	H03

Note. — Objects with traces of metals in their photosphere in this survey. References: E65 Eggen & Greenstein (1965); D93 Dupuis *et al.* (1993); W02, Wolff *et al.* (2002); H03, Holberg *et al.* (2003); K05, Koester *et al.* (2005); K06, Koester & Wilken (2006)

Chapter 6

Planet Limits with *Spitzer*

6.1 Introduction

The *Spitzer Space Telescope* (Werner *et al.* 2004) has opened a new window into our understanding of extra-solar planets and brown dwarf stars (BDs). In particular, the IRAC camera (Fazio *et al.* 2004) has been used to study the mid-infrared atmospheres of BDs (Patten *et al.* 2006), to study their formation and to directly detect the light from a transiting planet by comparing the brightness in and out of eclipse (Charbonneau *et al.* 2005; Deming *et al.* 2005). *Spitzer* also holds the distinction of recording the first spectrum of an extra-solar planet, taken with the IRS camera.

The greater wavelength sensitivity of IRAC in the mid-infrared allows surveys for companions with greater sensitivity than is possible with ground-based near infrared techniques. BDs and planets have absorption bands at 3.5 and 5.5 μm from methane and water, but are brightest at interval wavelengths. For nearby objects, the direct flux from a low-mass companion is much greater than the IRAC point source sensitivity (see Burrows *et al.* 2003). Unfortunately, the contrast between star and companion is so great as to often hide the companion from detection.

This problem is mitigated by studying white dwarf stars (WDs). A WD is the final stage of stellar evolution for approximately 98% of all stars (e.g. Weidemann 2000). Nuclear burning has effectively ceased and their evolution is one of slow and

predictable cooling. Although their masses are $\sim 0.6 M_{\odot}$, their radii are typically less than $2 R_{\oplus}$ and consequently WDs are orders of magnitude less luminous than their main sequence progenitors for all but their very early existence. A sufficiently massive unresolved companion will appear as an excess flux over the continuum near $4.5 \mu\text{m}$, while providing very little flux at other wavelengths. Figure 1.4 shows the expected contrast between 12,000 K WD and planets of different masses.

There are three main formation mechanisms for planets around WDs discussed in the literature. The first, and most obvious, is that the planets formed from a proto-stellar disk at the same time as the progenitor main sequence star and is as old as the system. We will refer to these as “old” planets. As discussed in Livio & Soker (1984), planets can be destroyed during the AGB phase of the star, accrete mass to become more massive objects, or survive unscathed. Second, material expelled by the AGB may not escape the system but collapse into a disk from which planets can form (Jura & Turner 1998). Third, Livio *et al.* (2005) point out that the merger of 2 WDs would need to create a disk to conserve angular momentum, and that planets could form from that disk. These recently formed, or young, planets have less time to cool down and are therefore hotter and brighter than an old planet. Planets that accrete matter from AGB ejecta will also be reheated to close to their zero-age temperature and should be considered as young objects.

We initiated a survey (described in Chapter 5) to search for companions to WDs by observing a sample at 4.5 and $8.0 \mu\text{m}$. We hoped to detect excess flux from the companion object at $4.5 \mu\text{m}$ over the WD continuum as determined from fitting models to optical and near infrared photometry. Our survey was successful in discovering a possible BD. In this chapter we place limits on the mass of companions to a sample of the other stars in the survey and compare these limits to predictions based on the different suggested pathways for planet formation.

6.2 Observations and Reductions

6.2.1 The Survey

We performed a magnitude limited survey of 124 WDs brighter than $K=15$ to detect excess at $4.5\,\mu\text{m}$ indicative of a companion. Our target selection and our data reduction technique are described in Mullally *et al.* (2007) and in Chapter 5. Briefly, we observed each WD simultaneously at 4.5 and $8.0\,\mu\text{m}$ with the IRAC camera on *Spitzer* for 5 dithered exposures of 30s each for a total integration time of 150s. We performed aperture photometry on the basic calibrated data (bcd) frames, applying the corrections suggested in the IRAC data handbook and Reach *et al.* (2005b). Our procedure is identical to that described in Chapter 5 except that we use the bcd frames from the newer version of the pipeline (S14.0.0 instead of version S11.4.0). The pipeline flux conversion for channel 4 data was changed by 3% in the interim¹. Of our 124 objects, we were successful in obtaining uncontaminated photometry at $4.5\,\mu\text{m}$ for 77 DAs, 19 DBs and 3 sundry objects.

6.2.2 Testing our models and photometry

Before proceeding to determine the excess flux at $4.5\,\mu\text{m}$ (or lack thereof) we need to check that our extraction method is producing a reasonable result. The obvious approach is to compare the flux of a known isolated object to that predicted from a model. Unfortunately our models are untested because this is one of the first surveys of WDs at these wavelengths; worse we do not know *a priori* which stars are free of companions. Fortunately, with such a large sample, we can compare the average properties of our stars against model predictions and look for bulk agreement between the two. This does not demonstrate that either one or the other is correct (i.e. that either the observations or the models are a close match to reality), but can at least confirm that they agree with each other.

We selected all DA stars between 7 and 60,000 K and fit their optical and near infrared fluxes to DA models kindly provided by D. Koester (see Finley *et al.*

¹See <http://ssc.spitzer.caltech.edu/archanaly/plhistory/irac.html>

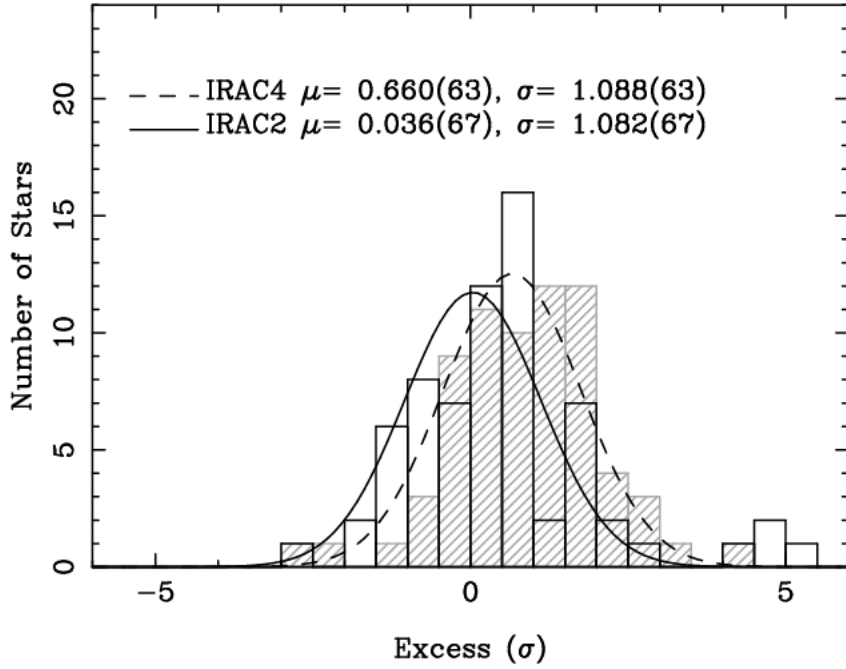


Figure 6.1 Histogram of distribution of excesses and deficits in the IRAC bands compared to models for DA WDs between 7,000 and 60,000 K. In channel 2, the distribution of excesses over models is well described by a Gaussian distribution of mean 0 and standard deviation 1 indicating that the models and photometry are in agreement. The measured fluxes in channel 4 are on average higher than predicted by models.

1997) with appropriate temperatures. We then subtracted the flux predicted by the model in the two IRAC channels from the measured value and divided this excess (or deficit) by the quoted error bar. If the models do a good job at predicting the flux, and there are no systematic effects in the photometry, the mean of this value over the sample should be zero and the observed excesses and deficits should scatter about this value according to a Gaussian distribution. Further, if the sizes of the error bars are correct, the standard deviation of this distribution should be one.

In Figure 6.1 we show a histogram of the excess or deficit in each band, and the parameters of the best fit Gaussian. Channel 2 shows a mean of zero and a variance of 1, within the uncertainties. This indicates that, on average, the observed flux from our WDs agrees with what is expected from the models at $4.5 \mu\text{m}$

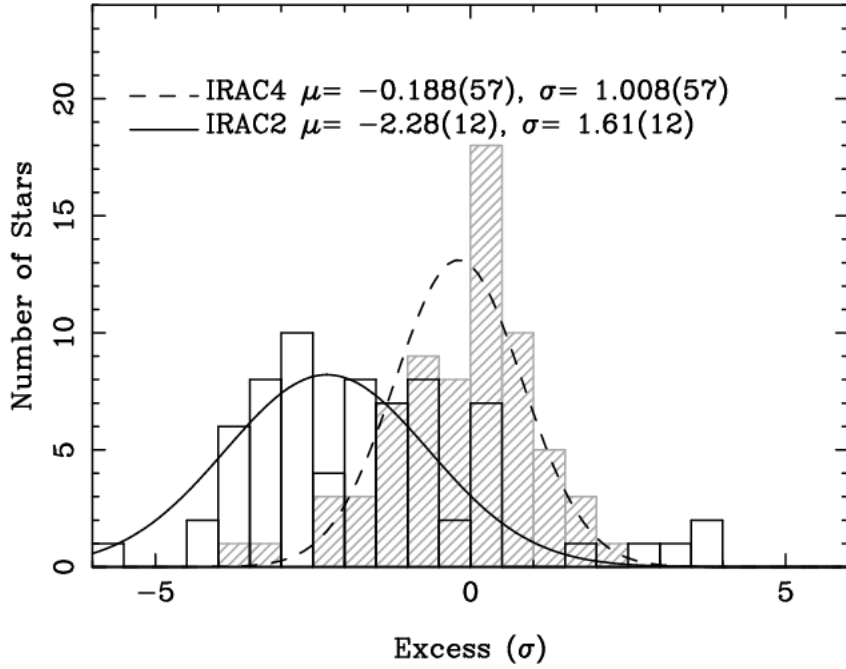


Figure 6.2 Same as Figure 6.1, but measuring the excess flux over a blackbody model. Due to its failure to accurately describe the SED in the optical and near-infrared, a blackbody consistently overestimates the flux at $4.5 \mu\text{m}$.

and demonstrates that our models and photometry are consistent.

For Channel 4, the variance is again close to one, but the mean of the distribution is significantly greater than zero. This could be due to a number of reasons. Firstly there may be a systematic offset in either the photometry or the models. An error existed in version S11 of the bcd pipeline for channel 4, and there may well still be an undiscovered problem in S14. The models may be missing an emission feature in this band, however it is difficult to think of any mechanism to create such a feature. It is also possible that observed flux is higher due to the presence of faint, cool circumstellar material around a significant number of stars.

As we do not have models available for the DBs and sundry WD spectral types, we investigated the use of a blackbody as a model of the spectrum. We repeat the test on the same sample of stars as shown in Figure 6.1 using a blackbody instead of a DA model. We show the results in Figure 6.2. The mean of the distribution

for channel 2 is significantly below zero indicating that the blackbody is a poor model choice. We reluctantly conclude that we currently have no good model for the non-DAs and discard them from the sample.

Notes on individual objects

Four objects show excesses greater than 4σ . We discuss these objects individually here.

WD1407-475.— The excess in channel 2 is 4.3σ higher than expected while channel 4 is 2σ , although only weakly detected. There are no significant deviations in the photometry at other wavelengths. The field is moderately crowded, but there is no evidence of a close companion. After removing the contribution from the WD photosphere we determined that the excess at $8\mu\text{m}$ is greater than that at $4.5\mu\text{m}$, leading to the conclusion that the source of the excess is more likely to be a debris disk than a companion planet. However, the low significance of the excess at $8\mu\text{m}$ means that neither hypothesis is strongly supported.

WD1716+020.— This star is very close to a bright object that is almost certainly leaking flux into the aperture.

WD1408+323.— The flux in channel 2 is 4.8σ higher than predicted. Examination of the images shows no evidence of contamination from a field object but the flux in channel 4 is also high by 2σ similar to WD1407, leading to a similar conclusion.

WD1713+332.— Shows the largest excess, 5.2σ in channel 2. However, the measured flux at $8\mu\text{m}$ is a strong function of the aperture size used, suggesting that the photometry is affected by flux from a nearby object. Examination of the mosaic image shows a faint object ≈ 5 pixels away which is the likely culprit for this excess.

6.2.3 Constraining the excess at $4.5\mu\text{m}$

To measure or constrain the excess at $4.5\mu\text{m}$, we need to first calculate the expected flux in this band. We do that by fitting a model atmosphere for the appropriate

temperature to the optical, near-infrared and $8\mu\text{m}$ photometry to determine the continuum flux. We obtained V, and where available B, photometry from McCook & Sion (1999), and near infrared fluxes (JHK) from the 2MASS survey (Skrutskie *et al.* 2006). Although the $8\mu\text{m}$ flux is on average slightly higher than expected, it still provides an important additional datum to constrain the fit. We determined the upper limit on the excess flux at $4.5\mu\text{m}$ using the formula

$$\begin{aligned} &\text{if } (F_{obs} > F_{mod}) \\ &\quad \text{excess} = F_{obs} - F_{mod} + \Delta F \\ &\text{else} \\ &\quad \text{excess} = \Delta F \end{aligned}$$

where F_{obs} is the observed flux at $4.5\mu\text{m}$, F_{mod} is the flux predicted by the model, and ΔF is the measured uncertainty in the observed flux.

6.2.4 Measuring the Contrast

Converting a fractional excess into a companion mass (or in this case a limit on companion mass) requires an estimate of the luminosity contrast between the star and any companion. We estimate the WD luminosity from spectroscopic parameters. The luminosity of a planet is more difficult to determine because it depends on the age. While the age can be estimated from the properties of the WD, there are considerable uncertainties in this calculation, as discussed below.

Table 6.1. Infrared Fluxes and Excesses

Name	Type	T _{eff} (K)	log <i>g</i>	IRAC 2 (mJy)	IRAC 4 (mJy)	Ap	Excess	Note
WD0004+330	DA	49593(200)	7.67(05)	0.2220(86)	0.062(20)	5	1.1638	
WD0047−524	DA	17660(200)	7.82(05)	0.1988(73)	0.088(14)	3	1.0351	
WD0050−332	DA	35636(200)	7.83(05)	0.311(10)	0.124(16)	3	1.0464	
WD0101+048	DA	8305(200)	8.01(05)	0.789(25)	0.313(25)	5	1.0740	
WD0126+101	DA	8614(200)	7.63(05)	0.471(15)	0.188(19)	3	1.0573	
WD0126−532	DA	16009(200)	7.94(05)	0.1796(66)	0.058(14)	3	1.0554	
WD0133−116	DAV	12229(200)	7.90(05)	0.302(10)	0.102(15)	3	1.0345	
WD0134+833	DA	18306(200)	7.94(05)	0.574(19)	0.199(21)	5	1.1103	
WD0148+467	DA	13710(200)	7.91(05)	1.256(39)	0.427(28)	5	1.0327	
WD0227+050	DA	19085(200)	7.78(05)	0.764(24)	0.288(26)	5	1.0521	
WD0231−054	DA	15569(200)	8.57(05)	0.2244(87)	0.087(27)	5	1.0437	
WD0255−705	DA	10582(200)	8.13(05)	0.412(13)	0.166(16)	3	1.0642	
WD0310−688	DA	15480(200)	8.02(05)	3.025(91)	1.106(39)	5	1.0298	
WD0316+345	DA	14880(200)	7.61(05)	0.2244(80)	0.080(18)	3	1.0337	
WD0407+179	DA	13620(200)	7.79(05)	0.280(10)	0.108(30)	5	1.0739	
WD0410+117	DA	20790(200)	7.94(05)	0.2611(97)	0.115(31)	5	1.0511	
WD0431+126	DA	21340(200)	8.04(05)	0.1815(76)	0.038(29)	5	1.0414	
WD0438+108	DA	27238(200)	8.07(05)	0.2141(76)	0.092(19)	3	1.0353	
WD0446−789	DA	22760(390)	7.70(06)	0.353(12)	0.153(13)	3	1.0958	
WD0507+045	DA	11630(200)	8.17(05)	0.2204(76)	0.231(20)	2	1.1041	(2)
WD0549+158	DA	32863(200)	7.77(05)	0.437(14)	0.245(20)	2	1.1343	
WD0612+177	DA	25133(200)	7.84(05)	0.449(15)	0.228(23)	2	1.2450	(2)
WD0644+375	DA	21009(200)	8.05(05)	1.347(42)	0.482(32)	5	1.0592	
WD0732−427	DAE	14540(370)	8.15(06)	0.2611(92)	0.117(24)	3	1.0345	
WD0839−327	DA	9129(200)	7.87(05)	4.20(13)	1.551(50)	3	1.0500	
WD1031−114	DA	25135(200)	7.79(05)	0.481(16)	0.187(25)	5	1.0320	
WD1053−550	DA	13575(200)	7.87(05)	0.2658(93)	0.103(15)	3	1.0654	
WD1105−048	DA	15540(200)	7.82(05)	0.655(21)	0.259(29)	5	1.0309	
WD1134+300	DA	21231(200)	8.42(05)	0.874(27)	0.283(29)	5	1.0306	
WD1202−232	DAZ	8791(200)	8.16(05)	2.034(62)	0.731(30)	3	1.0496	
WD1223−659	DA	7740(200)	8.13(11)	0.951(30)	0.382(18)	2	1.1048	
WD1236−495	DAV	11779(200)	8.82(05)	0.467(15)	0.164(15)	3	1.1007	
WD1254+223	DA	38899(200)	7.76(05)	0.310(10)	0.093(18)	3	1.0499	
WD1327−083	DA	13754(200)	7.88(05)	1.385(42)	0.476(25)	3	1.0294	
WD1337+705	DAZ	20414(200)	7.89(05)	0.754(24)	0.288(21)	5	1.0947	
WD1407−475	DA	21080(400)	8.00(06)	0.2094(77)	0.048(14)	2	1.2346	
WD1408+323	DA	18410(200)	7.97(05)	0.292(10)	0.120(20)	5	1.2432	
WD1425−811	DA	12304(200)	8.19(05)	0.594(20)	0.232(20)	5	1.0329	
WD1509+322	DA	14659(200)	8.00(05)	0.2629(89)	0.105(14)	3	1.0629	

Table 6.1—Continued

Name	Type	T _{eff} (K)	log <i>g</i>	IRAC 2 (mJy)	IRAC 4 (mJy)	Ap	Excess	Note
WD1531–022	DA	18870(200)	8.39(05)	0.2474(85)	0.104(17)	3	1.0545	
WD1559+369	DAV	11160(200)	8.04(05)	0.2679(89)	0.105(12)	2	1.0305	
WD1606+422	DA	12539(200)	7.71(05)	0.408(13)	0.160(13)	2	1.0327	
WD1611–084	DA	40400(300)	7.94(05)	0.1891(79)	0.096(28)	5	1.1300	
WD1615–154	DA	29711(200)	7.97(05)	0.318(11)	0.097(17)	3	1.0657	
WD1631+396	DA	52394(200)	8.00(05)	0.1655(61)	0.056(15)	3	1.0965	(1)
WD1637+335	DA	10059(200)	8.15(05)	0.2645(90)	0.083(15)	2	1.0324	
WD1647+591	DAV	12460(200)	8.28(05)	1.718(52)	0.628(28)	5	1.0304	
WD1655+215	DA	9274(200)	8.17(05)	0.518(16)	0.182(15)	3	1.0496	
WD1659–531	DA	14659(200)	8.02(05)	0.441(15)	0.114(16)	2	1.0322	
WD1713+332	DA	22107(200)	7.41(05)	0.1882(66)	0.062(12)	2	1.2667	
WD1716+020	DA	13222(200)	7.81(05)	0.296(10)	0.108(18)	2	1.2333	
WD1756+827	DA	7270(200)	7.98(05)	0.785(24)	0.277(20)	5	1.0538	
WD1919+145	DA	14880(200)	8.07(05)	1.102(40)	0.570(70)	2	1.6000	(2)
WD1935+276	DAV	12130(200)	8.05(05)	0.888(28)	0.311(20)	3	1.0620	
WD1936+327	DA	21245(200)	7.78(05)	0.331(11)	0.110(17)	3	1.0927	
WD1942+499	DA	34086(200)	7.97(05)	0.1103(50)	0.031(13)	3	1.1352	
WD1943+163	DA	19410(200)	7.80(05)	0.2339(89)	0.132(14)	2	1.0418	(2)
WD1953–011	DAP	7873(200)	8.24(05)	1.259(39)	0.491(23)	3	1.1450	(2)
WD2004–605	DA	43169(200)	8.25(05)	0.332(11)	0.169(27)	5	1.1105	
WD2007–303	DA	14840(200)	7.92(05)	1.440(44)	0.571(33)	5	1.0300	
WD2014–575	DA	27627(200)	7.80(05)	0.2308(80)	0.093(20)	3	1.0327	
WD2028+390	DA	24426(200)	7.88(05)	0.374(13)	0.125(75)	2	1.1449	
WD2032+248	DA	19925(200)	7.84(05)	2.330(71)	0.821(34)	5	1.0471	
WD2039–202	DA	19987(200)	7.88(05)	1.056(32)	0.370(23)	3	1.0301	
WD2039–682	DA	16189(220)	8.47(05)	0.498(16)	0.185(21)	5	1.0313	
WD2047+372	DA	14070(200)	8.21(05)	0.772(25)	0.217(17)	2	1.0497	
WD2105–820	DAZ	10418(200)	8.22(05)	0.735(23)	0.280(27)	5	1.1150	
WD2111+498	DA	39623(200)	7.93(05)	0.425(14)	0.109(20)	2	1.0894	
WD2117+539	DA	14239(200)	7.81(05)	1.316(40)	0.518(26)	3	1.0304	
WD2126+734	DA	15289(200)	7.84(05)	0.961(30)	0.366(16)	2	1.1320	(2)
WD2134+218	DA	18310(200)	8.07(05)	0.1771(73)	...	5	1.0956	(3)
WD2136+828	DA	16940(200)	7.84(05)	0.619(20)	0.210(19)	5	1.0308	
WD2149+021	DAZ	17616(200)	7.95(05)	0.786(25)	0.284(27)	5	1.0390	
WD2246+223	DA	10515(200)	8.71(05)	0.313(10)	0.139(15)	3	1.0329	
WD2331–475	DAZ	53046(200)	7.82(05)	0.2971(99)	0.135(16)	3	1.0325	
WD2333–165	DA	10634(200)	8.00(05)	0.557(18)	0.201(19)	3	1.0421	(1)
WD2359–434	DAP	8621(200)	8.74(05)	1.838(56)	0.666(32)	5	1.0736	

Note. — T_{eff} and log *g* taken from the literature, see text. The excess is defined so a value of 1.0 indicates no excess, and 1.1 is a 10% excess over that predicted by the model. (1) T_{eff} obtained from a blackbody fit, and log *g* assumed to be 8.0. (2) Flux at 8 μ m contaminated by light from a nearby field object. This value should be considered an upper bound only. (3) Object too faint to be detected at 8 μ m.

Determining the luminosity of the WD

The luminosity of any physical object is given by $L \propto R^2 T_{\text{eff}}^4$. Optical spectroscopy is a popular method to determine T_{eff} and $\log g$ of WDs and comparing these two values to models yields the radius. We performed a literature search to determine the effective temperature and gravity of each star. A large number of overlapping surveys exist and we took a weighted mean of the parameters listed in one or more of Bergeron *et al.* (2001, 2004); Finley *et al.* (1997); Gianninas *et al.* (2005); Holberg & Bergeron (2006); Karl *et al.* (2005); Kawka *et al.* (2007); Koester *et al.* (2001, 2005); Koester & Wilken (2006) and Liebert *et al.* (2005). Authors differ on whether the uncertainty they quote is the internal uncertainty of the fit or the systematic uncertainty, which is generally agreed to be ≈ 200 K and 0.05 for T_{eff} and $\log g$ respectively (e.g. Fontaine *et al.* 2003). To fairly weight these measurements we insisted that the uncertainty be no smaller than these values. We assumed the same uncertainties when no error bars were quoted.

We list the values for T_{eff} and $\log g$ used in Table 6.1. Having obtained these values, we then interpolate over the grid of models from Holberg & Bergeron (2006) to determine a radius and hence a luminosity.

Luminosity of Companions

Burrows *et al.* (2003) published atmosphere models for planets and BDs for 1–25 M_J and ages ranging from 100 million to 5 billion years. Similar to WDs, the evolution of sub-stellar objects is one of slow, monotonic cooling and dimming. To determine the flux from such an object with a given mass, it is therefore necessary to know the age. For young objects, the age is the cooling time of the WD, for old objects it is the total age of the system. In principle the age of a system containing a WD is straightforward to determine. Comparing the WD temperature and gravity to models determines the mass and cooling time. Comparing the mass to the initial-final mass relation (IFMR) for WDs gives the progenitor mass, from which the progenitor lifetime can be determined. The total age is just the sum of the cooling age and the progenitor lifetime.

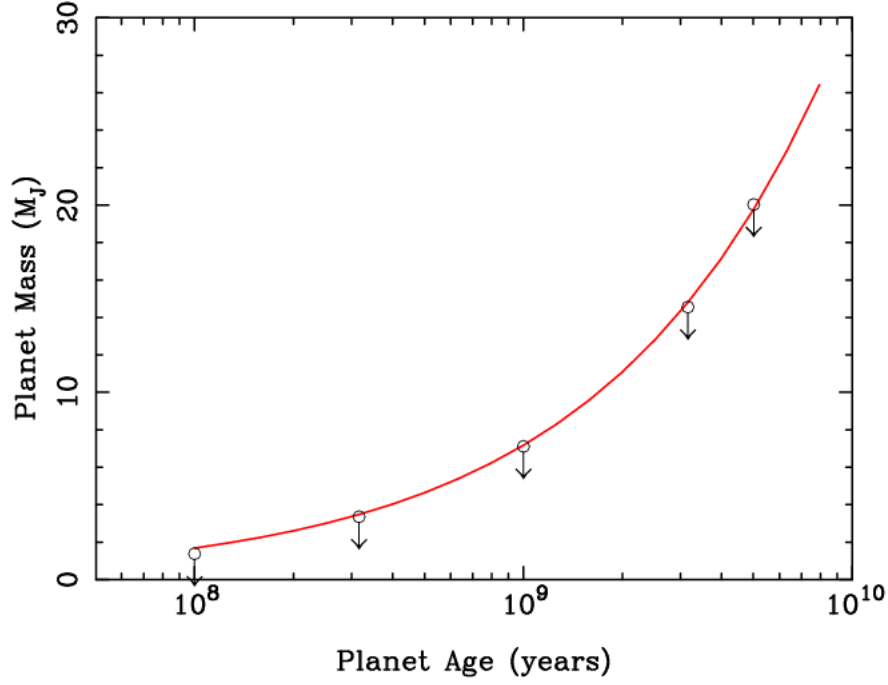


Figure 6.3 Our ability to detect planets decreases as the planet ages and cools. This plot shows the upper bound that can be placed on the mass of a planet around WD0316+345 as a function of the age of the planet. As the planet ages, it cools and becomes dimmer, reducing the contrast against the flux from the WD. The solid line is a fit of an exponential function to the data. For each age, the presence of planets with masses above the line can be ruled out, while masses below the line are undetectable.

In practice, this approach is much less certain than it appears. Although WD cooling models are well established and generally trustworthy, estimating the progenitor lifetime is more difficult. The IFMR is still not well constrained, especially at the low and high-mass ends, and the initial mass is a strong function of the final mass. Willams (2006) and Ferrario *et al.* (2005) differ in their determination of the initial mass of a $0.64 M_{\odot}$ WD by $\approx 0.4 M_{\odot}$. Also, it is not known to what extent the IFMR is valid for individual stars, or whether it is only statistically valid. Compounding the difficulty, small differences in initial mass can lead to wildly different lifetimes. For example the BD candidate system WD1234+481 discussed in

the previous chapter, has spectroscopic parameters of 55,040(975) K and $\log g = 7.78(05)$. These give a WD mass of $0.57(02) M_{\odot}$, a progenitor mass of between 1 to $1.8 M_{\odot}$ (Weidemann 2000), and a main sequence lifetime of between 1.2 and 12 Gyr (Girardi *et al.* 2000). Any calculation for the total age of a WD should therefore be treated with considerable skepticism.

Burrows' grid of planet models spans ages from 0.1 to 5 Gyr. For each star and model age, we calculate the maximum-mass planet that could be present in the system without producing an excess flux that would have been detectable in our data for that star. We fit an exponential curve to these mass limits as a function of $\log_{10}(\text{age})$ and interpolate to find the mass limit for the young and old ages. The exponential function is not chosen based on some theoretical understanding of the cooling process, but because empirically it fits the data well. For assumed ages older than 5 Gyr we extrapolate to determine a mass limit. For assumed ages less than 0.1 Gyr extrapolation is untrustworthy and so we conservatively choose the mass limit for 0.1 Gyr.

6.2.5 Range of orbital separation probed

As well as constraining the mass of any companions around the WD, we also want to determine the range of orbital separations for which these mass limits are applicable. Because we are only looking for unresolved companions, we are sensitive to companions close enough to their parent WD that their projected separation is less than the point response function of the star on the telescope. According to Table 6.1 of the *Spitzer* Observing Manual, the FWHM of a point source in channel 2 is $1.72''$. We measure the distance by interpolating the spectroscopic T_{eff} and $\log g$ over the model grid of Holberg & Bergeron (2006) to determine a bolometric magnitude, a bolometric correction and hence an absolute magnitude, which we then compare to the apparent magnitude to determine the distance. Distance and angular separation gives the projected orbital separation.

To test the validity of this method we obtained parallaxes for a subset of the sample from Simbad² and compared the distance as measured from parallax to

²<http://simbad.u-strasbg.fr/simbad/sim-fid>

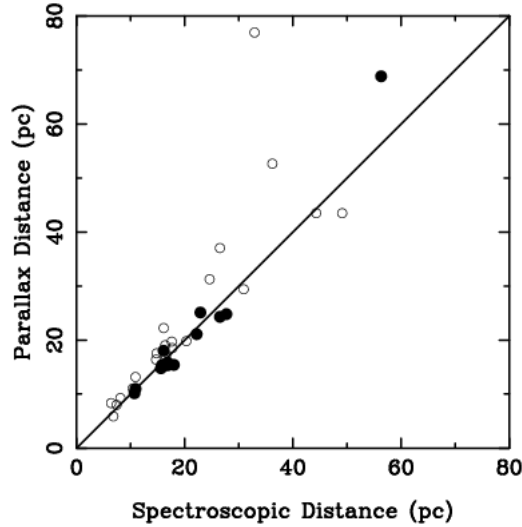


Figure 6.4 Comparison of distance to stars as determined by spectroscopy and from parallax measurements taken from Simbad. Filled circles are parallax measurements from Hipparcos (Perryman *et al.* 1997) while open circles indicate measurements assigned lower confidence by Simbad and are taken from Jenkins (1952); Harrington & Dahn (1980), and Holberg *et al.* (2002). The solid line is not a fit but indicates a one to one correspondence. With some exceptions, there is good agreement between the two methods of determining distance.. The 3 stars with abnormally high parallax based distance are, in order of increasing spectroscopic distance, WD0133-116 (R548), WD1509+322 and WD0501+527. R548 is known to have a parallax inconsistent with its magnitude and luminosity (Mullally & de Graff 2005)

that determined by our spectroscopic approach. Although Figure 6.4 shows that we obtain good agreement for most objects, it should be noted that this is not an independent test as our models are already tuned to give the best agreement between spectroscopic and parallactic distance for a subset of stars (see Bergeron *et al.* 1995, for a discussion). On the other hand, T_{eff} is much easier to measure for the more distant stars than parallax, so a spectroscopy based distance measurement averages over many good parallax measurements and often produces a better distance estimate than parallax could do alone.

6.3 Results and Discussion

In Figure 6.5 we show the limits we place on companions if we assume an age (and luminosity) consistent with the total age of the system. Each box represents the limits placed around one WD, with planets to the upper left detectable and planets to the lower right not detectable. We also show the population of known extra-solar planets as filled circles, although it should be remembered that the masses of most of these planets are lower bounds only. Our limits span a range from about $4 M_J$ up to the transition between BDs and main sequence stars at $75 M_J$. However, as discussed above, these limits are dependent on our estimates of the total age of the system which are subject to a number of theoretical uncertainties. At best, these

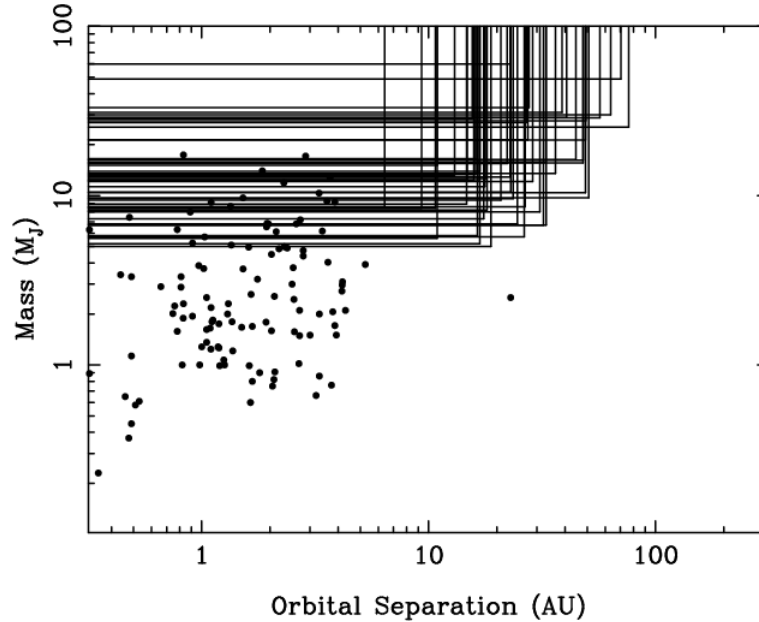


Figure 6.5 Limits on old planets with ages equal to the estimated total age of the system (WD cooling time plus progenitor lifetime). As discussed in the text, total lifetime is an uncertain quantity, and these limits should be treated with lower confidence than those shown in Figure 6.6. Each box represents the limit placed around one WD, with planets to the upper left detectable, and planets to the lower right too faint to be detected. These mass limits are in the range of known massive extra-solar planets (shown here as filled circles).

limits should be considered to be best guesses.

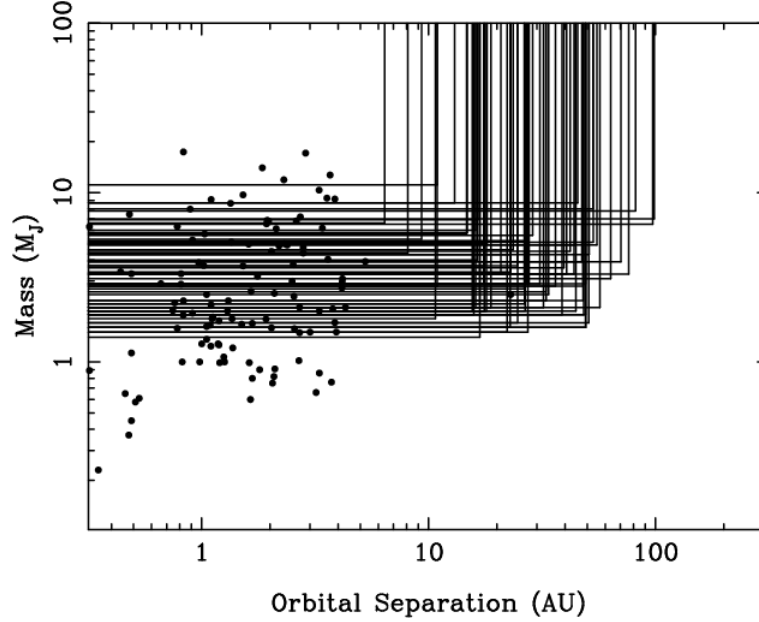


Figure 6.6 Same as Figure 6.5 but assuming the age of the planet is equal to the cooling time of the WD. These ages, and hence mass limits on young planets, are less uncertain than those calculated for older planets

Much more certain – and more interesting – are the limits we place on young planets, i.e. those formed or reheated during the AGB phase of stellar evolution. Based on the spectroscopically determined temperature and gravity, we can determine the time since the WD formation with much less uncertainty. The limits we place on hot, young planets are shown in Figure 6.6 and span a range from 1–10 M_J , well within the mass range of known extra-solar jovian planets. If these young planets existed, we would have detected them. The fact that we don't implies that the processes which have been suggested to create such planets do not apply, or at the very least do not efficiently create planets. We can be confident that the method of creating jovian planets directly from a disk of material left over from the AGB (Jura & Turner 1998) is not common. Also, we find no evidence of close non-interacting BD companions that we would expect if the mechanism suggested by (Livio & Soker 1984) applies. Livio's mechanism may still operate, but needs to be able to create close interacting binaries (CVs) without creating close non-interacting binaries.

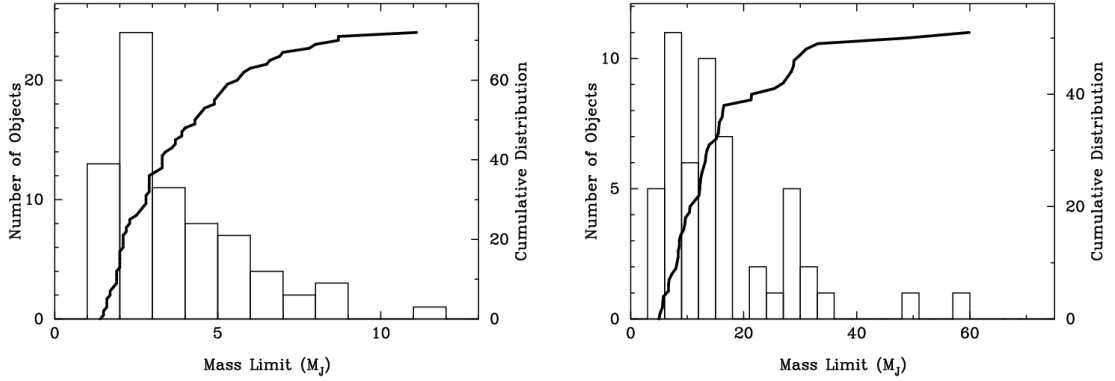


Figure 6.7 Histogram and cumulative distribution of upper mass limits. The histogram shows the number of stars with upper limits of a given mass (with numbers on the left axis), while the cumulative distribution shows the total number of systems with mass limits less than the given value (with numbers of the right axis). For example, in the figure on left, 24 objects have mass limits $\lesssim 2\text{--}3 M_J$, but 36 objects mass limits $< 3 M_J$. The figure on left is for young systems, with planetary ages equal to the cooling time of the WD, while the figure at right shows limits for companions as old as the total age of the system

Livio *et al.* (2005) suggest the formation of high-mass ($> 0.8 M_\odot$) WDs from the merger of two lower mass WDs will produce a metal-rich debris disk ripe for planet formation. By comparing the ratio of high and low-mass WDs to the ratio of their progenitor main sequence stars, Liebert *et al.* (2005) estimate that up to 80% of high-mass WDs are formed through mergers. We observe 8 WDs with masses greater than $0.8 M_\odot$, and in each case place limits on young companions of $< 3\text{--}7 M_J$ (see Figure 6.8). The radius, and hence luminosity, of a WD decreases with mass so our limits on companions generally improve with increasing mass. However, Livio *et al.* predict that a typical merger will produce a disk mass of $\sim 0.007 M_\odot$ or $\sim 7 M_J$. We would not expect a single planet to accrete all the mass from a disk, and so our results are not inconsistent with undetected planets $\lesssim 1 M_J$ around these stars. In any event, with such a small sample of high-mass stars, we can only place weak constraints on the frequency of companion planets.

Although we have placed tight constraints on the presence of young planets around WDs, this does not imply that planetary companions to WDs in general are rare. Our limits on planets that formed co-eval with the progenitor main sequence star, while uncertain, are at best sensitive to high-mass planets. Radial velocity

studies (Marcy *et al.* 2005) show that the frequency of planets is inversely proportional to mass, so massive planets are comparatively rare. The population of old Jupiter mass planets remains unconstrained.

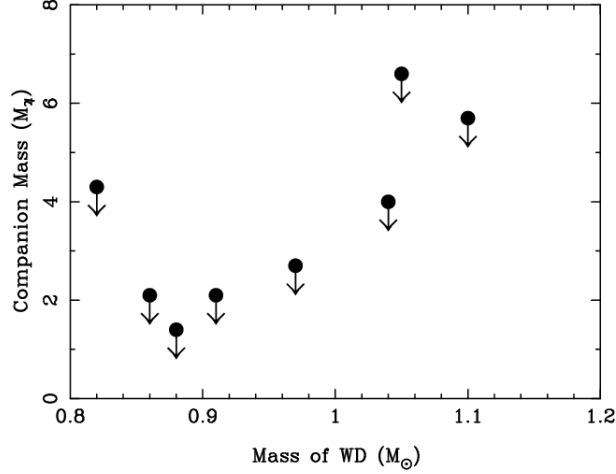


Figure 6.8 Limits on companions around massive WDs. Livio *et al.* (2005) predict that planets should be common around WDs in the high-mass range. Unfortunately, our sample size is too small, and our limits too loose, to constrain this hypothesis.

6.4 Conclusion

We place upper limits on the mass of planetary companions to a sample of 73 WDs. By fitting atmosphere models to optical and near infrared photometry, we calculate an upper bound on the excess flux observed at $4.5\mu\text{m}$ over the expected continuum. We then compare this excess to combined models of the WD with planets of different masses and ages to determine the upper limit on the mass of the companion. We place limits on companions for two ages, the cooling age of the WD, and the estimated total age of the system. Our findings are inconsistent with predictions of formation or reheating of planets during the AGB phase of stellar evolution, but still admit the possibility of a population of old, low-mass planets.

Table 6.2. Upper mass limits on Planets

Name	WD Age (Gyr)	Total Age (Gyr)	Initial Mass (M_{\odot})	Distance (pc)	Separation (AU)	Young (M_J)	Old (M_J)
WD0047–524	0.10	9.4(8.8)	1.10(26)	49.3	84.4	1.6	27.7
WD0050–332	0.01	3.1(1.2)	1.60(20)	63.5	108.6	3.1	30.0
WD0101+048	1.01	3.6(1.5)	1.73(24)	16.1	27.5	6.0	13.3
WD0126+101	0.62	—	—	26.5	45.4	5.2	—
WD0126–532	0.15	3.3(1.9)	1.60(26)	47.9	82.0	2.3	16.2
WD0133–116	0.32	5.8(4.4)	1.29(20)	32.9	56.3	2.6	15.7
WD0134+833	0.10	3.0(1.6)	1.65(26)	27.0	46.2	2.9	27.0
WD0148+467	0.24	4.7(3.5)	1.39(23)	16.8	28.8	2.2	13.9
WD0227+050	0.07	—	—	26.5	45.3	2.2	—
WD0231–054	0.49	1.75(10)	5.21(32)	26.4	45.2	2.7	5.7
WD0255–705	0.69	2.23(36)	2.52(25)	23.6	40.4	4.6	9.6
WD0310–688	0.19	2.35(69)	1.99(32)	10.7	18.3	1.8	8.4
WD0316+345	0.12	—	—	48.2	82.5	1.9	—
WD0407+179	0.21	—	—	39.5	67.6	3.6	—
WD0410+117	0.06	2.8(1.3)	1.70(26)	44.5	76.2	2.0	16.3
WD0431+126	0.07	1.91(43)	2.23(32)	49.1	84.0	1.6	10.4
WD0438+108	0.02	1.58(33)	2.51(32)	50.8	86.9	1.7	9.7
WD0446–789	0.03	—	—	47.3	81.0	3.9	—
WD0507+045	0.57	1.94(31)	2.80(33)	28.7	49.1	5.6	12.1
WD0549+158	0.01	5.8(4.0)	1.27(19)	53.0	90.8	8.0	—
WD0612+177	0.02	4.8(3.6)	1.36(22)	45.4	77.6	8.7	—
WD0644+375	0.07	1.86(40)	2.26(28)	18.0	30.9	2.0	12.6
WD0732–427	0.30	1.70(33)	2.74(37)	33.0	56.5	2.3	6.7
WD0839–327	0.68	—	—	8.1	13.8	4.4	—
WD1031–114	0.02	8.1(6.0)	1.14(22)	38.7	66.3	1.9	31.0
WD1053–550	0.23	7.1(4.7)	1.20(23)	40.6	69.5	3.3	28.9
WD1105–048	0.14	—	—	24.7	42.2	1.7	—
WD1134+300	0.15	1.31(10)	4.43(33)	16.8	28.7	1.4	5.2
WD1202–232	1.27	2.71(34)	2.67(26)	9.3	15.9	5.3	8.4
WD1223–659	1.66	3.2(1.3)	2.52(55)	13.0	22.3	8.7	13.2
WD1236–495	1.49	3.13(21)	6.49(37)	14.7	25.2	5.7	8.9
WD1254+223	<0.01	4.4(2.4)	1.40(19)	70.4	120.4	3.9	48.8
WD1327–083	0.23	6.5(3.5)	1.23(20)	16.1	27.6	2.1	16.5
WD1337+705	0.06	4.0(2.2)	1.45(20)	27.7	47.5	2.9	33.1
WD1407–475	0.06	2.21(77)	2.00(35)	53.2	90.9	5.1	—
WD1408+323	0.10	2.6(1.2)	1.79(28)	44.3	75.8	4.9	—
WD1425–811	0.50	3.36(87)	1.68(16)	23.2	39.7	2.9	9.1
WD1509+322	0.21	2.5(1.2)	1.85(32)	36.2	62.0	2.8	13.5
WD1531–022	0.21	1.35(10)	4.22(36)	32.1	54.9	2.1	6.7

Table 6.2—Continued

Name	WD Age (Gyr)	Total Age (Gyr)	Initial Mass (M_{\odot})	Distance (pc)	Separation (AU)	Young (M_J)	Old (M_J)
WD1559+369	0.50	2.64(72)	2.01(32)	30.9	52.9	2.9	8.0
WD1606+422	0.25	—	—	33.8	57.9	2.5	—
WD1611–084	<0.01	1.91(33)	2.17(26)	81.7	139.8	7.8	—
WD1615–154	0.01	2.15(35)	2.02(24)	49.1	84.0	2.9	21.3
WD1631+396	<0.01	1.45(15)	2.64(19)	98.6	168.7	7.0	—
WD1637+335	0.84	2.30(31)	2.63(26)	24.6	42.1	3.7	6.8
WD1647+591	0.56	1.73(10)	3.47(35)	10.9	18.6	2.8	5.6
WD1655+215	1.11	2.51(32)	2.74(26)	18.1	30.9	5.0	8.2
WD1659–531	0.22	2.39(79)	1.97(32)	26.6	45.5	2.0	8.6
WD1756+827	1.36	4.7(3.0)	1.55(26)	14.8	25.3	5.8	12.4
WD1935+276	0.41	2.40(59)	2.10(32)	17.7	30.3	3.7	11.3
WD1936+327	0.04	—	—	43.8	75.0	3.3	—
WD1942+499	0.01	1.94(35)	2.16(28)	97.1	166.2	6.5	—
WD1943+163	0.06	—	—	49.1	84.0	1.9	—
WD1953–011	1.98	3.23(23)	3.14(27)	10.9	18.7	11.1	15.1
WD2004–605	<0.01	1.16(10)	3.83(31)	51.0	87.3	4.3	—
WD2007–303	0.19	4.0(3.0)	1.48(26)	15.8	27.1	1.9	12.3
WD2014–575	0.01	6.1(3.6)	1.25(22)	56.9	97.4	2.1	28.8
WD2028+390	0.03	3.6(2.0)	1.51(23)	42.0	71.8	4.5	—
WD2032+248	0.06	6.4(3.9)	1.23(23)	15.6	26.7	2.0	28.4
WD2039–202	0.06	4.2(3.5)	1.42(26)	22.2	38.0	1.5	15.5
WD2039–682	0.35	1.51(10)	4.65(37)	18.8	32.1	2.1	5.0
WD2047+372	0.36	1.62(18)	3.08(34)	17.5	29.9	2.9	7.3
WD2105–820	0.85	2.11(18)	3.07(27)	16.5	28.3	6.9	12.2
WD2111+498	<0.01	2.00(28)	2.11(23)	55.2	94.5	4.9	—
WD2117+539	0.19	—	—	17.6	30.1	2.0	—
WD2126+734	0.16	8.6(7.8)	1.13(26)	22.9	39.3	4.3	59.9
WD2134+218	0.13	1.83(47)	2.34(32)	48.0	82.2	2.8	15.6
WD2136+828	0.11	7.6(6.2)	1.17(26)	27.4	46.8	1.5	21.4
WD2149+021	0.11	3.0(1.2)	1.65(21)	22.9	39.1	1.6	12.9
WD2246+223	1.64	3.11(21)	5.89(35)	16.4	28.1	4.0	5.8
WD2331–475	<0.01	2.17(36)	1.99(22)	76.2	130.3	3.3	25.4
WD2333–165	0.51	3.22(83)	1.70(16)	23.0	39.4	3.4	10.5
WD2359–434	2.66	4.15(32)	6.02(38)	6.4	10.9	6.6	8.6

Note. — Young refers to mass limits placed on young planets, i.e those with cooling ages consistent with the cooling age of the WD, while old refers to mass limits for planets as old as the total age of the system. For some stars, the age computed based on the initial mass is older than the Galaxy. These stars likely lost some mass through binary interaction, and the ages are therefore younger than computed. With no meaningful estimate of total system age we are unable to constrain the mass of any old planets. For some stars with very large excesses we were unable to extrapolate an age. The mass limit in these cases is likely very much greater than $25 M_J$.

Chapter 7

Finis

Strike another match, go start anew

And it's all over now, Baby Blue.

Bob Dylan

We used the extremely stable pulsations of a subset of variable white dwarves to search for, and find, evidence of planetary companions. Planets found in this way make enviable candidates for follow up with Spitzer, and in future with larger telescopes such as the GMT (Giant Magellan Telescope) and JWST (the James Webb Space Telescope). The low contrast between star and planet makes follow-up orders of magnitude easier than for planets around main sequence stars.

Out of a sample of 16 objects, we find evidence of a daughter planet in one system. The limits on companions placed around two stars with decades of archival data are among the most stringent for long period companions by any technique for any star. The fact that we find a planet in a relatively small sample supports the hypothesis that planets are at least as common around WDs as they are around main sequence stars.

The future direction of this project is clear — obtaining more and better data on the sample reported on here, while increasing the number of DAVs studied. This can be achieved both by increasing the number of 1-2m class telescopes which can obtain long timebases, with similar or slightly lower signal to noise, and using

bigger telescopes to obtain better data with lower timing uncertainties to obtain more stringent limits of companions.

We find a candidate brown dwarf companion to a white dwarf by observing an excess flux in the near and mid-infrared. The BD fraction we observe is consistent with that found by other surveys and with the frequency of BDs in short period orbits around main sequence stars found by radial velocity surveys. Although the statistics of these rare WD plus BD systems are uncertain, the good agreement between WD binarity fractions and those of main sequence stars suggests that companions have a strong chance of surviving the death throes of their parent star. We use the same observational technique to place limits on the presence of young planetary companions with cooling ages consistent with the cooling age of the WD. The mass limits we place disfavour various suggestions that planets can form or accrete from the material cast off from a star as it dies. This does not rule out formation of terrestrial sized rocky planets through a similar mechanism put forth to explain the existence of the pulsar planets.

This work takes a significant step towards addressing the question of the ultimate fate of the Earth by answering the question of whether planets can survive the death of their parent star.

Bibliography

- Abazajian, K., *et al.* 2003, AJ, 126, 2081
———. 2004, AJ, 128, 502
Adelman-McCarthy, J. K., *et al.* 2006, ApJS, 162, 38
Alcock, C., Fristrom, C. C., & Siegelman, R. 1986, ApJ, 302, 462
Allard, F., *et al.* 1994, AJ, 107, 1565
Aumann, H. H. 1988, AJ, 96, 1415
Becklin, E. E., & Zuckerman, B. 1988, Nature, 336, 656
Becklin, E. E., *et al.* 2005, ApJ, 632, L119
Benedict, G. F., *et al.* 2006, AJ, 132, 2206
Benvenuto, O. G., García-Berro, E., & Isern J., 2004, Phys. Rev. D, 69, 082002
Bergeron, P., Leggett, S. K., & Ruiz, M. T. 2001, ApJS, 133, 413
Bergeron, P., *et al.* 1994, ApJ, 423, 456
———. 1995, ApJ, 449, 258
———. 2004, ApJ, 600, 404
Bevington, P. R. 1969, “Data reduction and error analysis for the physical sciences”
(2nd ed.; New York: McGraw-Hill, 1969)
Boffin, H. M. J., *et al.* 1998, MNRAS, 300, 1189
Bohlin, R. C., Dickinson, M. E., & Calzetti, D. 2001, AJ, 122, 2118
Boss, A. P. 1995, Science, 267, 360
———. 1997, Science, 276, 1836
———. 2002, ApJ, 576, 462
———. 2005, ApJ, 629, 535
Bradley, P. A. 1998, ApJS, 116, 307
Brickhill, A. J. 1983, MNRAS, 204, 537
Burleigh, M. R., Clarke, F. J., & Hodgkin, S. T. 2002, MNRAS, 331, L41
Burleigh, M. R., *et al.* 2006, MNRAS, 373, L55
Burrows, A., Sudarsky, D., & Hubeny, I. 2006a, ApJ, 650, 1140
———. 2006b, ApJ, 640, 1063
Burrows, A., Sudarsky, D., & Lunine, J. I. 2003, ApJ, 596, 587
Burrows, A., *et al.* 2001, Reviews of Modern Physics, 73, 719

- Cai, K., *et al.* 2006, ApJ, 636, L149
- Cameron, A. G. W. 1978, Moon and Planets, 18, 5
- Carpenter, J. M., *et al.* 2005, AJ, 129, 1049
- Castanheira, B. G., *et al.* 2004, A&A, 413, 623
- Charbonneau, D., *et al.* 2005, ApJ, 626, 523
- Chary, R., Zuckerman, B., & Becklin, E. E. 1998, The Universe as Seen by ISO (astro-ph/9812090)
- Chu, Y. H., *et al.* 2001, ApJ, 546, L61
- Debes, J. H., & Sigurdsson, S. 2002, ApJ, 572, 556
- Debes, J. H., Ge, J., & Ftaclas, C. 2006, AJ, 131, 640
- Debes, J. H., Sigurdsson, S., & Woodgate, B. E. 2005a, AJ, 130, 1221
- . 2005b, ApJ, 633, 1168
- Deming, D., *et al.* 2005, Nature, 434, 740
- . 2006, ApJ, 644, 560
- Dolez, N., Vauclair, G., & Chevreton, M. 1983, A&A, 121, L23
- Duncan, M. J., & Lissauer, J. J. 1998, Icarus, 134, 303
- Dupuis, J., Fontaine, G., & Wesemael, F. 1993, ApJS, 87, 345
- Eggen, O. J. 1968, ApJS, 16, 97
- Eggen, O. J., & Greenstein, J. L. 1965, ApJ, 141, 83
- Endl, M., *et al.* 2006, ApJ, 649, 436
- Farihi, J., & Christopher, M. 2004, AJ, 128, 1868
- Farihi, J., Becklin, E. E., & Zuckerman, B. 2005a, ApJS, 161, 394
- Farihi, J., Zuckerman, B., & Becklin, E. E. 2005b, AJ, 130, 2237
- Fazio, G. G., *et al.* 2004, ApJS, 154, 10
- Ferrario, L., *et al.* 2005, MNRAS, 361, 1131
- Finley, D. S., Koester, D., & Basri, G. 1997, ApJ, 488, 375
- Fischer, D. A., & Valenti, J. 2005, ApJ, 622, 1102
- Fontaine, G., *et al.* 1982, ApJ, 258, 651
- . 2003, ApJ, 591, 1184
- Forrest, W. J., *et al.* 2004, ApJS, 154, 443
- Fukugita, M., *et al.* 1996, AJ, 111, 1748
- Gianninas, A., Bergeron, P., & Fontaine, G. 2005, ApJ, 631, 1100
- . 2006, AJ, 132, 831
- Giclas, H. L., Burnham, R., & Thomas, N. G. 1965, Lowell Observatory Bulletin, 6, 155
- Giovannini, O., *et al.* 1998, Baltic Astronomy, 7, 131
- Girardi, L., *et al.* 2000, A&AS, 141, 371
- Goldreich, P., & Tremaine, S. 1980, ApJ, 241, 425
- Gonzalez, G. 1997, MNRAS, 285, 403
- Greaves, J. S., *et al.* 2005, ApJ, 619, L187
- Grether, D., & Lineweaver, C. H. 2006, ApJ, 640, 1051

- Grillmair, C. J., *et al.* 2007, ApJ, 658, L115
- Gunn J. E. Carr, M., *et al.* 1998, AJ, 116, 3040
- Haisch Jr., K. E., Lada, E. A., & Lada, C. J. 2001, ApJ, 553, L153
- Harrington, R. S., & Dahn, C. C. 1980, AJ, 85, 454
- Hatzes, A. P., *et al.* 2000, ApJ, 544, L145
- Hessels, J. W. T., *et al.* 2006, Science, 311, 1901
- Hogg, D. W., *et al.* 2001, AJ, 122, 2129
- Holberg, J. B., & Bergeron, P. 2006, AJ, 132, 1221
- Holberg, J. B., Barstow, M. A., & Burleigh, M. R. 2003, ApJS, 147, 145
- Holberg, J. B., Barstow, M. A., & Sion, E. M. 1998, ApJS, 119, 207
- Holberg, J. B., Oswalt, T. D., & Sion, E. M. 2002, ApJ, 571, 512
- Homeier, D., *et al.* 1998, A&A, 338, 563
- Houck, J. R., *et al.* 2004, ApJS, 154, 18
- Hubickyj, O., Bodenheimer, P., & Lissauer, J. J. 2005, Icarus, 179, 415
- Ida, S., & Lin, D. N. C. 2004, ApJ, 604, 388
- Jeans, J. H. 1924, MNRAS, 85, 2
- Jenkins, L. F. 1952, “General catalogue of trigonometric stellar parallaxes.” (ed.; [New Haven, Yale University Observatory] 1952.)
- Jura, M. 2003, ApJ, 584, L91
- Jura, M., & Turner, J. 1998, Nature, 395, 144
- Karl, C. A., *et al.* 2005, A&A, 434, 637
- Kawka, A., *et al.* 2007, ApJ, 654, 499
- Kepler, S. O., *et al.* 1982, ApJ, 254, 676
- . 1988, *Advances in Helio- and Asteroseismology*, ed. Christensen-Dalsgaard J., & Frandsen S., 123, 325
- . 1991, ApJ, 378, L45
- . 2005, ApJ, 634, 1311
- . 2007, MNRAS, 375, 1315
- Kilic, M., *et al.* 2005, ApJ, 632, L115
- . 2006a, ApJ, 642, 1051
- . 2006b, ApJ, 646, 474
- Kilkenny, D., Heber, U., & Drilling, J. S. 1988, South African Astronomical Observatory Circular, 12, 1
- Kirkpatrick, J. D. 2005, ARA&A, 43, 195
- Kirkpatrick, J. D., *et al.* 1999, ApJ, 519, 834
- Kleinman S. J. Harris, H. C., *et al.* 2004, ApJ, 607, 426
- Kleinman, S. J., *et al.* 1994, ApJ, 436, 875
- Koen, C. 2006, MNRAS, 365, 489
- Koester, D., & Wilken, D. 2006, A&A, 453, 1051
- Koester, D., *et al.* 2001, A&A, 378, 556
- . 2005, A&A, 432, 1025

- Kuchner, M. J., Koresko, C. D., & Brown, M. E. 1998, *ApJ*, 508, L81
- Kumar, P., & Goodman, J. 1996, *ApJ*, 466, 946
- Kumar, S. S. 1963, *ApJ*, 137, 1121
- Kurucz, R. L. 1979, *ApJS*, 40, 1
- Laughlin, G., & Adams, F. C. 1997, *ApJ*, 491,
- Liebert, J., Bergeron, P., & Holberg, J. B. 2005, *ApJS*, 156, 47
- Lin, D. N. C., Bodenheimer, P., & Richardson D. C. , 1996, *Nature*, 380, 606
- Lisker, T., *et al.* 2005, *A&A*, 430, 223
- Livio, M., & Soker, N. 1984, *MNRAS*, 208, 763
- Livio, M., Pringle, J. E., & Wood, K. 2005, *ApJ*, 632, L37
- Marcy, G., *et al.* 2005, *Progress of Theoretical Physics Supplement*, 158, 24
- Marcy, G. W., & Butler, R. P. 2000, *PASP*, 112, 137
- Maxted, P. F. L., Marsh, T. R., & Moran, C. K. J. 2000, *MNRAS*, 319, 305
- Maxted, P. F. L., *et al.* 2006, *Nature*, 442, 543
- McCook, G. P., & Sion, E. M. 1999, *ApJS*, 121, 1
- McLaughlin, D. B. 1924, *ApJ*, 60, 22
- Mendoza V., E. E. 1966, *ApJ*, 143, 1010
- . 1968, *ApJ*, 151, 977
- Monet, D. G., *et al.* 2003, *AJ*, 125, 984
- Motch, C., Werner, K., & Pakull, M. W. 1993, *A&A*, 268, 561
- Muench, A. A., *et al.* 2002, *ApJ*, 573, 366
- Mukadam, A. S., *et al.* 2003, *ApJ*, 594, 961
- . 2004a, *ApJ*, 607, 982
- . 2004b, *ApJ*, 612, 1052
- Mullally, F. 2003, Masters thesis, University of Texas at Austin
- Mullally, F., & de Graff, M. 2005, *14th European Workshop on White Dwarfs*, ed. Koester D., & Moehler S., 334, 506
- Mullally, F., *et al.* 2005, *ApJ*, 625, 966
- . 2007, *ApJS* in press (astro-ph/0611588)
- Nather, R. E., & Mukadam, A. S. 2004, *ApJ*, 605, 846
- O'Donoghue, D., & Warner, B. 1987, *MNRAS*, 228, 949
- Oke, J. B. 1990, *AJ*, 99, 1621
- Oke, J. B., Weidemann, V., & Koester, D. 1984, *ApJ*, 281, 276
- Pajdosz, G. 1995, *A&A*, 295, L17
- Patten, B. M., *et al.* 2006, *ApJ*, 651, 502
- Perryman, M. A. C., *et al.* 1997, *A&A*, 323, L49
- Pesnell, W. D. 1985, *ApJ*, 292, 238
- Pier, J. R., *et al.* 2003, *AJ*, 125, 1559
- Pollack, J. B., *et al.* 1996, *Icarus*, 124, 62
- Pols, O. R., *et al.* 1998, *MNRAS*, 298, 525
- Probst, R. G. 1983, *ApJS*, 53, 335

- Quillen, A. C., & Thorndike, S. 2002, ApJ, 578, L149
- Raffelt, G. G. 1986, Physics Letters B, 166, 402
- Rasio, F. A., *et al.* 1996, ApJ, 470, 1187
- Reach, W. T., *et al.* 2005a, ApJ, 635, L161
- . 2005b, PASP, 117, 978
- Reipurth, B., & Clarke, C. 2001, AJ, 122, 432
- Rice, W. K. M., *et al.* 2003, MNRAS, 346, L36
- Richardson, L. J., *et al.* 2007, Nature, 445, 892
- Rossiter, R. A. 1924, ApJ, 60, 15
- Santos, N. C., Israelian, G., & Mayor, M. 2004, A&A, 415, 1153
- Sartoretti, P., & Schneider, J. 1999, A&AS, 134, 553
- Saumon, D., & Guillot, T. 2004, ApJ, 609, 1170
- Schatzman, E. L. 1958, “White dwarfs” (1st ed.; Amsterdam, North-Holland Pub. Co.; New York, Interscience Publishers, 1958.)
- Silverstone, M. D., *et al.* 2006, ApJ, 639, 1138
- Silvotti, R., *et al.* 2007, astro-ph/0703753
- Sion, E. M., *et al.* 1988, AJ, 96, 251
- Skrutskie, M. F., *et al.* 2006, AJ, 131, 1163
- Smith, J. A., *et al.* 2002, AJ, 123, 2121
- Sozzetti, A. 2004, MNRAS, 354, 1194
- Stoughton, C., *et al.* 2002, AJ, 123, 485
- Stover, R. J., *et al.* 1980, ApJ, 240, 865
- Struve, O. 1952, The Observatory, 72, 199
- Stumpff, P. 1980, A&AS, 41, 1
- Sudarsky, D., Burrows, A., & Hubeny, I. 2003, ApJ, 588, 1121
- Thejll, P., MacDonald, J., & Saffer, R. 1991, A&A, 248, 448
- Tremblay, P.-E., & Bergeron, P. 2007, ApJ, 657, 1013
- Varnière, P., *et al.* 2006, ApJ, 640, 1110
- Villaver, E., & Livio, M. 2007, astro-ph/0702724
- von Hippel, T., *et al.* 2007, astro-ph/0703473
- Wegner, G., & Swanson, S. R. 1990, AJ, 99, 330
- Weidemann, V. 2000, A&A, 363, 647
- Werner, K., Heber, U., & Fleming, T. 1994, A&A, 284, 907
- Werner, K., *et al.* 1996, A&A, 307, 860
- Werner, M. W., *et al.* 2004, ApJS, 154, 1
- Wickramasinghe, D. T., Allen, D. A., & Bessell M. S. , 1982, MNRAS, 198, 473
- Wickramasinghe, N. C., Hoyle, F., & Al-Mufti, S. 1988, Ap&SS, 143, 193
- Williams, K. A. 2006, astro-ph/0610254
- Winget, D. E. 1998, Journal of the Physics of Condensed Matter, 10, 11247
- Winget, D. E., *et al.* 1990, ApJ, 357, 630
- Winn, J. N., *et al.* 2005, ApJ, 631, 1215

- . 2006, *ApJ*, 653, L69
- Wolff, B., Koester, D., & Liebert, J. 2002, *A&A*, 385, 995
- Wolszczan, A., & Frail, D. A. 1992, *Nature*, 355, 145
- Wood, M. A. 1992, *ApJ*, 386, 539
- Wynands, R., & Weyers, S. 2005, *Metrologia*, 42, 64
- Yeates, C. M., *et al.* 2005, *ApJ*, 635, 1239
- York, D. G., *et al.* 2000, *AJ*, 120, 1579
- Zuckerman, B., & Becklin, E. E. 1987, *Nature*, 330, 138
- . 1992, *ApJ*, 386, 260
- Zuckerman, B., *et al.* 2003, *ApJ*, 596, 477

Vita

Fergal Mullally was born in Dublin, Ireland 1 May 1979, the son of Paul and Maeve Mullally. He completed Leaving Certificate at Coláiste Éanna in 1997, before reading Science at the University College Dublin. In October 2001, he graduated with Second Class Honours from the Experimental and Mathematical Physics Departments. He immediately entered the graduate school at the University of Texas obtaining a Master of Arts in Astronomy in 2003.

He is pleased that this ordeal is nearly over.

Permanent Address: 11 Ashton Grove,
Knocklyon,
Dublin 16,
Ireland

This dissertation was typeset with $\text{\LaTeX} 2_{\epsilon}$ ¹ by the author.

¹ $\text{\LaTeX} 2_{\epsilon}$ is an extension of \LaTeX . \LaTeX is a collection of macros for \TeX . \TeX is a trademark of the American Mathematical Society. The macros used in formatting this dissertation were written by Dinesh Das, Department of Computer Sciences, The University of Texas at Austin, and extended by Bert Kay, James A. Bednar, and Ayman El-Khashab.